Investigation of the lysosomal proteome in neuronal ceroid lipofuscinosis caused by CLN6 deficiency and interactome studies to identify novel interaction partners of CLN6

Dissertation

zur Erlangung des Doktorgrades (Dr. rer. nat.)
der Mathematisch-Naturwissenschaftlichen Fakultät
der Rheinischen Friedrich-Wilhelms-Universität Bonn

vorgelegt von

Andreas Türmer

aus Balingen

Bonn, November 2023

Angefertigt mit Genehmigung der Mathematisch-Naturwissenschaftlichen

Fakultät der Rheinischen Friedrich-Wilhelms-Universität Bonn

1. Gutachter: Prof. Dr. Volkmar Gieselmann

2. Gutachter: Prof. Dr. Oliver Gruß

Tag der Promotion: 25. März 2024

Erscheinungsjahr: 2024

Table of Contents

Abbreviations

°C	degree celsius
µL	microliter
µM	micromolar
ACN	acetonitrile
Amp	ampicillin
APS	ammonium persulfate
ASAH1	acid ceramidase
ATP	adenosine triphosphate
BHK cells	baby hamster kidney cells
BiFC	bimolecular fluorescence complementation
CALR	calreticulin
CANX	calnexin
CD	cation-dependent
cDNA	complementary desoxyribonucleic acid
CI	cation-independent
CLN	ceroid-lipofuscinosis neuronal
CLNX	ceroid-lipofuscinsosis neuronal protein x
Co-IP	Co-immunoprecipitation
COP	coat protein complex
CPT2	carnitine o-palmitoyltransferase 2
CTSC	cathepsin C
CTSD	cathepsin D
CTSF	cathepsin F
CTSZ	cathepsin Z
DB	digestion buffer
DCA	deoxycholic acid
DMSO	dimethyl sulfoxide
DNA	desoxyribonucleic acid
E. coli	Escherichia coli
EDTA	ethylenediaminetetraacetic acid
EGRESS	ER-to-Golgi relaying of enzymes of the lysosomal system

eIF-4G1	eukaryotic translation initiation factor 4 gamma 1
ER	endoplasmic reticulum
ERAD	ER-associated degradation
ERES	endoplasmic reticulum exit site
FA	formic acid
FSC	forward scatter
GANAB	catalytic alpha subunit of glucosidase 2
GBA	β-glucocerebrosidase
GlcNAc	N-acetylglucosamine
GNTP	N-acetylglucosamine-1-phosphate transferase
GPLD1	phosphatidylinositol-glycan-specific phospholipase D
HEK cells	human embryonic kidney 293 cells
HPLC	high pressure liquid chromatography
Kan	kanamycin
L	liter
LAMP1	lysosomal-associated membrane protein 1
LC	liquid chromatography
LIMP2	lysosomal integral protein 2
LSD	lysosomal storage disease
M	molar
M6P	mannose-6-phosphate
mFA2H	mutated fatty acid 2-hydroxylase
mg	milligram
min	minute
mL	milliliter
mM	millimolar
MPR	mannose 6-phosphate receptor
MS	mass spectrometry
NAAA	N-acylethanolamine-hydrolyzing acid amidase
NAGPA	α-N-acetylglucosaminidase
NC	nitrocellulose
NCL	neuronal ceroid lipofuscinosis
o/n	overnight

OST	oligosaccharyltransferase
PBS	phosphate-buffered saline
PDI	protein disulfide isomerase
pH	potential of hydrogen
PNS	post nuclear supernatant
PPT1/2	palmitoyl-protein thioesterase 1/2
PVDF	polyvinylidene fluoride membrane
rpm	revolutions per minute
RT	room temperature
SAX	strong anion exchange
SDC	sodium deoxycholate
SDS-PAGE	sodium dodecyl sulphate-polyacrylamide gel electrophoresis
SEC16A	protein transport protein SEC16A
SEH1	nucleoporin SEH1
SILAC	stable isotope labeling by amino acids in cell culture
SMPD1	sphingomyelin phosphodiesterase
SPE	solid phase extraction
SSC	side scatter
STAGE	stop and go extraction
STT3B	dolichyl-diphosphooligosaccharide--protein glycosyltransferase subunit STT3B
TANGO1	transport and golgi organization protein 1 homolog
TBS	Tris-buffered saline
TBS-T	Tris-buffered saline with Tween-20
TEAB	triethylammonium bicarbonate
TEMED	tetramethylethylenediamine
TMT	tandem mass tag
TPP1	tripeptidyl peptidase 1
UGGT	UDP-glucose:glycoprotein glucosyltransferase
V	volt
wt	wild-type
xg	earth’s gravitational acceleration
YFP	yellow fluorescent protein

Abstract

Neuronal ceroid lipofuscinoses (NCLs) account for the majority of genetic neurodegenerative diseases in infancy. However, for most forms of this serious disease there is no adequate treatment available. In the NCL6 subtype, which is caused by deficiency in ceroid- lipofuscinosis neuronal protein 6 (CLN6), poor understanding of CLN6's function and its pathomechanisms impede the development of a proper treatment. Therefore, this thesis comprises a detailed examination of pathological changes in the lysosome and investigations to identify novel interaction partners of CLN6 with the purpose to elucidate its function. First, mass spectrometric analysis of the lysosomal fraction from wild-type (wt) and *nclf* mouse liver were conducted, which for the first time presented a large-scale study of proteomic changes in CLN6 deficiency and indicated a significant depletion of specific lysosomal proteins. This reduction of mainly soluble hydrolases was validated through examining selected proteins by western blotting of tritosomes as well as 20.000 g brain and liver pellets from wt and *nclf* mice. However, western blots of whole liver and brain lysates in comparison to the lysosomal fractions showed no differences or even an increase in the protein amount of most investigated proteins, which might indicate an impaired transport to the lysosome. Second, the BioID approach was applied for CLN6 and resulted in numerous proteins, which are located in close proximity of CLN6 and, therefore, are potential interaction partner candidates. Bimolecular fluorescence complementation (BiFC) assays of selected candidates from the BioID data sets verified an association of CLN6 with the chaperones calnexin (CANX) and calreticulin (CALR), which are known interaction partners of lysosomal soluble hydrolases.

This thesis contributes to a better understanding of the development of NCL6 and the molecular biology of CLN6 in multiple ways. The investigations of the lysosomal proteome provide with the reduction of many lysosomal hydrolases a concrete link to CLN6's function and a conceivable explanation for the accumulation of storage material in CLN6 deficiency. The interaction partner studies provide an enormous number of proteins, which are acting in various different biological pathways and are potentially associated with CLN6. The inclusion of a considerable number of proteins playing a

role in the calnexin-cycle along with CANX and CALR, whose association with CLN6 was validated by the BiFC assay, suggest an involvement of CLN6 in the biogenesis of lysosomal proteins and potentially also a direct interaction with soluble hydrolases in the endoplasmic reticulum (ER).

Zusammenfassung

Neuronale Ceroid-Lipofuszinosen stellen die am häufigsten vorkommenden genetisch bedingten neurodegenerativen Erkrankungen im Kindesalter dar. Für die meisten Formen dieser ernsten Krankheit sind jedoch keine angemessenen Behandlungsmöglichkeiten vorhanden. Ebenso wie bei der NCL6 Form, die durch einen Defekt im CLN6 Protein hervorgerufen wird. Die Entwicklung einer geeigneten Behandlung wird unter anderem durch fehlende Kenntnisse über die genauen Pathomechanismen und die Funktion von CLN6 erschwert. Das Ziel dieser Arbeit war, einen Beitrag zur Aufklärung der Funktion von CLN6 zu leisten. Hierzu wurden zwei Ansätze verfolgt: eine detaillierte Untersuchung der pathologischen Veränderungen im Lysosom und Versuche zur Identifikation von CLN6 Interaktionspartner. Zunächst wurden massenspektrometrische Analysen der lysosomalen Fraktion von wildtyp und *nclf* Mausleber durchgeführt, die erstmals ein umfassendes Bild von proteomischen Veränderungen bei einem CLN6 Defekt lieferten und einen signifikanten Verlust spezifischer lysosomaler Proteine anzeigten. Diese Verringerung hauptsächlich löslicher Hydrolasen wurde durch den Nachweis ausgewählter Proteine in Western Blots aus 20.000 g Gehirn- und Leberpellet Proben von wt und *nclf* Mäusen bestätigt. Außerdem zeigten Western Blots von Lysaten der gesamten Leber und des gesamten Gehirns für den Großteil der untersuchten Proteine keinen Unterschied bzw. sogar einen Anstieg der Proteinmenge bei CLN6 Defizienz an, was auf einen beeinträchtigten Transport oder eine fehlerhafte Verarbeitung hinweisen könnte. Im zweiten Teil dieser Arbeit wurde die BioID Methode für CLN6 angewandt und ergab eine große Anzahl von Proteinen, die sich in unmittelbarer Nähe von CLN6 befinden und daher potenzielle Interaktionspartner darstellen. Bimolekulare Fluoreszenzkomplementationstests ausgewählter Kandidaten aus den BioID Datensätzen bestätigten eine Assoziation von CLN6 mit den Chaperon Proteinen CANX und CALR, die bekannte Interaktionspartner lysosomaler löslicher Hydrolasen sind.

Diese Arbeit trägt in mehrfacher Hinsicht zu einem besseren Verständnis der Krankheitsentstehung bei NCL6 und der Molekularbiologie von CLN6 bei. Die Untersuchungen des lysosomalen Proteoms liefern mit der Verringerung vieler

lysosomaler Hydrolasen eine konkrete Verbindung zur Funktion von CLN6 und eine denkbare Erklärung für die Akkumulation von Speichermaterial bei CLN6 Defizienz. Des Weiteren liefern die Interaktionspartnerstudien eine enorme Anzahl von Proteinen, die möglicherweise mit CLN6 in Verbindung stehen und in ganz unterschiedlichen biologischen Prozessen mitwirken. Eine beträchtliche Anzahl von diesen Proteinen einschließlich CANX und CALR, deren engere Verbindung zu CLN6 in Fluoreszenzkomplementationstests bestätigt wurde, spielen eine Rolle in der Prozessierung glykosylierter Proteine und deuten darauf hin, dass CLN6 an der Biogenese lysosomaler Proteine und möglicherweise auch an einer direkten Interaktion mit löslichen Hydrolasen im ER beteiligt ist.

1 Introduction

1.1 Lysosomes

To carry out and maintain its physiological function each cell relies on the concerted effort of different organelles. Each of these cellular subunits serves a specific purpose important for cell survival, growth and proliferation. In mammalian cells the lysosome is one of these organelles. It was discovered in 1955 by Christian de Duve (De Duve et al. 1955), who had observed unexpected low enzyme activities of acid phosphatase in homogenized cell fractions. De Duve and his team assumed the enzyme had to be surrounded by a membrane and for this reason does not have access to the added substrate. This hypothesis could soon be verified and even more hydrolases were assigned to the newly found compartment (Bainton 1981). To point out its lytic properties de Duve referred to this newly discovered organelle as lysosome. Since then, the knowledge about the lysosome has grown continuously, which made our understanding of this cellular compartment more and more complete. The size of the lysosome varies between 0,1 and 1,2 µm (Kühnel et al. 2003) and there are between 50 and 1000 lysosomes distributed in every mammalian cell (Meyer-Schwesinger 2021). The lumen of this membrane-bound organelle has an acidic pH, which is established and maintained by the vacuolar ATPase (Mellman 1989) and ranges from 3,5 to 5,5 (Wu et al. 2011). For lysosomal hydrolases this presents a suitable environment to carry out their function (De Duve et al. 1966, Ng et al. 2012), as the majority of these enzymes show a pH optimum between pH 4,5 and 5,5 (Mellman et al. 1986). As of today, over 60 soluble lysosomal hydrolases (Schroder et al. 2010), numerous of their associated cofactors (Sleat et al. 2005), and over 100 lysosomal membrane proteins (Schwake et al. 2013) and many proteins associated with the lysosomal membrane (Schroder et al. 2007) were identified. Discovering these proteins and determining the function of many of these proteins increased our understanding of the lysosome enormously. However, the lysosomal proteome is still not completely known and numerous questions about the lysosome are still to be answered.

1.1.1 Biogenesis of lysosomes

The genesis of lysosomes is a complex process, involving various pathways and many different assisting proteins. Lysosome's site of origin is the ER, where the biosynthesis, processing and folding of the lysosomal proteins take place (Kornfeld 1986). In the ER most lysosomal proteins are N-glycosylated. Among other functions, it protects the protein against degradation by proteases especially in the lysosome and the oligosaccharides also serve as specific marker molecules used for intracellular targeting and transport (Kornfeld 1998). After processing and proper folding lysosomal proteins are sorted into coat protein complex (COP) II vesicles and transported to the Golgi. There are two known principle transport concepts existing, which soluble lysosomal proteins potentially rely on in the early secretory pathway, the bulk flow and the receptor mediated transport (Barlowe et al. 2016). Ergic53 and ceroid lipofuscinosis neuronal protein 8 (CLN8) are postulated receptors for various soluble hydrolases in the ER and were shown to deliver their cargo to the Golgi (Appenzeller et al. 1999, di Ronza et al. 2018). Another known receptor as well as a lysosomal membrane protein is lysosomal integral protein 2 (LIMP2), which binds in the ER specifically to β-glucocerebrosidase (GBA) and mediates its transport through the Golgi and endosomes to the lysosome (Schwake et al. 2013). From the Golgi to the lysosome the main path for soluble lysosomal hydrolases is the mannose-6-phosphate (M6P) dependent pathway. In the cis-Golgi network the N-acetylglucosamine-1-phosphate transferase (GNTP) transfers N-acetylglucosamine-1-phosphate to mannose residues of glycosylated lysosomal proteins. Subsequently, the N-acetylglucosamine-1-phosphodiester α-N-acetylglucosaminidase (NAGPA) removes the N-acetylglucosamine (GlcNAc) in the trans-Golgi and uncovers the M6P residues (Coutinho et al. 2012, Khan et al. 2020), the binding site of mannose 6-phosphate receptors (MPRs). The two MPRs, the cation-independent (CI) and the cation-dependent (CD) MPR, bind to the M6P-tagged proteins in the trans-Golgi network (TGN) and transport them in clathrin-coated vesicles to endosomes (Ghosh et al. 2003). After the vesicles fuse with early endosomes MPRs and lysosomal proteins dissociate because of the acidic pH. Finally, late endosomes fuse with lysosomes and provide new supply of soluble lysosomal proteins. Furthermore, mistargeted and secreted lysosomal proteins containing M6P residues can be reinternalized by the CI-MPR, as it also cycles

between the plasma membrane and the endosomal-lysosomal system and reach the lysosome by the endocytic pathway (Storch et al. 2005). In addition to the common and well known M6P pathway accounting for the transport of most hydrolases, there are also M6P-independent pathways. Besides the already mentioned LIMP2, which transports GBA, which does not bear M6P residues to the lysosome, several other receptors are known to be involved in the transport of soluble lysosomal proteins. For example, sortilin is known to transport GM2 activator protein, acid sphingomyelinase, prosaposin and cathepsins D and H from the Golgi to the lysosome (Staudt et al. 2016). Seizure 6-like protein 2 was shown to target procathepsin D to the lysosome specifically in neuronal cells (Boonen et al. 2016). And yet another example is the mannose receptor at the plasma membrane, which binds to high mannose type glycans of proteins also if they do not contain M6P residues, internalizes secreted proteins and transports them from the plasma membrane to the lysosome (Elvevold et al. 2008). The majority of these pathways are cell-type specific or include a few or even only a single protein. Overall, the M6P-independent pathways are less well characterized compared to M6P-dependent pathway so far and it is not exactly clear how important and extensive their role is for the biogenesis of lysosomes (Staudt et al. 2016). The transport of lysosomal membrane proteins does not rely on the M6P sorting signal at all, but on specific sequence motifs in their cytoplasmic tails. Membrane proteins require di-acidic or di-hydrophobic motifs for their integration into the COPII vesicles and ER export (Barlowe 2003). After being transported to the TGN some proteins, for example the LIMP/LAMP class, are targeted directly to endosomes, which fuse later with lysosomes and others like the lysosomal acid phosphatase follow the constitutive secretory pathway to the plasma membrane, where they again are internalized and reach the endosomal-lysosomal system by endocytosis. In both cases the membrane protein requires either the YXXØ or the [DE]XXXL[LI] signal motif located in the cytoplasm closely to the transmembrane domain in general at or near the C-terminus to be transported to the lysosome (van Meel et al. 2008, Braulke et al. 2009).

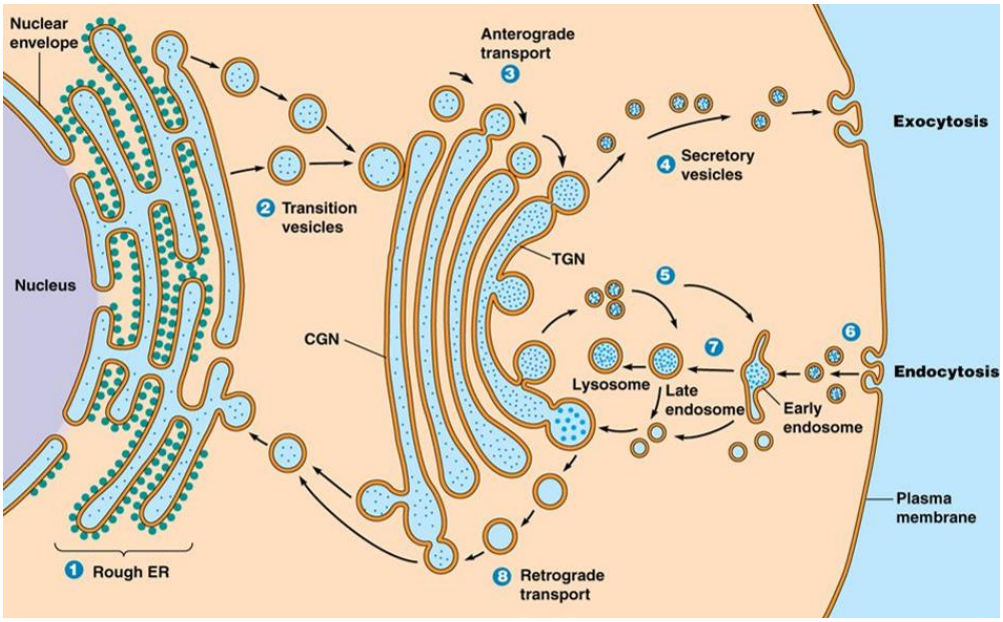

Figure 1.1: Schematic overview of the transport routes of lysosomal proteins
Lysosomal proteins are synthesized in the ER (1) and are transported to the Golgi by COPII vesicles (2). During Golgi transit soluble lysosomal proteins receive M6P residues (3). Lysosomal proteins reach the endosome after secretion or integration into the plasma membrane (4) by endocytosis (6) or directly by M6P-dependent or -independent pathways (5) and, finally, the lysosomal compartment upon fusion of late endosomes with lysosomes (7). Retrograde transport (8) recycles receptors and other components of the trafficking machinery for further transport rounds (https://slideplayer.com/slide/10613641(Owen)).

1.1.2 Lysosomal functions

The central function of the lysosome is the degradation of intra- and extracellular lipid, carbohydrate, nucleic acid and protein substrates. Extracellular biological components reach the lysosome mainly by endocytosis and phagocytosis, whereas intracellular materials are delivered into the lysosomal compartment by autophagy (Settembre et al. 2013). After reaching the lysosome the substrates are broken down by lysosomal hydrolases to their respective building blocks, which are either exported by specific transporters into the cytoplasm and reused for new cellular components and generating energy (Ballabio 2016) or released into the extracellular space via vesicle exocytosis (Buratta et al. 2020). This process serves a crucial role in regulating the cellular metabolism and eliminating toxic protein aggregates, damaged organelles and pathogens (Huber et al. 2016). However, the lysosomal function is broader and not only restricted to degradation and recycling. In addition, the lysosome assists in the plasma membrane repair by lysosome exocytosis (McNeil et al. 2005) and is an essential

signaling hub. The lysosome is an intracellular storage organelle of Ca^{2+} and is involved in Ca^{2+} signaling (Lloyd-Evans et al. 2010). Furthermore, the lysosome plays a role in recycling receptors to the plasma membrane by the endocytic pathway, which also affects cellular signaling (Meyer-Schwesinger 2021). The most important role of the lysosome in cell signaling is the regulation of different nutrition states. Nutrition availability is monitored at the lysosomal membrane and in times of starvation a cellular program is initiated, leading to the transcription of a certain set of proteins, which are needed for managing the state of nutrient deficiency. If enough nutrients are available again the cell signaling changes starting from the lysosome and the cell switches back to an anabolic state (Liu et al. 2020). Another process involving the lysosome is protein exocytosis, in which the lysosomal content is released in the extracellular space. Among others it plays a role in immune response and antigen presentation (Blott et al. 2002). While lysosomes fulfill all these functions and more, it is clear that lysosomal malfunction has serious consequences and can lead to various diseases. Many lysosomal diseases cause devastating symptoms and affect general body functions underscoring the importance of lysosomes for the health of mammalian organisms. Besides deficiency of proteins directly involved in and necessary for lysosomal functions, lysosomal malfunction can also be caused by disruption of lysosomal biogenesis (Cox et al. 2012).

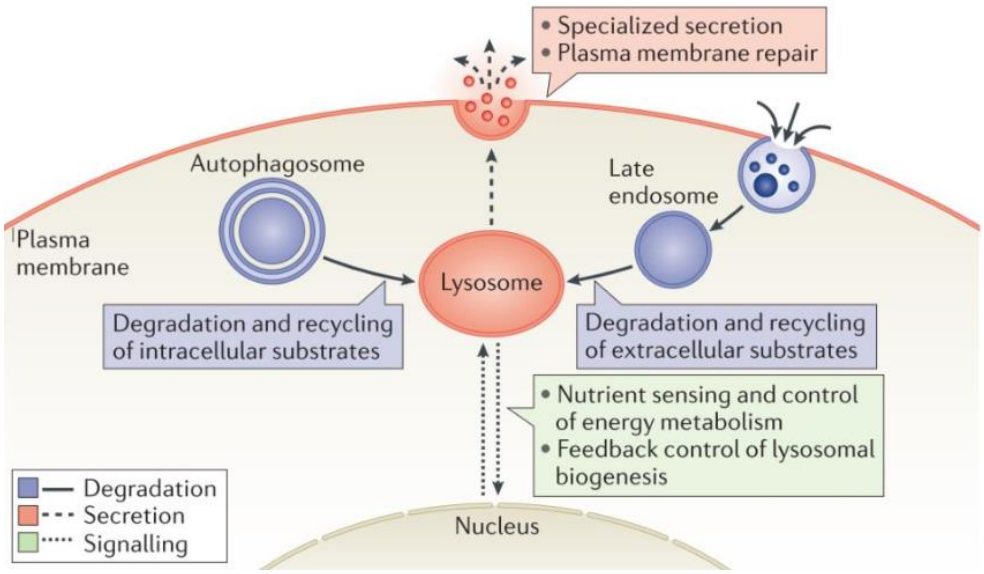

Figure 1.2: Main functions of the lysosome
Illustrated are the main cellular functions of the lysosome, which are degradation, secretion and signaling (Settembre et al. 2013).

1.2 Lysosomal storage diseases

Lysosomal storage diseases (LSDs) are a group of genetic diseases characterized by lysosomal dysfunction and accumulation of storage material inside the lysosomal lumen. The storage material is often the result of enzyme substrates, which cannot be fully degraded or exported from the lysosome (Ballabio et al. 2009). LSDs are caused by gene mutations leading to deficient proteins involved in lysosomal biogenesis or degradation pathways, which are therefore impaired (Gieselmann 1995). At present, there are over 70 LSDs known, which are mainly inherited autosomal recessively and hence, show a relatively low prevalence in the general population (Platt et al. 2018). Furthermore, the clinical pictures of LSDs are heterogenous and among other things differ in the type of the storage material, which is determined by the accumulating substrates. There are also considerable differences in the severity and the onset of symptoms in LSDs, depending on how indispensable the deficient protein is for the lysosomal function and cellular homeostasis. The appearance of symptoms, which in general aggravate over time, ranges from the neonatal period to the late adulthood. The central nervous system is most affected by LSDs, which show neurological symptoms in two of three cases and cause neurodegeneration and mental deterioration. However, all other organs and biological systems are affected as well indicated by visceral, ocular, hematological and skeletal manifestations (Winchester et al. 2000, Parenti et al. 2015). The origin of these diverse symptoms is found on the cellular and molecular level. The primary impairment, namely the accumulation of specific lysosomal substrates, entail various secondary effects, which significantly determine the pathology of the disease. These secondary effects associated with LSDs include the accumulation of additional undegraded macromolecules, disruption of calcium signaling, oxidative stress, inflammation, impairment of autophagy and ER stress (Vitner et al. 2010). Eventually, accumulation of storage material leads to apoptosis and cell death (Bellettato et al. 2010). Interestingly, neurons compared to other cell types are more affected by LSDs indicated by the fact that symptoms are mostly neurological. One reason is that most neurons are postmitotic and therefore lack the possibility to reduce the number of cellular substrates by dividing and solely rely on autophagy and lysosomes for substrate clearance (Onyenwoke et al. 2015).

1.2.1 Neuronal ceroid lipofuscinosis

NCLs are a specific group of LSDs characterized by their common storage material resembling a mixture of ceroid and lipofuscin and neurodegeneration especially in the cerebral and cerebellar cortices (Jalanko et al. 2009). As ceroid and lipofuscin, the storage material is a formation of oxidized and polymerized lipids and proteins, which show autofluorescence, are insoluble by lipid solvents and display a wax-like nature (Pappenheimer et al. 1946, Haltia 2003, Terman et al. 2004). Typical ultrastructural patterns for the storage in NCLs are fingerprint profiles and granular, curvilinear or rectilinear structures mostly found in neurons (Radke et al. 2015). Furthermore, NCLs show common clinical features mainly manifesting in the central nervous system. Among others cognitive decline, progressive cerebellar atrophy, retinopathy, and myoclonic epilepsy are associated with NCL diseases, which eventually almost in all cases lead to premature death (Nita et al. 2016). Despite these similarities NCLs have diverse genetic origins as 14 different ceroid lipofuscinosis neuronal (CLN) genes and proteins are known. Mutated CLN genes, which lead to a deficient protein, cause NCL. The CLN genes and proteins are numbered from 1 to 14 successively according to the time of their discovery. Interestingly, although dysfunction of CLN proteins leads to similar symptoms, known molecular functions of CLN proteins and also their subcellular locations differ widely (Kollmann et al. 2013). Furthermore, also the time of disease onset and the severity varies between NCLs significantly. Except NCL4, which can also be inherited in an autosomal dominant manner, all other types of NCL are inherited only as autosomal recessive traits (Nita et al. 2016). The heredity of these diseases is also the reason for its relatively low prevalence with a combined worldwide incidence of 1:30,000 (Ramirez-Montealegre et al. 2007). There are various approaches available to diagnose NCLs like for instance ultrastructural examination of storage material, enzyme activity assays and genetic tests (Rakheja et al. 2018). However, therapeutic approaches for NCLs are still very limited. Mainly there are only symptomatic and supportive therapies available. The only exception is NCL2, for which there is an enzyme replacement therapy approved (Platt et al. 2018).

Table 1.1: NCL disease onset, protein name, function and location of CLN genes

Gene	NCL onset	Protein	Protein function	Location
CLN1	Infantile, juvenile or adult	Palmitoyl-protein thioesterase 1 (PPT1)	Palmitoylthioesterase	Lysosome
CLN2	Late infantile or juvenile	Tripeptidyl peptidase 1 (TPP1)	Serine protease	Lysosome
CLN3	Juvenile	Battenin	Unknown, modulation of vesicular trafficking and fusion, pH regulation predicted	Late endosomal/ lysosomal membrane
CLN4	Adult	DnaJ homolog subfamily C member 5 (DNAJC5)	Hsc70 co-chaperone, involved in exocytosis and endocytosis	Cytosolic
CLN5	Late infantile, juvenile or adult	CLN5	Functions in endosomal sorting[1]	Lysosome
CLN6	Late infantile[2], juvenile or adult	CLN6	Unknown; involvement in Golgi transport of lysosomal hydrolases postulated[3]	ER-membrane
CLN7	Late infantile or juvenile	Major facilitator superfamily domain containing 8 (MFSD8)	Unknown, transmembrane transporter function predicted	Lysosomal membrane
CLN8	Late infantile or juvenile	CLN8	Receptor of various lysosomal hydrolases for ER-Golgi transport[4]	ER, Golgi[4]
CLN9	Juvenile	CLN9	Unknown	Unknown
CLN10	Congenital, late infantile, juvenile or adult	Cathepsin D (CTSD)	Aspartyl endopeptidase	Lysosome
CLN11	Adult	Progranulin (PGRN)	Regulation of lysosomal pH[5], CTSD chaperone[6]	Secreted, lysosome[7]
CLN12	Juvenile	Cation-transporting ATPase13A2 (ATP13A2)	Polyamine export[8]	Lysosomal membrane
CLN13	Adult	Cathepsin F (CTSF)	Cysteine protease	Lysosome
CLN14	Infantile	Potassium channel tetramerization domain containing 7	Unknown, modulation of ion channel activity predicted	Cytosolic

(Platt et al. 2018)

(Kollmann et al. 2013)

[1] (Mamo et al. 2012)

[2] (Chin et al. 2019)

[3] (Bajaj et al. 2020)

[4] (di Ronza et al. 2018)

[5] (Tanaka et al. 2017)

[6] (Beel et al. 2017)

[7] (Hu et al. 2010)

[8] (van Veen et al. 2020)

1.2.2 Ceroid lipofuscinosis neuronal protein 6

CLN6 is one of 14 proteins, whose deficiency is linked to NCL disease. In total 82 DNA sequence alterations in the CLN6 gene were identified so far. Only twelve are classified as gene mutations with a pathogenic effect. One shows no negative functional impact and is classified as a polymorphism. The impact and the effect of the other remaining sequence alterations could not be clearly determined as of yet (https://www.ucl.ac.uk/ncl-disease/mutation-and-patient-database/mutation-and-patient-datasheets-human-ncl-genes/cln6). Among other things, the type of mutation also affects the degree of CLN6's deficiency, the severity and the onset of the disease. In the more severe forms of NCL6 first symptoms occur in the majority of cases between the years 3 and 5 due to a complete or almost complete loss of CLN6's function. Mutations related to these severe forms often cause frameshifts and result in a truncated CLN6. However, there are also milder forms of NCL6, which become first apparent in adulthood and are associated with mutations, which do not compromise CLN6's structural integrity and cause only a partial loss of function. Clinical features of NCL6 include visual loss, motor impairment, developmental delay, dysarthria, ataxia, seizures. Furthermore, NCL6 is accompanied by premature death occurring in the most severe forms already between the age of 5 and 12 years (Nita et al. 2016, Berkovic et al. 2019). Since this devastating disease led to the discovery of the CLN6 gene and its corresponding protein, many insights have been revealed about both. The CLN6 gene was mapped to the chromosome 15q21-23 comprises 6 introns and 7 exons, which span a genomic region of approximately 22 kb. After splicing an approximately 2,4 kb transcript is translated ubiquitously (Wheeler et al. 2002). The CLN6 protein consists of 311 amino acids with a predicted mass of 36 kDa (Gao et al. 2002) and contains no glycosylation sites (Thelen et al. 2012). Furthermore, it is a membrane protein with 7 transmembrane domains and has been located to the ER membrane. Its N-terminus is present in the cytoplasm, whereas its C-terminus is found in the ER lumen (Heine et al. 2007). This location is especially interesting when considering CLN6's relevance for lysosomal homeostasis and health. As for many other proteins, self-dimerization was also shown for CLN6 (Heine et al. 2004). Additionally, no homologues of CLN6 are known and the protein is highly conserved in vertebrates (Mole et al. 2004).

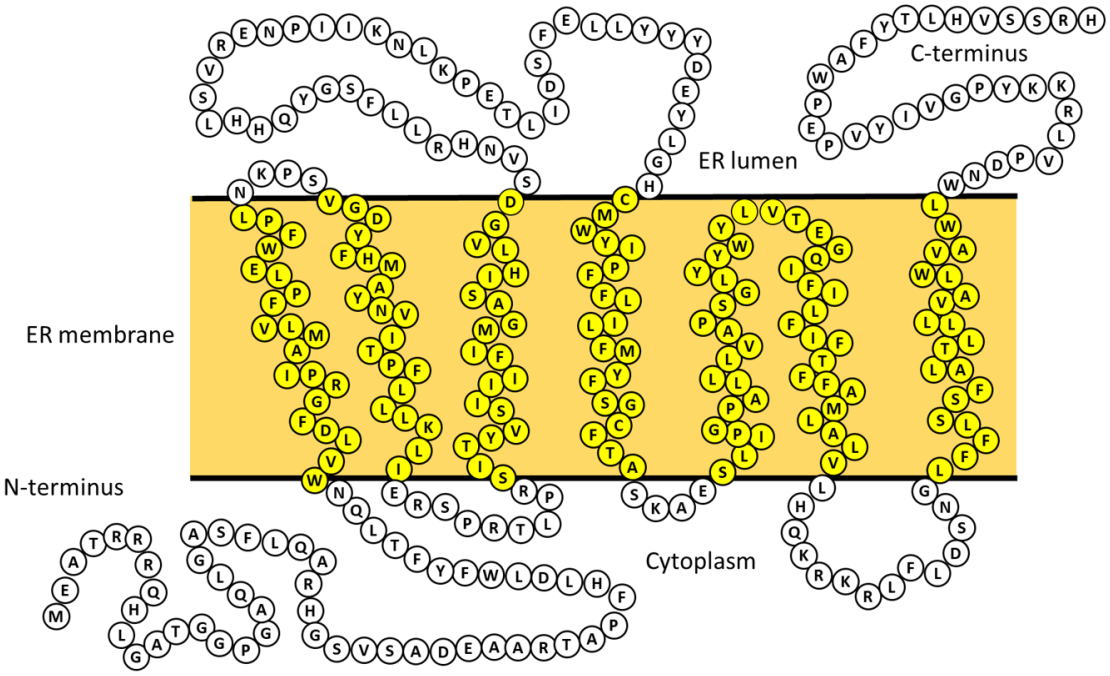

Figure 1.3: CLN6's primary structure and topology
In the illustration the amino acid sequence and the cytoplasmic, luminal and transmembrane domains (yellow) of CLN6 are shown.

At the beginning of this thesis in 2018 only two interaction partners of CLN6, namely CLN5 and collapsin-response-mediator protein 2, were identified (Benedict et al. 2009, Lyly et al. 2009). The functional relations of these interaction partners with CLN6 were not resolved as of yet. Moreover, no functions of CLN6 were described previously of 2018, which are related to lysosomal function and explain the pathology of NCL6. In 2020 CLN8 was identified as a novel interaction partner of CLN6 and a mechanism was proposed that outlines the function of CLN6. According to this mechanism CLN6 and CLN8 form the ER-to-Golgi relaying of enzymes of the lysosomal system (EGRESS) complex, which is required for proper and efficient transport of specific lysosomal hydrolases from the ER to the Golgi. Just recently CLN8 was shown to act as a receptor, which binds to various lysosomal hydrolases in the ER, transports them to the Golgi and recycles back for further rounds of transport (di Ronza et al. 2018). The similarity in the clinical picture of NCL forms caused by CLN8 and CLN6 deficiency also suggests a functional relation of these two proteins. This presumption was further supported by BiFC experiments, which identified an interaction of CLN6 and CLN8. Moreover, CLN6 was found to interact as well with lysosomal hydrolases associated with NCLs, namely PPT1, TPP1 and CTSD as they were co-immunoprecipitated with

CLN6. These interactions depend on the large second loop of CLN6 in the ER lumen, because they could not be detected in absence of the second loop. Immunoprecipitation experiments with CLN6 and CLN8 knock-out cells also indicated that CLN6 and CLN8 are mutually dependent to bind to lysosomal hydrolases. Interestingly, lysosomal hydrolases, which do not interact with CLN8 and apparently use different pathways to travel to the Golgi like for example ß-hexosaminidase, have also not been found to interact with CLN6, what additionally verifies clearly a functional link between these two proteins. For three proteins, CTSD, PPT1 and N-acetylgalactosamine-6-sulfatase which were determined to interact with CLN8 and CLN6, it was shown that CLN6 deficiency leads to an impaired and inefficient ER-Golgi transport. In conclusion, CLN6 was proposed to be an adapter protein, which is essential for the binding of specific lysosomal proteins to CLN8 and therefore their ER-Golgi transport (Bajaj et al. 2020). These findings were considered carefully with regard to the planning of experiments and the assessment of results in this PhD project.

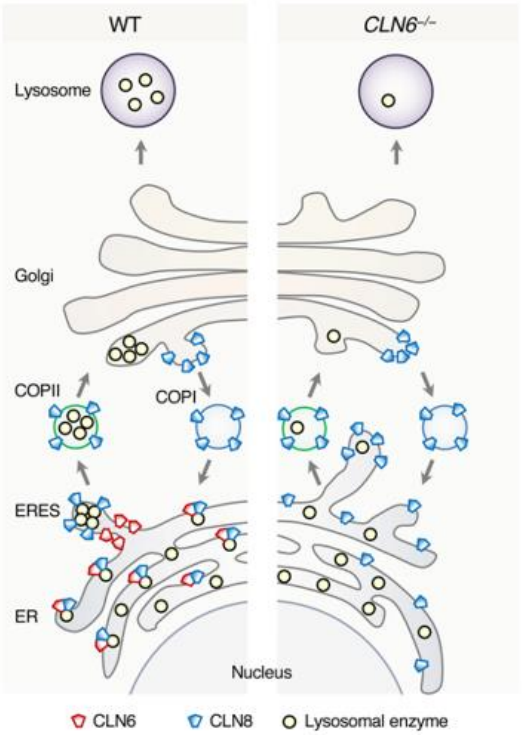

Figure 1.4: Schematic model of soluble lysosomal hydrolases ER-to-Golgi trafficking
Shown in comparison is the transport of EGRESS dependent lysosomal hydrolases in wt and CLN6 deficient cells (Bajaj et al. 2020).

1.3 Endoplasmic reticulum

Since CLN6 is an ER protein and the ER also constitutes the site of biosynthesis for lysosomal proteins a few relevant key aspects of ER biology are discussed in the following chapters. The ER is a cellular, membrane-enclosed organelle consisting of tubules and cisternal sheets and verging directly on the nucleus (Westrate et al. 2015). In general, the ER can be divided into two units, the rough and the smooth ER (Shibata et al. 2006). The rough ER is characterized by ribosomes being present across the ER membrane and its function is primarily the synthesis, folding and modification of proteins (English et al. 2009). The smooth ER is devoid of ribosomes and fulfills different cellular functions, namely membrane lipid biogenesis, detoxification, carbohydrate metabolism, Ca^{2+} storage, hormone synthesis and vesicle trafficking in the translational ER, a specific ribosome-free subdomain. (Miller 1988, Mancias et al. 2005, Csala et al. 2006, Gorlach et al. 2006, Iyanagi 2007, Fagone et al. 2009). In the following, the focus lies on the processes in the rough ER and the vesicle export in the transitional ER as they are especially relevant regarding lysosomal proteins.

1.3.1 Protein translation and translocation in the endoplasmic reticulum

Besides the cytosol, the ER presents another major site of protein biosynthesis for secretory and integral membrane proteins as well as for luminal and membrane ER resident proteins. Polypeptides with a signal sequence at the N-terminus are recruited by signal-recognition particle to the Sec61 translocon at the ER membrane following their translation and import into the ER lumen. Afterwards the signal sequence of almost all soluble proteins is cleaved by the signal peptidase complex co- or post-translationally and upon the termination of the translation soluble proteins are released into the ER lumen. (Nicchitta 2002, Ellgaard et al. 2016).

1.3.2 Glycoprotein processing in the early secretory pathway – the calnexin cycle

This chapter deals with the processing and maturation of glycoproteins, as glycosylation is an essential modification for most lysosomal proteins. N-glycosylation, which occurs exclusively in the ER, determines the structure, stability and function of proteins (Lis et al. 1993). Especially for lysosomal proteins glycosylation additionally serves as

protection against degradation and also plays a role in proper targeting of soluble lysosomal proteins (Shepherd et al. 1983). Before the $GlcNAc_2Man_9Glc_3$ N-glycan structure is attached to the protein, it is built up stepwise in the ER by many different enzymes primarily encoded by the ALG genes. Another enzyme, the oligosaccharyltransferase (OST) transfers the previously assembled N-glycans to asparagine residues of the glycosylation sequence motif (NxT/S) (Abeijon et al. 1992, Breitling et al. 2013). In mammalians N-glycosylation is performed by two complementary OST isoforms, which act either co- or post-translational (Ruiz-Canada et al. 2009). Next to glycosylation, disulfide-bond formation is another very important modification in the ER, in which two cystine residues are covalently linked by oxidation. Disulfide-bonds can be formed already during translation. However, after translation most of them undergo isomerization until the correct cysteine residues are connected. Oxidation and reduction are both catalyzed by thiol-disulfide oxidoreductases of the protein disulfide isomerase (PDI) family (Ellgaard et al. 2016). Disulfide bonds contribute to the stability and play an essential role in proper folding (Feige et al. 2011, Fass 2012). The folding process is also assisted by various chaperones. Membrane-anchored CANX and its soluble homologue CALR are the most important chaperones for glycoproteins, as they bind to mono-glucosylated glycan intermediates after N-glycans were trimmed by glucosidase I and II (Williams 2006).

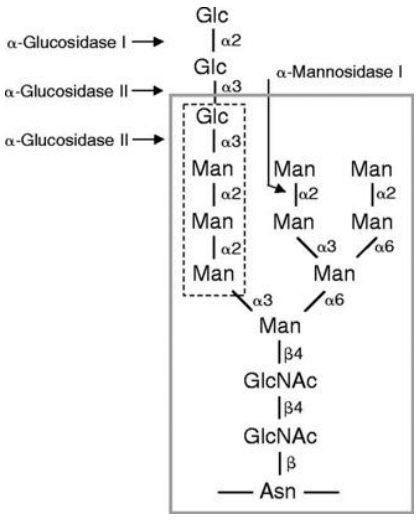

Figure 1.5: N-Glycan structure and enzymes cleavage sites
The figure shows the N-glycan assembly of two GlcNAc monosaccharides, nine branching mannose units and three glucose residues attached to an asparagine. Glucosidases I and II are removing the three external glucose residues and ER α-mannosidase I trims the outer middle mannose residue at the depicted cleavage sites (Williams 2006).

Moreover, the lectin chaperones bind other function-specific chaperones like cyclophilin B and facilitate apart from general protein folding additional assembly steps like proper disulfide-bond formation by recruiting the protein disulfide isomerase ERp57 (Kozlov et al. 2020). Upon protein release from CANX and CALR the last glucose residue is cleaved by glucosidase II and the protein is subjected to the ER quality control system, which for glycoproteins is primarily embodied by the UDP-glucose:glycoprotein glucosyltransferase (UGGT). This enzyme reglucosylates incompletely or incorrectly folded proteins, enables rebinding to CANX and CALR and therefore, prevents their export from the ER and further transport (Adams et al. 2020).

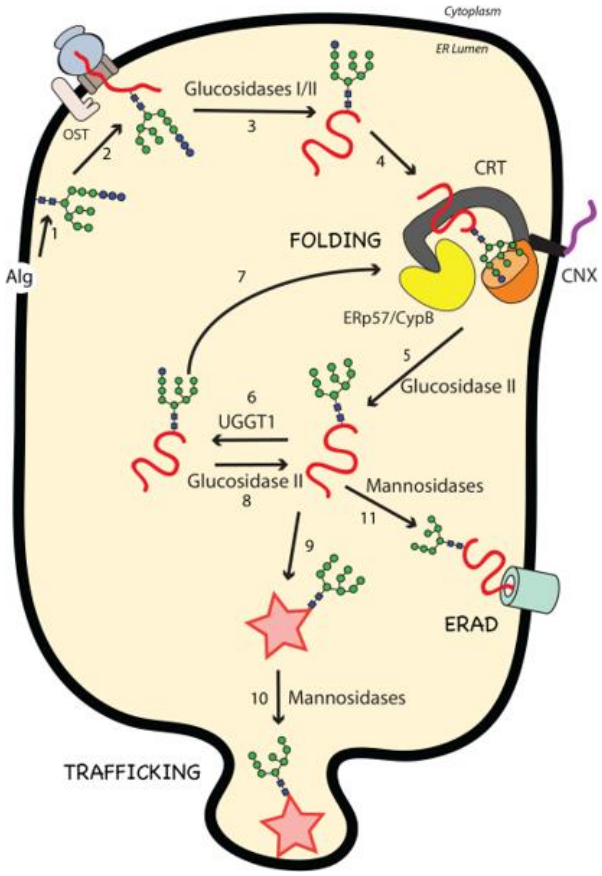

Figure 1.6: The calnexin cycle
De novo synthesized N-glycans (1) are transferred to translocated nascent polypeptide chains (2). After trimming of the first two glucoses (3) monoglucosylated immature proteins bind to CANX and CALR, which facilitate protein folding and modification (4). Upon release proteins are deglucosylated (5) and become substrates of UGGT, which reglucosylates incompletely or misfolded proteins (6). These proteins reenter the calnexin cycle (7+8). Mature proteins leave the calnexin cycle (9), which might be further trimmed before ER export (10), while misfolded proteins are directed to ERAD by mannose trimming (11) (Lamriben et al. 2016).

Misfolded glycoproteins, which undergo this process repeatedly without refolding into their native forms, are targeted to a degradation pathway. In general, these proteins become substrates of the ER α-mannosidase I, which removes a mannose residue and gives rise to GlcNAc2Man8 glycan intermediates. As a consequence, these glycans are recognized not as efficiently by UGGT anymore and serve in combination with misfolding as signal directing proteins to the ER-associated degradation (ERAD) pathway, in which the misfolded proteins are eventually degraded by the proteasome (Ellgaard et al. 2003). Glycans of native proteins might also be trimmed by ER α-mannosidase I, however this alone leads not to degradation. Correctly folded proteins are exported and transported to the Golgi-apparatus (Aebi et al. 2010).

1.3.3 Transport and export of proteins in the endoplasmic reticulum

After protein processing is completed and the protein passed the ER quality control system, it is loaded into budding COPII vesicles at ER exit sites (ERESs) to be transported to the Golgi. This process is assisted by many proteins, which are required for the formation, packaging and the scission of COPII vesicles (D'Arcangelo et al. 2013). ER transport and export of soluble and membrane proteins along the secretory pathway is realized by two basically distinct mechanisms. One relies on receptor-mediated cargo capture, whereas the other depends on bulk flow (Barlowe et al. 2016). The term cargo capture describes the association of cargo proteins with the ER membrane by adaptor or receptor proteins, which transport their cargo to ERESs. There, cargo proteins are incorporated into the COPII vesicles by the interaction of vesicle coat components with their receptors, which are either integrated into the vesicle coat or excluded from the vesicle structure prior to vesicle scission (Budnik et al. 2009). An example for such a receptor is Ergic53, one of the first discovered glycoproteins receptors in the ER, which binds to high-mannose-type glycans as well as monoglucosylated N-glycans and, as demonstrated, interacts also with the lysosomal hydrolases cathepsins C and Z (CTSC, CTSZ) (Nyfeler et al. 2005). Another example is CLN8, which binds numerous lysosomal hydrolases and transports them to the Golgi. After cargo release in the Golgi, both receptors are recycled back to the ER in COPI vesicles for further rounds of transport (Kappeler et al. 1997, di Ronza et al. 2018). Moreover, some membrane proteins can directly bind to specific vesicle coat

components for instance the Sec24 isoforms and do not require additional adaptors for the integration into COPII vesicles and cargo capture transport (Miller et al. 2003). Bulk flow driven protein transport and export however is understood as random and undirected inclusion of proteins into COPII vesicles as part of the vesicle membrane or fluid (Barlowe et al. 2016). As also proteins not destined for ER exit are falsely incorporated into vesicles by default, ER resident proteins contain sorting signals like for soluble proteins the motif KDEL or for membrane proteins KKXX in their C-terminus, which allow retrieval of these proteins from the Golgi to the ER (Gaynor et al. 1994, Newstead et al. 2020). Receptors, which travel to the Golgi, are retrieved by the same mechanism. In comparison to the bulk flow, the transport by receptor-mediated cargo capture is a concerted, directed, efficient, closely controlled and regulated process, in which incompletely or misfolded proteins are excluded (Dancourt et al. 2010). Even though bulk flow is undirected, in some cases bulk flow rates were shown to be relatively high, which indicates that bulk flow can also contribute in a physiologically relevant way to the transport of the secretory pathway (Thor et al. 2009). After all, both transport types complement each other and contribute to the trafficking of all proteins destined to be secreted or transported to another compartment like the lysosome.

2 Objective

The main objective of this study was to increase the understanding of CLN6 and determine its functional relation to the lysosome. The lysosomal storage disorder NCL6 clearly outlines the importance and impact of CLN6 for lysosomal homeostasis and health. However, the link between CLN6 dysfunction and the accumulation of storage material in the lysosome has not been resolved. To address this issue this study dealt with two research questions with different emphases concerning CLN6 biology.

In the first part of the project investigations aimed to determine proteomic changes of the lysosome due to CLN6 deficiency, which could explain the NCL development and indicate involved proteins. Therefore, lysosomal fractions generated by tritosomes and 20.000 g pellets from wt and *nclf* mouse liver samples were compared by mass spectrometry and western blot analyses. As NCL shows mainly neurological symptoms 20.000 g brain pellets were also investigated. Furthermore, whole liver and brain homogenates from wt and *nclf* samples were analyzed with the objective to get possible information on the causes for the proteomic differences.

The second part of this project aimed to identify novel interaction partners of CLN6. At the beginning of this study only two interaction partners were known, which could not be put into context with the NCL6 disease. Therefore, the BioID approach was utilized for the discovery of proteins in close proximity of CLN6. Subsequently, selected candidates were analyzed by the BiFC assay to examine their interactions with CLN6. These investigations aimed to determine interaction partners of CLN6, which give new insights into the function of CLN6 and explain its relevance for lysosomal health. Finally, another aim of this project was to generate insights about CLN6, which promote the development of therapies for NCL6, which go beyond the current symptomatic and supportive approaches.

3 Materials and Methods

3.1 Materials

3.1.1 Consumables

Table 3.1: List of used consumables

Product	Manufacturer/Provider
Axygen® Maxymum Recovery® Pipet Tips (10 µL, 200 µL and 1000 µL)	Corning (Corning, NY, USA)
Pipet tips (10 µL, 200 µL and 1000 µL)	Greiner (Kremsmünster, Austria)
Axygen® 1.5 mL Maxymum Recovery® Snaplock Microcentrifuge Tubes	Corning (Corning, NY, USA)
C18 empore extraction-membrane	Merck (Darmstadt, Germany)
Centrifuge tubes (polypropylene)	Beckman Coulter (Brea, CA, USA)
Centrifuge tubes (Ultra-clear™)	Beckman Coulter (Brea, CA, USA)
Flacon® centrifuge tubes (15 and 50 mL)	Corning (Corning, NY, USA)
Disposable scalpels	Feather Safety Razor (Osaka, Japan)
Gel blotting paper 3 mm thickness	Whatman (Maidstone, UK)
Folded filter papers	Whatman (Maidstone, UK)
Glass beakers	Carl Roth (Karlsruhe, Germany)
Measuring cylinders	Carl Roth (Karlsruhe, Germany)
96-well plate (transparent)	BD Falcon (Heidelberg, Germany)
96-well plate (black)	Greiner (Kremsmünster, Austria)
Nitrocellulose (NC) membrane	GE Healthcare (Little Chalfont, UK)
Oasis HLB cartridges	Waters (Eschborn, Germany)
Petri dishes (Ø 6 and 10 cm)	Sarstedt (Nümbrecht, Germany)
Polyvinylidene fluoride membrane (PVDF)	GE Healthcare (Little Chalfont, UK)
Reaction tubes 1.5 ml, 2 ml	Sarstedt (Nümbrecht, Germany)
6-well plate	Corning (Corning, NY, USA)

3.1.2 Equipment

Table 3.2: List of used equipment

Description	Model	Manufacturer
Analytical balance	A 200S	Sartorius (Göttingen, Germany)
Basic power supply	Power Pac 200	Bio-Rad Laboratories (Hercules, CA, USA)
Gel documentation system	BioDoc Analyze live	Biometra (Göttingen, Germany)
Cell counter	Eve™	NanoEntek (Seoul, Korea)
Centrifuges:		
Benchtop centrifuge	5702, 5425	Eppendorf (Hamburg, Germany)
	Allegra X-15R	Beckman Coulter (Brea, USA)
Microcentrifuge	Galaxy MiniStar	VWR (Darmstadt, Germany)
Refrigerated centrifuge	5810 R, 5417 R	Eppendorf (Hamburg, Germany)
Ultracentrifuge	Optima L-80 XP	Beckman Coulter (Brea, USA)
Vacuum centrifuge	ScanSpeed 40	ScanVac (Lynge, Denmark)
Cryo storage tank	Forma Scientific 8030	Thermo Fisher Scientific (Waltham, US)
Dounce homogenizer	1 ml	Wheaton (Millville, USA)
	5 ml	Sigma-Aldrich (St. Louis, USA)
Electrophoresis system	Mini-PROTEAN® Tetra Cell	Bio-Rad (Hercules, USA)
Electrotransfer system	Trans-Blot® Cell	Bio-Rad (Hercules, USA)
Flow cytometry system	CyFlow Space	Sysmex Partec (Görlitz, Germany)
Fume hood	EN 14175	ARGE (Wathlingen, Germany)
HPLC column	ReproSil-Pur 120 C18-AQ	Dr. Maisch (Ammerbuch-Entringen, Germany)
Ice machine	Scotsman AF124	Scotsman Ice Systems (Vernon Hills, IL, USA)
Imaging system	Fusion Solo	Vilbert Lourmat (Collégien, France)
Incubator	Forma™ Series II 3110	Thermo Fisher Scientific (Waltham, US)
Laboratory rocker	Rotamax 120	Heidolph (Schwabach, Germany)
Magnetic stirrer	RH basic	IKA Werke (Staufen, Germany)
	RCT classic	IKA Werke (Staufen, Germany)

Mass spectrometers:	Orbitrap Fusion Lumos	Thermo Fisher Scientific (Waltham, USA)
	Orbitratp Velos	Thermo Fisher Scientific (Waltham, USA)
Micro scale	CP 124-OCE	Sartorius (Göttingen, Germany)
Micropipettes	Research Plus	Eppendorf (Hamburg, Germany)
Microplate reader	GENios	Tecan (Männedorf, Switzerland)
Microplate reader	Infinite 200 Pro	Tecan (Männedorf, Switzerland)
Nano HPLC system	Ultimate 3000 RSLC	Dionex (Idstein, Germany)
	easy-nLC1000	Thermo Fisher Scientific (Waltham, USA)
Offgel fractionator	3100	Agilent Technologies (Waldbronn, Germany)
pH electrode	WTW SenTix 50	Xylem (Weilheim, Germany)
pH-meter	Calimatic 761	Knick (Berlin, Germany)
Photometer		
Pipetboy		Eppendorf (Hamburg, Germany)
Roller mixer	RS-TR05	Carl Roth (Karlsruhe, Germany)
Rotor	Ti-50	Beckman Coulter (Brea, USA)
	SW41	Beckman Coulter (Brea, USA)
Scale	PC4400 DeltaRange	Mettler Toledo (Columbus, USA)
Semi-dry blotter	PerfectBlue M	VWR International (Darmstadt, Germany)
Shaker	ThermoMixer C	Eppendorf (Hamburg, Germany)
Spectrophotometer	NanoDrop 2000	PeQlab (Ehrlangen, Germany)
Tissue homogenizer	HOMGEN	Schütt Labortechnik (Göttingen, Germany)
Tweezer	7 Dumont INOX	Dumont (Montignez, Switzerland)
Ultra Thurrax	T 10 basic	IKA Werke (Staufen, Germany)
Ultrasonic bath	2510	Branson (Danbury, USA)
Vortex mixer	UNIMAG ZX3	UniEquip (Leipzig, Germany)
	Vortex Genie	Scientific Industries (Bohemia, USA)
Water bath	ED	Julabo (Seelbach, Germany)

3.1.3 Chemicals and reagents

Table 3.3: List of used chemicals and reagents

Chemical/reagent	Manufacturer/Provider
2-Mercaptoethanol	Sigma-Aldrich (St. Louis, USA)
4-Methylumbelliferyl 6-thio-palmitate-β-D-glucopyranoside	Santa Cruz Biotechnology, Inc. (Dallas, USA)
4-Methylumbelliferyl β-D-glucopyranoside	Sigma-Aldrich (St. Louis, USA)
Acetic acid	Biosolve (Valkenswaard, Netherlands)
Acetonitrile (ACN)	Biosolve (Valkenswaard, Netherlands)
Acrylamide	Merck KGaA (Darmstadt, Germany)
Adenosine 5′-triphosphate (ATP) magnesium salt	Sigma-Aldrich (St. Louis, USA)
Almond ß-glucosidase	Sigma-Aldrich (St. Louis, USA)
Ammonium persulfate (APS)	Carl Roth (Karlsruhe, Germany)
Bacto™ yeast extract	Thermo Fisher Scientific (Waltham, USA)
Boric acid	Thermo Fisher Scientific (Waltham, USA)
Bovine serum albumin (BSA)	Carl Roth (Karlsruhe, Germany)
Bromophenol blue	Merck KGaA (Darmstadt, Germany)
Calcium chloride	Merck KGaA (Darmstadt, Germany)
Citric acid monohydrate	Carl Roth (Karlsruhe, Germany)
Deoxynucleoside triphosphates (dNTPs)	Thermo Fisher Scientific (Waltham, USA)
Dibasic sodium phosphate dihydrate	Merck KGaA (Darmstadt, Germany)
Dimethyl sulfoxide (DMSO)	Sigma-Aldrich (St. Louis, USA)
Dithiothreitol (DTT)	Sigma-Aldrich (St. Louis, USA)
Ethanol	AppliChem (Darmstadt, Germany)
Ethyl acetate	AppliChem (Darmstadt, Germany)
Ethylenediaminetetraacetic acid (EDTA)	Sigma-Aldrich (St. Louis, USA)
Formic acid (FA)	Biosolve (Valkenswaard, Netherlands)
Glycerol	Carl Roth (Karlsruhe, Germany)
Glycine	Merck KGaA (Darmstadt, Germany)
Halt™ phosphatase inhibitor cocktail	Thermo Fisher Scientific (Waltham, USA)
HEPES	Carl Roth (Karlsruhe, Germany)
Hydrochloric acid	Carl Roth (Karlsruhe, Germany)
Hydroxylamine	Sigma-Aldrich (St. Louis, USA)
Isopropanol	Merck KGaA (Darmstadt, Germany)

Lennox agar	Thermo Fisher Scientific (Waltham, USA)
Lithiumchloride	Merck KGaA (Darmstadt, Germany)
Magnesium acetate	Merck KGaA (Darmstadt, Germany)
Magnesium chloride	Merck KGaA (Darmstadt, Germany)
Manganese(II) chloride tetrahydrate	Merck KGaA (Darmstadt, Germany)
Mercaptoethanol	Sigma-Aldrich (St. Louis, USA)
Methanol (MeOH)	Merck KGaA (Darmstadt, Germany)
Milk powder	Carl Roth (Karlsruhe, Germany)
MOPS	Merck KGaA (Darmstadt, Germany)
N,N,N`,N`-Tetramethylethylenediamine (TEMED)	Carl Roth (Karlsruhe, Germany)
NP-40	VWR (Darmstadt, Germany)
Nuclease-free distilled water	Thermo Fisher Scientific (Waltham, USA)
Pageruler™ prestained protein ladder	Thermo Fisher Scientific (Waltham, USA)
Phosphoric acid	Sigma-Aldrich (St. Louis, USA)
Phusion™ High-Fidelity DNA-Polymerase (2 U/µl)	Thermo Fisher Scientific (Waltham, USA)
PonceauS	AppliChem (Darmstadt, Germany)
Potassium acetate	Merck KGaA (Darmstadt, Germany)
Potassium chloride	Merck KGaA (Darmstadt, Germany)
Protease inhibitor cocktail cOmplete™	F. Hoffmann-La Roche (Basel, Switzerland)
Ribonuclease A from bovine pancreas	Sigma-Aldrich (St. Louis, USA)
Rubidium chloride	Merck KGaA (Darmstadt, Germany)
Sequencing grade modified trypsin, porcine	Promega (Madison, USA)
Sodium bicarbonate	Merck KGaA (Darmstadt, Germany)
Sodium carbonate	Carl Roth (Karlsruhe, Germany)
Sodium chloride	Carl Roth (Karlsruhe, Germany)
Sodium deoxycholate (SDC)	Thermo Fisher Scientific (Waltham, USA)
Sodium dodecyl sulfate (SDS)	Bio-Rad (Hercules, USA)
Sodium hydroxide	Merck KGaA (Darmstadt, Germany)
Sodium taurocholate hydrate	Sigma-Aldrich (St. Louis, USA)
Sucrose	Carl Roth (Karlsruhe, Germany)
T4 DNA Ligase (5 U/µl)	Thermo Fisher Scientific (Waltham, USA)
T4 DNA Ligase, HC (30 U/µl)	Thermo Fisher Scientific (Waltham, USA)
T4-Polynukleotid-Kinase (10 U/µl)	Thermo Fisher Scientific (Waltham, USA)
TMT10plex™ Isobaric Label Reagent Set	Thermo Fisher Scientific (Waltham, USA)
TMTsixplex™ Isobaric Label Reagent Set	Thermo Fisher Scientific (Waltham, USA)

Triethylammonium bicarbonate (TEAB)	Thermo Fisher Scientific (Waltham, USA)
Trifluoroacetic acid (TFA)	Biosolve (Valkenswaard, Netherlands)
Tris(hydroxymethyl)aminomethane	Carl Roth (Karlsruhe, Germany)
Triton WR1339 (tyloxapol bioXtra)	Sigma-Aldrich (St. Louis, USA)
Triton X-100	Sigma-Aldrich (St. Louis, USA)
TRIzol® reagent	Thermo Fisher Scientific (Waltham, USA)
Tryptone-Peptone, Difco™	Thermo Fisher Scientific (Waltham, USA)
TurboFect™ transfection reagent	Thermo Fisher Scientific (Waltham, USA)
Tween-20	Sigma-Aldrich (St. Louis, USA)
Water	Biosolve (Valkenswaard, Netherlands)

Fast digest restriction enzymes and buffers were purchased from Thermo Fisher Scientific (Waltham, USA)

3.1.4 Buffers and solutions

All buffers, media and solutions were prepared in ddH2O. MS-related buffers and solutions were either HPLC or MS grade.

Table 3.4: List of used buffers and solutions

Buffers	**Composition**
10x SDS-running buffer	250 mM Tris 1,92 M Glycin 1 % (w/v) SDS
10x Tris-buffered saline (TBS), pH 7.4	1.21 % (w/v) Tris-HCl 8.76 % (w/v) NaCl
4x Laemmli buffer, pH 6.8	250 mM Tris-HCl 8 % (w/v) SDS 40 % (v/v) Glycerol 10 % (v/v) Mercaptoethanol 0.004 % (w/v) Bromophenol blue
4x Running gel buffer, pH 8.8	1.5 M Tris-HCl
4x Stacking gel buffer, pH 6.8	0.5 M Tris-HCl
BioID Lysis buffer, pH 7,4	50 mM TRIS-HCl 500 mM NaCl 2 % (v/v) Triton X-100 0,4 % (w/v) SDS 5 mM EDTA

Blocking buffer	1x TBS 0.1 % (v/v) Tween-20 5 % (w/v) Milk powder or BSA
Blotting buffer	48 mM Tris 39 mM Glycine 0.037 % (w/v) SDS 20 % (v/v) Methanol
Buffer A	250 mM Sucrose 15 mM potassium chloride 1 M Magnesium acetate 1 M Hepes 1 mM Calcium chloride 1 mM Magnesium chloride 1 mM EDTA 10 mM DTT 1x Protease inhibitor cocktail
Digestion buffer (DB)	20 mM TEAB 0.5 % (w/v) SDC
LB agar plates	32 g Lennox agar 5 g NaCl 1 L H_2O for Amp plates: + 2 mL Ampicillin for Kan plates: +800 µL Kanamycin
LB-Medium	10 g Tryptone-Peptone 5 g Bacto yeast extract 10 g NaCl H_2O was added to a final volume of 1L and the pH was adjusted to 7,2
P1 buffer, pH 8	50 mM Tris-HCl 10 mM EDTA
P2 buffer	200 mM NaOH 1 % SDS
P3 buffer, pH 5,5	3 M KAc
Running gel solution 12.5 %	12.5 % (v/v) Acrylamide 25 % (v/v) Running gel buffer 0.1 % (w/v) SDS 0.1 % (w/v) APS 0.1 % (v/v) TEMED
SAX buffer	20 mM acetic acid 20 mM phosphoric acid 20 mM boric acid
Solvent A	0.1 % (v/v) FA

Solvent B	90 % (v/v) ACN 0.1 % (v/v) FA 5 % (v/v) DMSO (optional)
Stacking gel solution 5 %	5 % (v/v) Acrylamide 25 % (v/v) Stacking gel buffer 0.1 % (w/v) SDS 0.1 % (w/v) APS 0.2 % (v/v) TEMED
Substrate solution (CLN1 activity assay), pH 4	77 mM disodium phosphate 61 mM citric acid 15 mM DTT 0.375 % (w/v) Triton X-100 0,64 mM 4-Methylumbelliferyl 6-thio-palmitate-β-D-glucopyranoside
Substrate solution (GBA activity assay), pH 5,2	100mM citric acid monohydrate 200 mM dibasic sodium phosphate dehydrate 0.25 % (w/v) sodium taurocholate hydrate 0,1 % (w/v) Triton X-100 5 mM Methylumbelliferyl-ß-D-glucopranosidase
Sucrose gradient solutions	ρ 1.21 Sucrose solution ρ 1.15 Sucrose solution ρ 1.14 Sucrose solution ρ 1.06 Sucrose solution
TAE buffer, pH 8,3	30 mM Tris-HCl 20 mM acetic acid (100 %) 2 mM EDTA
Tfb I buffer	30 mM Potassium acetate 50 mM Manganese(II) chloride 100 mM Rubidium chloride 10 mM Calcium chloride 15 % Glycerol (v/v)
Tfb II buffer	10 mM MOPS 75 mM Calcium chloride 10 mM Rubidium chloride 15 % Glycerol (v/v)
Tissue homogenization buffer, pH 7.4	10 mM Tris 250 mM Sucrose 1 mM EDTA 1x Protease inhibitor cocktail 1x Phosphatase inhibitor cocktail
Tris-buffered saline with Tween 20 (TBS-T)	1x TBS; 0.1 % (v/v) Tween-20

3.1.5 Kits and assays

Table 3.5: List of used kits and assays

Name	Manufacturer
Bio-Rad DC™ Protein Assay	Bio-Rad Laboratories (Hercules, CA, USA)
Clarity™ Western Blotting ECL Substrate Kit	Bio-Rad Laboratories (Hercules, CA, USA)
NucleoBond Xtra Midi Plus kit for transfection-grade plasmid DNA	MACHEREY-NAGEL GmbH & Co. KG (Düren, Germany)
Pure Link® Quick Gel Extraction Kit	Thermo Fisher Scientific (Waltham, USA)
Cathepsin D Activity Kit	PromoCell (Heidelberg, Germany)

3.1.6 Media and supplements for bacteria and cell culture

Table 3.6: List of purchased media and supplements for bacteria and cell culture

Name	Manufacturer
Ampicillin (Amp)	Carl Roth (Karlsruhe, Germany)
Dialyzed Fetal Bovine Serum	Thermo Fisher Scientific (Waltham, USA)
DMEM for SILAC	Thermo Fisher Scientific (Waltham, USA)
Dulbecco's Modified Eagle Medium (DMEM)	Thermo Fisher Scientific (Waltham, USA)
Fetal Bovine Serum	Thermo Fisher Scientific (Waltham, USA)
Kanamycin (Kan)	Merck (Darmstadt, Germany)
L-Arginine-HCl, 13C6 for SILAC	Thermo Fisher Scientific (Waltham, USA)
L-Arginine-HCl, 13C6, 15N4 for SILAC	Thermo Fisher Scientific (Waltham, USA)
L-Glutamine	Thermo Fisher Scientific (Waltham, USA)
L-Lysine-2HCl, 13C6, 15N2 for SILAC	Thermo Fisher Scientific (Waltham, USA)
L-Lysine-2HCl, 4,4,5,5-D4 for SILAC	Thermo Fisher Scientific (Waltham, USA)
Penicillin-Streptomycin	Thermo Fisher Scientific (Waltham, USA)
Phosphate Buffered Saline (PBS) (10X)	Thermo Fisher Scientific (Waltham, USA)
Trypsin-EDTA	Thermo Fisher Scientific (Waltham, USA)

3.1.7 Bacterial strain and cell lines

Escherichia coli:

Dh5α

Human embryonic kidney 293 (HEK) cells

Baby hamster kidney (BHK) cells

3.1.8 Mouse strains

Mice were housed according to the respective institutional guidelines in the animal facility at the University Hospital Bonn, and experimental procedures were performed according to the institutional guidelines and approved by the Landesamt fuer Natur, Umwelt- und Verbraucherschutz Nordrhein-Westfalen. The *nclf* mice that were used in this study come from a homozygous breeding, were originally provided to us by the group of Prof. Dr. Thomas Braulke (UKE Hamburg) and have C57/Bl6J substrain background. Our wildtype control mice were C57/Bl6J substrain as well.

3.1.9 Antibodies

3.1.9.1 Primary antibodies

Table 3.7: List of used primary antibodies

Name/product number	Host	Manufacturer
Cathepsin D antibody (C-20), sc-6486	Goat	Santa Cruz Biotechnology, Inc. (Dallas, USA)
Polyclonal Anti-PPT1 Antibody, HPA021546	Rabbit	Atlas Antibodies (Bromma, Sweden)
CLN2 antibody (G-3), sc-393961	Mouse	Santa Cruz Biotechnology, Inc. (Dallas, USA)
Anti-Protein Disulfide Isomerase antibody, P7496	Rabbit	Sigma-Aldrich (St. Louis, USA)
CPT2 Polyclonal antibody, 26555-1-AP	Rabbit	Proteintech Group Inc. (Rosemont, USA)
LAMP1 antibody, 1D4B	Rat	Developmental Studies Hybridoma Bank (DSHB) (Iowa, USA)
Anit-peptide hCLN6-2-20 antibody	Rabbit	Pineda - Antikörper Service (Berlin, Germany)
Human/Mouse/Rat Cathepsin X/Z/P Antibody, AF934	Goat	R&D Systems (Minneapolis, USA)
c-Myc Antikörper (9E10), sc-40	Mouse	Santa Cruz Biotechnology, Inc. (Dallas, USA)
6x-His Tag Monoclonal Antibody (HIS.H8)	Mouse	Thermo Fisher Scientific (Waltham, USA)

3.1.9.2 Secondary antibodies

Table 3.8: List of used secondary antibodies

Antigen/Tag	Host	Manufacturer/product number
Mouse IgG (H+L)/HRP	Goat	Dianova (Hamburg, Germany), 115-035-044
Rabbit IgG (H+L)/HRP	Goat	Dianova (Hamburg, Germany), 111-035-003
Rat IgG (H+L)/HRP	Goat	Dianova (Hamburg, Germany), 112-035-167
Goat IgG (H+L)/HRP	Bovine	Dianova (Hamburg, Germany), 805-035-180

3.1.10 Primer

3.1.10.1 Used cloning primer for the C-terminal BioID construct

Table 3.9: List of purchased primers for the C-terminal BioID construct

Name	Sequence 5'-3'
BioID+Gly_EcoRI_for	ACGAATTCGGTGGTGGTGGTGGTGGTGACAAGGACAACACCG
BioID+His_XbaI_rev	ACTTCTAGATCAATGATGATGATGATGATGCTTCTCTGCGCTTCTCAGGGAGAT
CLN6_BamHI_for	ACTGGATCCATGGAGGCGACGCGGAG
CLN6_EcoRI_rev	ACGAATTCGTGCCGACTGCTGACGTG

3.1.10.2 Used cloning primer for BiFC constructs

Table 3.10: List of purchased primers for the YFP construct

AAName	Sequence 5'-3'
Calr_XbaI_rev	CCCTCTAGACTACAGCTCGTCCTTGGCCTG
Calr_XhoI_for	GGGCTCGAGTTGAGCCTGCCGTCTACTTCAAGGAGCA
Canx_XbaI_rev	CCCTCTAGATCACTCTCTTCGTGGCTTTCTG
Canx_XhoI_for	CCCTCGAGTTCATGATGGACATGATGATGATGT

CLN6_ClaI_rev	GGGGATCGATGTGCCGACTGCTGACGTGAAG
CLN6_HindIII_for	GGGAAGCTTATGGAGGCGACGCGGAGGCGGCAG
CLN6Δ2Loop_muta_for	CTGGGTCACTGCATGTGGTACATCCC
CLN6Δ2Loop_muta_rev	GTTGACAGAGTCACCCACCAGGTGG
CLN6ΔC-term_muta_for	CTGGCTGTGGAATGACGGCGGCAGCGGCGGCAGCGGCG GATCCGGCGGCAGCGGCGGCAGCGGCGGCAGCATCGAT GGTGGCGGTG
CLN6ΔC-term_muta_rev	GCGACCCAGAGCGCCACAAGCAAGAGG
CLN8_XbaI_rev	CCCTCTAGACTATGGCCTCTTCTTCCGCAGCAGC
CLN8_XhoI_for	GGGCTCGAGTTATGAATCCTGCGAGCGATGGG
Ctsd_XbaI_rev	GTATCTAGACTAGAGGCGGGCAGCCTCGG
Ctsd_XhoI_for	GTACTCGAGTTCTCGTCAGGATCCCGCTGCACA
Ctsz_XbaI_rev	CGCTCTAGATTAAACGATGGGGTCCCCAAATGT
Ctsz_XhoI_for	GTTCTCGAGTTGGCCTCTACTTCCGCCGGGGACAGA
Ganab_ClaI_rev	GGGGATCGATTCGCAGGTGAATACTCCAATCAGAT
Ganab_HindIII_for	GATAAGCTTATGGCGGCGGTAGCGG CAGTGGC
Ganab_XbaI_rev	CCTCTAGATCATCGCAGGTGAATACTCCAATCAGAT
Ganab_XhoI_for	GGCTCGAGTTATTACCCTTGCTGTGGATAGAAGCAACTT
Ppt1_ClaI_rev	GGGGATCGATTCCAAGGAATGGTATGATGTGGGC
Ppt1_HindIII_for	GTATAAGCTTATGGCGTCGCCCGGCTGCCTGTGGC
Ppt1_XbaI_rev	GGGGTCTAGATCATCCAAGGAATGGTATGATGTGGGC
Ppt1_XhoI_for	ATATCTCGAGTTGACCCGCCGGCGCCGCTGCCGTTGG
YFP1_XbaI_rev	GCTCTAGATCACTGCTTGTCGGCCATGATATAGACGTT
YFP1_XhoI_for	TATCTCGAGTTGTGAGCAAGGGCGAGGAGCTGTTCAC
YFP2_XbaI_rev	GTCTAGATTAGTACAGCTCGTCCATGCCGAGAGTG
YFP2_XhoI_for	GCTCGAGTTAAGAACGGCATCAAGGTGAACTTCAAGATC CGC

3.1.11 Sequencing primer

Table 3.10: List of purchased sequencing primers

Name	Sequence 5'-3'
BGHrev	TAGAAGGCACAGTCGAGG
CMVfor	AGGCGTTTTGCGCTGCTTCG
Seq_Ganab_for	GGAAGACCCTGTTTGGGAAG
T7	TAATACGACTCACTATAGGG

3.1.12 Software

Table 3.9: List of used software

Software	Provider
DAVID Bioinformatics Resources	https://david.ncifcrf.gov
Flowing Software 2.5.1	Turku Bioscience (Turku, Finland)
FusionCapt Advance Solo 4	Vilber Lourmat (Collégien, France)
GraphPad Prism 9.4.1	GraphPad Software Inc. (San Diego, USA)
i-control™ (Infinite 200 Pro)	Tecan (Männedorf, Switzerland)
Mascot server 2.6.1	Matrix Science Ltd (London, UK)
Microsoft Office Home and Student 2019	Microsoft Corporation (Redmond, USA)
Proteome discoverer	Thermo Fisher Scientific (Waltham, USA)
Thermo Xcalibur 2.2	Thermo Fisher Scientific (Waltham, USA)
UniProt	www.uniprot.org
Venny 2.1	https://bioinfogp.cnb.csic.es/tools/venny/
Xfluor4 (GENios)	Tecan (Männedorf, Switzerland)

3.2 Methods

3.2.1 Preparation of chemically competent Escherichia coli

Bacteria of the Dh5α strain was plated on a LB-Agar dish and grown overnight (o/n) at 37°C. On the next day, one isolated colony was picked and a 5 mL starter culture was made (LB-Broth, 37°C o/n). The following day, 100 mL prewarmed LB-Broth was inoculated with 2 mL of the starter culture (1 L flask). This culture was incubated at 37°C, 250 rpm for 2-3 h until an OD600 of 0,5 was reached. Then the suspension was cooled down on ice for 5-10 min, transferred to two precooled 50 mL tubes and

centrifuged at 4°C and 6000 rpm for 10 min. Afterwards the supernatant was quickly discarded. The pellets were resuspended in 30 mL Tfbl (4°C, on ice) and vortexed vigorously. Then the suspension was incubated on ice for 5-10 min and centrifuged for 10 min at 6000 rpm and 4°C. Subsequently, the supernatant was again quickly discarded. The pellets were resuspended in 4 mL ice-cold TfbII, vortexed gently and incubated on ice for 10-20 min. Finally, 50 µL aliquots were prepared in precooled tubes that were snap freezed in liquid nitrogen and stored at -80°C.

3.2.2 Transformation of chemically competent Escherichia coli

An aliquot of chemically competent Dh5α was put on ice for 10 min prior to adding 5 µL ligation preparation or 50 ng plasmid. The mixture was incubated on ice for 30 min, then for 45 Sec at 42°C and again on ice for 2 min. Afterwards 1 mL LB medium was added and the transformed bacteria were incubated at 37°C, 550 rpm for 30 min prior to centrifugation at 3000 g for 5 min. The supernatant was discarded and the pellet was resuspended in 200 µL LB medium including antibiotics of which the transformed bacteria are resistant against. Finally, the suspension was plated on LB-Agar dishes (with Amp/Kan) and incubated o/n at 37°C. On the following day single colonies were picked (Reinard 2018).

3.2.3 Purification of circular DNA

The purification of desoxyribonucleic acid (DNA) was needed in the cloning process and to obtain contaminant-free plasmid DNA for cell transfection.

3.2.3.1 Mini-preparation

For Mini-preps 5mL LB medium (+antibiotics) was inoculated with a single colony containing the desired plasmid one day before the isolation and incubated o/n at 37°C and 180 rpm. Then 2 x 2 mL of the suspension were centrifuged at 8.000 rpm for 1 min in a 2 mL Eppendorf tube and the supernatant was discarded. The pellet was resuspended in 400 µL P1 (RNAse was added before use, final conc. 100 µg/mL) by vortexing. Next, 400 µL P2 was added and the suspension was mixed gently by inverting 2-4 times. After 5 min P2 was neutralized by the addition of 400 µL P3 and

mixed gently, until white precipitate has been formed. The precipitate was spun down at 14.000 rpm for 10 min and the clear supernatant was transferred into a fresh tube with 840 µL isopropanol. After repeated centrifugation at 14.000 rpm for 10 min, the supernatant was discarded and the pellet was washed with 500 µL ethanol (70 %), which was again removed by two brief centrifugation steps. Finally, the DNA pellet was dried and reconstituted in 30-50 µL ddH_2O (Reinard 2018).

3.2.4 Midi-Preparation

For midi-preps the NucleoBond Xtra Midi Plus kit for transfection-grade plasmid DNA was used. In short, 50 mL LB medium (+antibiotics) was inoculated with one single colony of bacteria containing the desired plasmid and incubated o/n at 180 rpm and 37°C. On the following day, the cell suspension was centrifuged down at 6.000 g and 4°C for 15 min. The pellet was resuspended in 8 mL buffer RES, lysed with 8 mL buffer LYS for max. 5 min at room temperature (RT) and then 8 mL buffer NEU was added. The cell disruption was mixed until it became colorless. In the meantime, the column was prepared by pipetting 12 mL buffer EQU on the filter edge. Afterwards the cell disruption was loaded onto the column and 5 mL buffer EQU were added to wash the filter. Then the filter was removed and 8 mL of buffer WASH were added. 5 mL of buffer ELU were used for the elution of the DNA, that was collected in a 15 mL Falcon. 3,5 mL isopropanol were added prior to centrifugation at 15.000 g and 4°C for 30 min. The white pellet was washed with 2 mL ethanol (70 %), which was discarded after a repeated centrifugation step for 5 min. Finally, the pellet was dried until it became transparent and reconstituted in 100-200 µL ddH_2O.

3.2.5 Determination of nucleic acid concentrations

NanoDrop 2000 spectrophotometer was used to determine the DNA concentration and purity as follows. The medium was blanked, in which the DNA was solved. Then the sample absorbance was determined. Important wavelengths for DNA concentration and purity are 230, 260 and 280 nm. The absorbance of DNA displays a peak at 260 nm. The DNA concentration can be calculated by means of the Lambert-Beer law and the extinction coefficient of single stranded or doubled stranded DNA. The absorbance ratio

260/230 is used to assess organic contaminants and the ratio 260/280 indicates protein contamination.

3.2.6 DNA sequencing

The sequence of DNA segments was provided by the GATC service (LightRun Tube). Therefore, 5 µL of DNA plasmid with a concentration between 80 and 100 ng/µL and 5 µL of the appropriate primer with a concentration of 5 µM were mixed and sent to Eurofins.

3.2.7 Polymerase chain reaction

DNA fragments were amplified by the polymerase chain reaction (PCR) for molecular cloning and site-directed mutagenesis. The used polymerase was the Phusion® High-Fidelity DNA-Polymerase.

PCR premix:

10µL Phusion buffer (normally 5x HF was used; 5x GC was used, if GC content was higher than 60 %)
0,5 µL Polymerase
5 µL 2 mM dNTPs
2,5 µL Primer fwd (10 pmol/µL)
2,5 µL Primer rev (10 pmol/µL)
1,5 µL DMSO
x µL DNA plasmid template: 25 ng/µL for molecular cloning; 1-20 ng for site-directed mutagenesis
x µL H_2O

50 µL in total

PCR program for molecular cloning:

1.	98°C	30 Sec	
2.	98°C	10 Sec	**35 cycles**
3.	*°C	20 Sec	
4.	72°C	depends on the length of the DNA fragment that is amplified	
5.	72°C	5 min	
6.	4°C	hold	

*annealing temperature depends on melting temperature of used primers

PCR program for site-directed mutagenesis:

1.	98°C	1-2 min	
2.	98°C	30 Sec	**25 cycles**
3.	*°C	1 min	
4.	72°C	depends on the length of the DNA fragment that is amplified	
5.	72°C	5 min	
6.	4°C	hold	

*annealing temperature depends on melting temperature of used primers

3.2.8 Agarose gel electrophoresis

DNA fragments, PCR products, restriction digestions and plasmids were load onto an 0,5-2 % agarose gel to separate fragments of different sizes. The agarose was boiled in TAE buffer, the solution was cooled down and ethidium bromide was added to a final concentration of 0,5 µg/mL. Then mixture was poured into a gel mold, the gel hardened in about 20 min and the DNA samples premixed with loading dye could be pipetted into the gel-pockets. The gel was run between 90 and 120 V until a sufficient separation was reached. Finally, either an image of the gel was captured by the gel documentation system BioDoc Analyze live or the desired DNA fragments were cut out for further cloning processes (Reinard 2018).

3.2.9 Ligation

By ligation is understood the recombination of insert(s) and vector. Therefore, the vector and insert(s), which were cleaved by one or more restriction enzymes, T4 ligase buffer, T4 ligase and H_2O were mixed and incubated o/n at 16°C. Thereby the insert(s) was/were present in 10-fold excess.

3.2.10 Molecular cloning

Molecular cloning is a set of experimental methods, whose purpose is the alteration of the DNA sequence by introducing, deleting or replacing DNA fragments. Therefore,

restriction enzymes are utilized, which cleave the DNA at or near a certain recognition site. In the classical molecular cloning approach, the plasmid and a DNA fragment are incubated with two restriction enzymes. The emerging cutting ends are ligated afterwards and leading to the insertion of the DNA fragment into the plasmid. In the following the most common workflow will be explained in more detail. First of all, the vector and the insert(s) were chosen. Second, the composition of the construct was specified. Therefore, the position and order of the utilized restriction sites, start and stop codon, gene sequence(s) and possible linkers or tags were determined, which all together form the open reading frame. Then the primers for the insert(s) were designed. The primer sequence included the restriction site and the sequence of the beginning/ending of the insert and a few base pairs ahead of the restriction sequence as a binding site for the restriction enzyme. Other critical parameters for the primer design were the melting temperature, the overall length and the G/C content of the primers. The primers were ordered at biomers or eurofins. Then the insert was amplified by PCR. The correct amplification was checked by agarose gel electrophoresis. If the band was located at the accurate size of the marker, the band was excised and the DNA was extracted with the Pure Link® Quick Gel Extraction Kit. Afterwards 1 µg of the insert(s) and the vector were separately digested by the restriction enzyme(s). The digestion products were loaded onto another agarose gel. The bands were again examined on their correct size, excised and the DNA extracted by the above-mentioned kit. Then the insert(s) and the vector were ligated o/n. The ligation product was transformed into Escherichia coli (E. coli). One day later single colonies were picked and cultivated o/n in 5 mL LB medium (+antibiotics). The DNA plasmids were isolated on the next day. Then a test digestion and another agarose gel electrophoresis with the digestion products were performed to check, if the ligation was successful. Finally, DNA plasmids with the correct size were sent for sequencing to ensure no undesired mutation(s) occurred during the process (Reinard 2018).

3.2.11 Site-directed mutagenesis

As the name already suggest, site-directed mutagenesis is used to make specific, intentional changes to a DNA sequence. It is possible to substitute, delete and/or introduce DNA sections by this technique. Starting point of the mutagenesis was a PCR

with a reverse primer that bound next to the site, where the sequence changes should be introduced and a forward primer that bordered directly the reverse primer and included the desired DNA changes. Afterwards 5 µL of the PCR product were run in a gel electrophoresis to check if the correct sequence was amplified. The second step consisted of the Phosphorylation, Ligation and DpnI digestion. These 3 reactions happened all in parallel in the same tube.

Premix:

2 µL	PCR product
2 µL	T4 polynucleotide kinase buffer A
2 µL	10 mM ATP
1 µL	T4 DNA Ligase HC
1 µL	DNA polynucleotide kinase
11 µL	H_2O

The reaction mixture was incubated for 1 h at RT. The polynucleotide kinase phosphorylated the 5' ends of the PCR product, the ligase fused the phosphorylated 5' with the 3' end, which is a blunt end ligation and the DpnI restriction enzyme digested the PCR template that was carried over. Finally, 10 µL of the reaction mixture were transformed in E. coli and the DNA was isolated. The sequence was checked for correctness by a test digest and GATC sequencing like described in the previous chapter.

3.2.12 Vector maps and cloning design

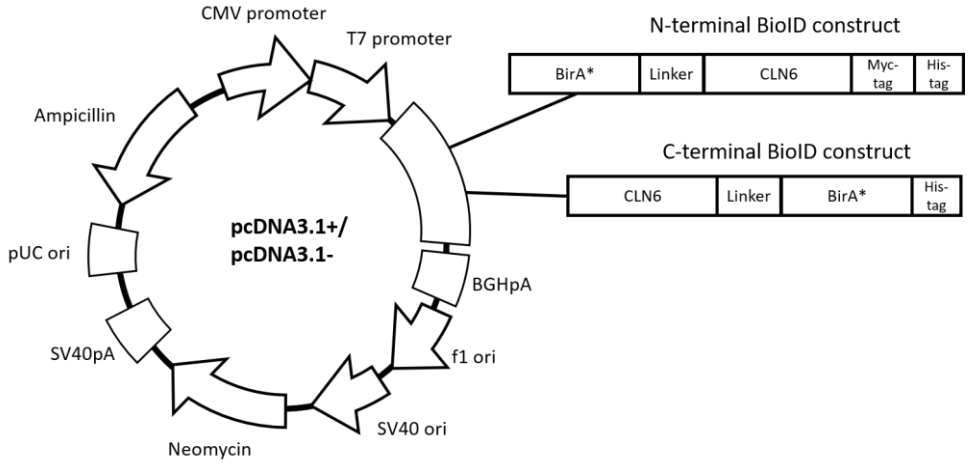

Figure 3.1: Vector map of the BioID constructs
Shown is the schematic representation of the vector components and organization for the N- and the C-terminal BioID constructs

NCBI reference sequences: NM_017882.3 (CLN6), in position 330 an adenosine is replaced by a thymine, but this difference leads to no change in the amino acid sequence; the BirA* sequence was derived from the pcDNA3.1 mycBioID vector (https://www.addgene.org/browse/sequence/228311/) by PCR

Linker sequence: GGTGGTGGTGGTGGTGGTGGATCCGCG

The N-terminal BioID construct has already been created previously in the working group by inserting the BirA* and linker cDNA into the pcDNA3.1(-)myc/His-CLN6 plasmid using the XbaI and BamHI cutting sites. The C-terminal BioID construct was created by integrating the inserts into the pcDNA3.1(+) vector using the BamHI, EcoRI and XbaI cutting sites.

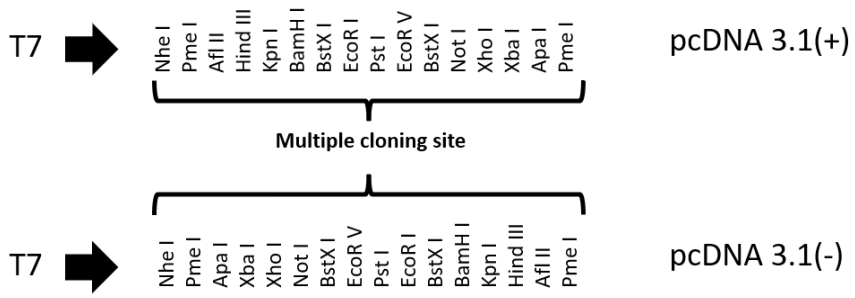

Figure 3.2: Multiple cloning site of the pcDNA3.1(+) and pcDNA3.1(-) vectors
Shown are restriction enzymes with an available cutting site following the T7 promotor.

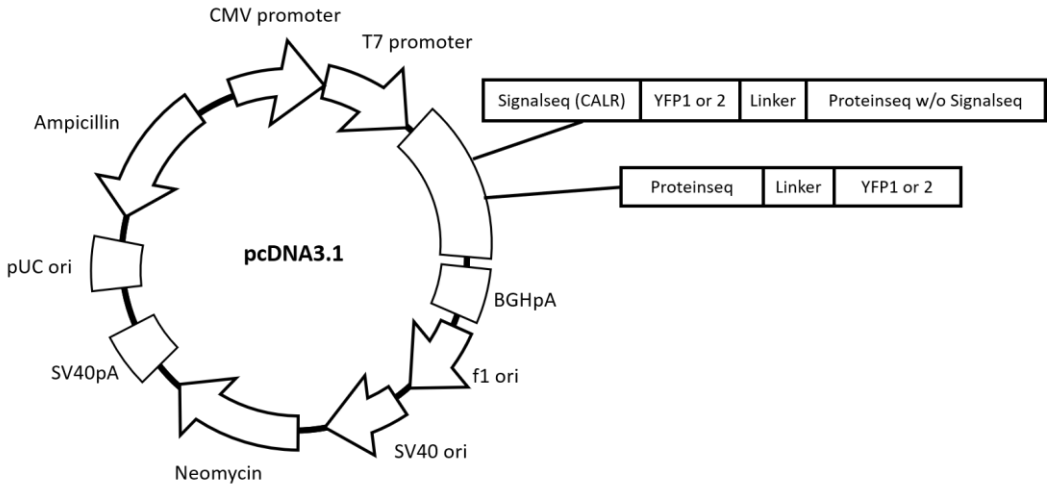

Figure 3.3: Vector map of the YFP constructs
Shown is the schematic representation of the vector components and the vector organization for the YFP constructs.

NCBI reference sequences: NM_017882.3 (CLN6), in position 330 an adenosine was substituted by thymine, but this difference leads to no change in the amino acid sequence; NM_018941.4 (CLN8); NM_000310.4 (PPT1); NM_005570.4 (Ergic53); NM_198335.4 (GANAB); NM_001024649.2 (CANX); NM_004343.4 (CALR); NM_001909.5 (CTSD); BC042168.1 (CTSZ); LT726804.1 (YFP), in position 471 a guanin is replaced by an adenosine with no effect on the amino acid structure.

Linker sequence:
ATCGATGGTGGCGGTGGCTCTGGAGGTGGTGGGTCCGCTCGAGTT

The YFP1/2-Ergic53 and YFP1/2-MCFD2 constructs were kindly provided by Prof. Dr. Hans-Peter Hauri, Biozentrum Basel. The sequences were inserted by using the restriction cutting sites HindIII and XhoI. These constructs were used as templates to generate the other YFP constructs. The N-terminal YFP-CLN6 constructs have already been created. For constructs, in which the YFP fragments were positioned in front of the respective protein, the Erig53 sequence was replaced using the XhoI and XbaI restriction cutting sites. For constructs, in which the positioning of the YFP fragment and the protein sequence was reverse the Ergic53 sequence was replaced by the YFP fragments and the respective protein was inserted in front of the linker using the restriction cutting sites HindIII and ClaI.

3.2.13 Cultivation of cell lines

All eukaryotic cell lines were cultivated at 37°C, under 5 % CO_2 and in a water-saturated atmosphere. Media and other solutions were prewarmed in a 37°C water bath. Standard medium was DMEM with 10 % (v/v) fetal bovine serum, penicillin/streptomycin and L-glutamine for all cell lines except Cbc cells.

3.2.14 Trypsination of cells

First of all, the medium and the solution were heated up. Now the old medium was removed from the cells and they were washed once with PBS. Afterward PBS was removed, 0,05 (w/v) trypsin/EDTA was pipetted onto the cells and incubated until the adherent cells were detached. At the end, 10 % supplemented medium or PBS was added to stop trypsin digestion.

3.2.15 Cryoconservation and revitalization of cells

Cells were trypsinated as described above and spun down by 700 g for 4 min. The supernatant was removed and the cells were resuspended with premixed 900 µL media and 100 µL DMSO. The cell suspension was transferred in cryovials, put into a freezing container filled with isopropanol, which was placed in a -80°C freezer and transferred to the liquid nitrogen tank on the next day. For revitalization the vial was taken out of the tank and put into the 37°C water bath briefly until the cell suspension was thawed and then transferred into 5 mL of media to dilute DMSO concentration. Cells were spun down and the supernatant with DMSO was removed. Finally, cells were resuspended in normal growth media and seeded in culture dishes.

3.2.16 Stable isotope labeling by amino acids in cell culture

For stable isotope labeling by amino acids in cell culture (SILAC) cells were treated with light (R+0, K+0), medium (R+6, K+4) or heavy (R+10, K+8) isotope labeled arginine and leucin. To ensure sufficient incorporation of the isotope labeled amino acids, the cells were passaged at least 6 times in SILAC media and the experiments were also conducted in the respective media. This labeling led to mass shifts between proteins and peptides of differently labeled samples. These shifts could be detected by mass spectrometry and consequently, proteins could be assigned to their respective label.

3.2.17 Transient transfection of cells

Transient transfections were carried out with Turbofect® as the transfection reagent. First, cells were seeded 24 h before the addition of the reagent with a cell density that led to a confluency of about 70 to 90 % at the time of transfection. Then the plasmid DNA was pipetted into 1x DMEM. Turbofect was added, the mixture was vortexed gently and incubated at RT for 20 min. Finally, the mixture was pipetted up and down rigorously and pipetted to the cell media dropwise. In case of cell lines with high sensitivity against turbofect the media with turbofect was removed after 4 h and exchanged by fresh media.

3.2.18 Cell harvest and lysis

In every single step the cells were put on ice if possible. First, cells were washed twice with PBS and scraped in ice-cold PBS. The cell suspension was transferred to a tube and centrifuged at 1.000 g and 4°C for 10 min. Then the supernatant was removed and the cells were resuspended in the BioID lysis buffer. The cells were lysed by three cycles of a freezing step in liquid nitrogen and followed by a thawing step, in which cells were treated either 5 min in an ultrasonic bath or 2 times with an ultrasonic rod for 15 sec. Then the tubes were put on ice for 1 h. Finally, the cell debris was centrifuged down at maximal speed and 4°C for 20 min and the cell lysate was transferred to a new tube.

3.2.19 Enrichment of the lysosomal fraction from mouse liver

First, the mouse had to be sacrificed by cervical dislocation. Then the liver was removed. Hereby, it was attempted to keep the gallbladder intact. The liver was separated from the gallbladder, washed with homogenization buffer and dissected. If possible, every step was performed on ice or 4°C.

3.2.19.1 Generation of 20.000 g pellets

The 20.000 g pellets are a fraction that contain besides lysosomes also mitochondria and peroxisomes. The dissected mouse liver was homogenized by a douncer with 20 strokes in 1:5 (m/v) mL homogenization buffer. The homogenate was centrifuged at 1.000 g and 4°C for 15 min. The post-nuclear supernatant (PNS) was again centrifuged at 20.000 g and 4°C for 20 min. The pellet was resuspended in buffer A. Finally, the protein concentration was determined and the 20.000 g pellet could be further analyzed by mass spectrometry and western blotting. For mass spectrometric analysis the samples were first alkylated, reduced and digested by the filter-aided sample preparation method. Afterwards peptides were tandem mass tag (TMT)-labeled, desalted by solid phase extraction (SPE), separated by OffGel and once more desalted by the stop and go extraction (STAGE)-tips before being measured on the LC/MC device.

3.2.19.2 Isolation of tritosomes

Tritosomes are a highly purified lysosomal fraction devoid of any notable contamination through peroxisomes or mitochondria. First, 3-4 days before sacrificing of the mouse and removing of the liver, 4 µL/g of body weight 17 % tyloxapol (Triton WR1339) were injected intraperitoneally. After the extraction and dissection of the liver, it was transferred into a dounce homogenizer and homogenized at 1000 rpm by adding 4,5 mL 0,25 M sucrose and moving the douncer up and down three times. Then the homogenate was emptied into a 15 mL Falcon and the douncer was rinsed with 0,5 mL 0,25 M sucrose, which was also transferred to the Falcon. The liver homogenate was centrifuged at 1.000 g and 4°C for 10 min and the supernatant was transferred to another 15 mL falcon tube. The homogenization step was repeated with the pellet and 3 mL 0,25 M sucrose. The douncer was again rinsed with 0,5 mL 0,25 M sucrose and the total 3,5 mL were centrifuged with the conditions as mentioned above. Then the supernatant was added to the supernatant of the first centrifugation step and the pellets were discarded. The PNS was now centrifuged at 25.000 rpm and 4°C for 10 min in an ultracentrifuged using the fix angle rotor Ti-50 and the corresponding plastic tubes. The supernatant was removed carefully and the pellet was mixed well first in 1 mL 0,25 M sucrose by a glass stick and later 9 mL were added and the suspension was resuspended up and down. The ultracentrifugation step was repeated and the supernatant was removed once again carefully without causing any disturbance to the pellet. Next, the pellet was mixed well by a glass stick with first 1 mL of p1.21 sucrose and then with another milliliter. The homogenate was transferred to the douncer and the centrifugation tube was rinsed with 0,5 mL p1.21 sucrose, which were added to the douncer. The total of around 3 mL were homogenized 3 times at low speed. Another 0,5 mL were added and the complete homogenate was transferred to a SW41 rotor plastic tube. Now the other gradients were pipetted carefully on top. First, 2,5 mL p1.15, then 2,5 mL p1.14 and at the end, 1,5 mL p1.06 of sucrose were added on each other one by one. A clear layer should have been visible between each sucrose densities. After the sucrose gradient was completed, another ultracentrifugation step was conducted at 25.500 rpm and 4°C for 150 min using the SW41 rotor. Following centrifugation, the lysosomal fraction appeared as a whitish ring and presents the most upper layer of the 3 existing layers in the tube. Finally, the fraction was removed and transferred in to a new tube.

The tritosomes were stored at -20 or -80°C. For mass spectrometry measurements the tritosome samples were prepared similar as the 20.000 g pellet samples (see 3.2.18.1 generation of 20.000 g pellets).

3.2.20 Determination of protein concentrations

The BioRad DC assay was used to determine the protein concentration in cell lysates, tissue homogenates or subcellular fractions. Therefore, calibration solutions with known protein concentrations of 2; 1; 0,5; 0,25; 0,125 and 0,650 mg/mL were prepared from a 20 mg/mL BSA stock. Next, 5 µL of every calibration solution and sample were pipetted in a well of a transparent 96 Well Plate. Triplicates were performed. Then solution A' was prepared (1:50 solution S/solution A) and 25 µL were added into the wells. Afterwards 200 µL of solution B was pipetted to the mixture. Finally, the well was measured at 750 nm by a plate reader after an incubation of at least 15 min at RT. The relevant product absorbing light at 750 nm was stable for about 1 h.

3.2.21 Sodium dodecyl sulphate-polyacrylamide gel electrophoresis

Sodium dodecyl sulphate-polyacrylamide gel electrophoresis (SDS-PAGE) is a method to separate proteins according to their different masses. First of all, the running gel was prepared. Therefore, the ingredients were mixed together, TEMED and APS were added for the initiation of the polymerization, the solution was poured into a gel cast and a layer of isopropanol was put on top. After complete polymerization, which takes normally around 15-20 min, the isopropanol was removed and the stacking gel was mixed and poured on top of the running gel. The comb with the right number of wells was shoved/pushed between the glass plates. After the polymerization of the stacking gel took place, the gel was loaded with the appropriate protein ladder and the samples. The samples were mixed with 4x Lämmli buffer and boiled at 95°C for 5 min. The gel was run with a voltage of 90 V for the first 15 min and then the voltage was increased to 120 V. When the loading dye has reached the desired endpoint, the gel was stopped and taken out of the glass plates. Subsequently, a western blot was performed as described underneath.

3.2.22 Western blot

Western blot is a method, in which proteins are separated by SDS-PAGE and blotted onto a NC or PVDF membrane for subsequent identification and quantification with specific antibodies. One 3 mm thick filter paper was soaked in blot buffer and placed into the western blotter. Either a NC or a PVDF membrane was wetted in blot buffer and put on top of the filter paper. If a PVDF membrane was used, it was activated prior to that in MeOH for 5 min. The gel with the separated proteins was then placed on top of the membrane following another filter paper wetted in blot buffer. The blotter was closed and 2,5 mA/cm^2 were applied and 25 V was set as limit. The blotter was run for 1 h, then stopped and the membrane was taken out. In case of a NC membrane, the protein bands and over all blotting performance could be observed by a ponceau staining. Afterwards the membrane was blocked in 5 % milk solution for 1h and washed with TBS-T for 15 min. Then the membrane was incubated with the primary antibody at 4°C o/n. On the following day, the membrane was washed thrice with TBS-T and incubated for 45 min at RT with the secondary antibody, to which a horse radish peroxidase was coupled. Again, the membrane was washed thrice with TBS-T for 10 min each. Finally, the membrane was developed in the Fusion, shortly after adding premixed enhanced chemiluminescence substrate solution (1:1). For relative protein quantification the FusionCapt Advance Solo 4 software was used.

3.2.23 Enzyme assays

Enzyme assays are used to determine the enzymatic activity. Besides methods for the evaluation of the protein quantity, following three enzyme assays of lysosomal hydrolases were performed to obtain additional information about their functionality.

3.2.23.1 CTSD activity assay

The Ctsd activity in tritosomes was determined using the Cathepsin D Activity Kit and was performed following the manual instructions. Therefore, 62,5 ng protein of wt and *nclf* tritosome samples were added in triplicates into wells of a black 96-well plate and filled up to 50 µL with lysis buffer. After addition of the master mix, the plate was

incubated at 37°C and measured every 5 min at Ex/Em=328/460 nm. For our analysis the values measured after 15 min were taken.

3.2.23.2 GBA activity assay

Gba activity was determined for tritosome samples. Therefore, for each wt and *nclf* tritosome sample 15 µg of protein in 20 µL of the 0,25 M sucrose together with 30 µL substrate solution were incubated in a black 96-well plate for 45 min at 37°C. Then enzyme activity was inhibited by addition of 200 µL 100 mM Glycin with a pH of 10,6. Finally, the plate containing triplicates of wt and *nclf* samples was measured at Ex/Em=365/405 nm.

3.2.23.3 PPT1 activity assay

The activity of Ppt1 was determined by a slightly modified assay, which was previously described (van Diggelen et al. 1999). 5 µg of three wt and three *nclf* whole liver samples were each filled up to 10 µL with the homogenization buffer and mixed with 20 µL of substrate solution. The reaction mixture was incubated for 1 h at 37°C. Then the samples were boiled for 2 min and allowed to cool down. Afterwards, the solution was adjusted to pH 5 by adding 10 µL phosphate/citrate buffer with almond ß-glucosidase (0,1 U dissolved in 0,02 % BSA) and the reaction mixture was incubated again for 1 h at 37°C. All enzymatic reactions were terminated by the addition of 200 µL of 0.5 M Na_2CO_3/$NaHCO_3$ with a pH of 10.7, containing 0,025 % Titon X-100. Finally, 230 µL of the reaction mixture were transferred into a black 96-well plate and the fluorescence of the released 4-methylumbelliferone was measured at 365 nm excitation and 405 nm emission wavelength in the tecan Infinite 200 Pro microplate reader.

3.2.24 The BioID experiment

The BioID approach is utilized to identify proteins in close proximity and potential interaction partners of one specific protein. Here, it was coupled with an SILAC labeling and mass spectrometric analysis. Three SILAC labels were used, as cells were labeled with light, medium and heavy isotopes. HEK cells were seeded one day prior to transfection at a confluency of 70-90 %. Two differently labeled HEK cells were transfected with cDNA (complementary desoxyribonucleic acid) encoding the BioID

fusion protein consisting of the biotin ligase BirA* and the protein of interest combined by a linker. The cells containing the third SILAC label were transfected with an empty vector. Another 24 h later, biotin was added into the cultivation media of one sample transfected with the BioID fusion protein and the sample transfected with the empty vector to a final concentration of 50 µM. After cells were cultivated for another 24 h, they were harvested, lysed and the protein concentration of the cell lysates was determined. The HEK cells transfected with the BioID fusion protein an added biotin is expected to contain biotinylated proteins. The other two samples are negative controls, in which biotinylation is not supposed to take place due to the absence of either the fusion protein or biotin. As a label switch experiment the three treatments were conducted with every label, resulting in a total of nine different samples. These were combined to three sets each containing 1 mg protein of every treatment with a different label.

	Light	Medium	Heavy
1	Transf. with the addition of biotin (sample)	Transf. without the addition of biotin (control 1)	Untransf. with the addition of biotin (control 2)
2	Untransf. with the addition of biotin (control 2)	Transf. with the addition of biotin (sample)	Transf. without the addition of biotin (control 1)
3	Transf. without the addition of biotin (control 1)	Untransf. with the addition of biotin (control 2)	Transf. with the addition of biotin (sample)

Table 3.10: Sample and control combinations of one SILAC label switch experiment

The differently SILAC labeled proteins from the label switch experiment were pooled to three sets with each set containing the sample, control 1 and control 2.

Next, the biotinylated proteins were purified and prepared for mass spectrometry analysis. Therefore, 100 µL streptavidin sepharose beads were centrifuged at 500 g for 1 min to remove the storage solution. Afterwards, the beads were washed 3 times with 1 bead volume BioID lysis buffer and the beads were mixed with the pooled lysates, volumes were adjusted and the mixture was incubated O/N at 4°C on a rotator. On the next day, the beads were spun down and washed 2 times with 2 % SDS in H_2O, then in a buffer consisting of 0,1 % sodium deoxycholate; 0,91 % Triton X-100; 500mM NaCl; 1mM EDTA and 50 mM Hepes with a pH 7,5 and a buffer containing 250 mM LiCl; 0,5 % NP-40; 0,5 % sodium deoxycholate; 1 mM EDTA and 10 mM Tris-HCl with a

pH 8,1. Finally, the beads were washed twice in H_2O with 50 mM Tris and 50 mM NaCl at a pH 7,4. After the washing steps the purified proteins were reduced. Therefore, 300 µL of 10 mM DTT in 100 mM TEAB were added to the beads and incubated at 56°C for 30 min while shaking. Then acrylamide was added to a final concentration of 56 mM and incubated again for 30 min at RT while shaking. The beads were spun down with 800 g for 1 min and the supernatant was removed. Now, beads were washed three times with 1 mL of 100 mM TEAB and 1 µg trypsin in 300 µL 100 mM TEAB was added to the beads for the digestion O/N at 37°C. On the next day, the peptides were extracted by incubating the beads two times in 300 µL 5 % ACN and 0,1 % FA at RT while shaking at 800 rpm. The supernatants were combined and the beads were discarded. After the digest an Oasis was performed to desalt the peptides and subsequently either an OffGel or a strong anion exchange (SAX) fractionation was conducted. Finally, samples were again desalted by STAGE-tipping and loaded onto the autosampler 96 well plate for LC/MS measurements. At the end the mass spectrometry data was analyzed with the Proteome Discovery software from Thermo Scientific.

3.2.25 Bimolecular fluorescence complementation assay

The BiFC assay is utilized to identify protein-protein interactions. It relies on the reconstitution of two fluorescent protein fragments. One is fused to the protein of interest and the other one to the potential interaction partner candidate. Both fragments can be coupled to either the N- or the C-terminus of the proteins. An emerging fluorescent signal indicates a possible interaction of these two proteins. Here, the yellow fluorescent protein (YFP) was used as the fluorescent protein and the first fragment YFP1 included amino acids from 1-158 and the second fragment YFP2 consisted of the remaining amino acids 159-239. First, 300.000 BHK cells were seeded in a 6 well plate. Then 24 h later the cells were cotransfected with two DNA plasmids encoding for different proteins, which are fused by a linker to either YFP1 or YFP2. Therefore, 2 µg DNA plasmid of each construct and 8 µL Turbofect® were applied. After another 48 h cells were washed with PBS and trypsinated. BHK cells were washed again twice with PBS and finally resuspended in 200 µL PBS. The cells were now measured by flow cytometry using a GFP filter. For the data analysis BHK cells transfected with an empty

vector were gated and the means of the cells showing a higher fluorescent level were determined and statistically evaluated (Nyfeler et al. 2005, Kerppola 2006).

3.2.26 Mass spectrometry

Tritosome, 20.000 g pellets and BioID samples were analyzed by mass spectrometry for protein identification and quantification. In the following used preparation methods, measurement parameters and data evaluation are specified in detail.

3.2.26.1 Filter-aided sample preparation method

First, the filter unit was washed with 500 µL 60 % methanol (MeOH) twice, H_2O and DB. The solutions were passed through the filter device by centrifugation at 10,000 g and RT for 10 min, if not stated otherwise. After the washing steps 50 µg protein in 100 µL were transferred onto the filter and 300 µL DB were added. The flowthrough was discarded and the sample was reduced with 100 µL of 20 mM DTT at 55°C for 30 min. The solution was removed by a brief centrifugation and the filter was washed twice with 400 µL DB. Subsequently, the sample was alkylated by adding 100 µL DB with 40 mM acrylamide and incubating for 30 min at RT in the dark. Again, the solution was removed and the filter device was washed twice with DB. For digestion 50 µL DB with trypsin at a 1:100 mass ratio (enzyme:protein) was added and incubated for 10 h at 37°C. Afterwards, the filter device was centrifuged and the flowthrough containing the peptides was collected in a new tube. 200 µL DB were passed through the filter to elute remaining peptides and combined with the previous flowthrough. Now, the volume was estimated and 25 % FA was added for a final concentration of 2,5 % to remove deoxycholic acid (DCA). The sample was vortexed briefly and centrifuged at 14,000 g and RT for 5 min. The supernatant was transferred carefully into a new tube. Then the pellet was washed with 250 µL 0,1 % FA and the centrifugation step was repeated. Again, the supernatant was removed and combined with the first one. Finally, the remaining DCA was removed. Therefore, 500 µL ethyl acetate was added to the supernatants, the mixture was vortexed and centrifuged at 10,000 g and RT for 2 min. The upper layer was carefully discarded. This step was repeated twice and the sample was vacuum dried.

3.2.26.2 Tandem mass tag-labeling

TMT-labeling is a method enables to quantify peptides of multiple different samples in one mass spectrometry measurement. TMT molecules have got the same mass and chemical structure. Therefore, pooled peptides labeled with TMT elute and are measured at the same time. However, they are fragmented into reporter ions of differing masses. In this way, the TMT labels can be assigned to the different samples. First, reduced, alkylated and digested samples were solved in 100 mM Triethylammonium bicarbonate (TEAB) and sonicated for 5 min. In the meantime, the TMT-reagents from Thermo Scientific were taken out of the freezer and acclimatized to RT in a desiccator, because the reagents are highly hygroscopic and react in the presence of H_2O. Then 0,8 mg of each TMT label was solved in 41 µL anhydrous ACN. The vials were kept on the bench for around 5 min and vortexed occasionally. Then the solutions were centrifuged down briefly, added to the peptides separately and incubated for 1 h at RT. Afterwards, the reaction was stopped by the addition of 10 µL 5 % hydroxylamine, which was vortexed and incubated for 15 min at RT. Finally, samples were combined at equal amounts and vacuum dried.

3.2.26.3 Peptide purification by solid phase extraction

Prior to mass spectrometry measurements or fractionation, it is critical to desalt the sample and remove all interfering components. One possible method for desalting peptides is the SPE.

First, the sample was acidified with FA that an end concentration of 0,1 % FA was reached. Then the Water Oasis HLB column was activated with 3 mL of 70 % ACN and 0,1 % FA and washed with 4 mL 0,1 % to remove the ACN. Now, the sample was flushed through the column three times allowing the peptides to bind to the column. Afterwards, desalting of the peptides took place by washing the column with 10 mL 0,1 % FA. Finally, peptides were eluted with 1,5 mL ACN containing 0,1 % FA and vacuum dried.

3.2.26.4 Strong anion exchange fractionation

In proteomics a high complexity of the sample can be an issue in mass spectrometry measurements. If the complexity is too high, not all peptides can be detected properly. To reduce sample complexity there are different fractionation methods like the SAX fractionation. Here peptides bind to a positively charged resin and are eluted according to their negative charge at different pH values.

First, a tip with 10 disks of an anion-SR empore extraction membrane was prepared. The membrane resin was equilibrated by 100 µL of MeOH, 1 M NaOH and SAX buffer with a pH of 11. Each solution was passed through the tip by centrifugation at 5,000 g for 3 min. The peptides were solved in 200 µL SAX buffer with a pH of 11 and passed through the tip for binding on the membrane resin. The flowthrough was collected as the first fraction. Afterwards, 5 more fractions were eluted by sequentially passing through 200 µL of SAX buffers with declining pH value (6, 5, 4 and 3). The last SAX buffer with a pH of 3 for the elution of peptides additionally contained 0,25 M NaCl. Finally, collected eluates were acidified with 0,1 volumes FA and vacuum dried.

3.2.26.5 Peptide fractionation by isoelectric focusing - OffGel

Another way of fractionate peptides is to separate them based on their different isoelectric points. The Aligent 3100 fractionator device was used to generate 12 fractions by isoelectric focusing. First, the peptides were dissolved in 1,9 mL IPG buffer. Then the immobilized pH gradient gel strip (ranging from pH 3 to 10) was placed into the tray between anode and cathode according to the manufacture's instruction. A frame with 12 wells was put on top of the gel strip and the gel as well as the electrode pads were wettened with IPG buffer. Then the dissolved peptides were added into the wells and the electrode pads were attached to the ends of the gel strip. The frame was sealed and mineral oil was pipetted onto the anode and cathode. Then the tray was put into the fractionator and voltage was applied. Now, the peptides were moved toward the sector on the gel strip, where the pH correspond to their isoelectric point. Afterwards the solution in the wells containing the single fractions were pipetted into new tubes. 200 µL of 0,1 % FA was pipetted in each well to elute remaining

peptides, which were combined with their respective fractions. At the end samples were vacuum dried.

3.2.26.6 Stop and go extraction tips desalting procedure

After Offgel or SAX fractionation samples again contain salts, which have to be removed before the mass spectrometry measurement. This was achieved by STAGE-tips. These were prepared by putting 6 layers of C18 membrane disks tightly into a 200 µL pipette tip. For every elution a centrifugation step of 5 min and 5,000 rpm was applied. The disks were activated by centrifuging 20 µL MeOH, buffer B and buffer A sequentially through the tips. Next, the sample was dissolved in 20 µL 5 % FA and 5 % ACN and sonicated for 5 min. Then 80 µL H_2O were added and the solution was spun down for 5 min at 13,000 rpm. The sample was passed through the STAGE tip for peptide binding and washed with 100 µL buffer A. Then the desalted peptides were eluted twice with 20 µL buffer B and collected in a new tube. Finally, peptides were vacuum dried to remove excess of organic solvent.

3.2.26.7 LC-MS measurement for 20,000 g pellets and tritosomes

Peptides from 20,000 x g samples were separated on a Dionex Ultimate 3000 RSLC nano HPLC system (Dionex GmbH). The autosampler was operated in µl-pickup mode. Peptides were dissolved in 10 µl 0.1 % FA (solvent A). 3 µl were injected onto a C18 analytical column made in-house (200 mm length, 75 (20,000 x g pellets)/100 (tritosomes) µm inner diameter, ReproSil-Pur 120 C18-AQ, 1.9/5 µm). Peptides were separated during a linear gradient from 1 % to 35% solvent B (90 % ACN, 0.1 % FA, for tritosomes + 5 % DMSO) within 60 min at 300nl/min. The nanoHPLC was coupled online to an Orbitrap Fusion Lumos mass spectrometer (ThermoFisher Scientific). Peptide ions between 330 and 1500 m/z were scanned in the Orbitrap detector every 3 seconds with a resolution of 120,000 (maximum fill time 50 ms, AGC target400,000). Polysiloxane (445.12002 Da) was used for internal calibration (typical mass error ≤1.5 ppm). In a top-speed method peptides were subjected to collision induced dissociation for identification (CID: 0.7 Da quadrupole isolation, threshold intensity 5000, normalized energy 35 %) and fragments analyzed in the linear ion trap („Turbo“ scan rate) with target 104 and maximum filltime 50 ms. Fragmented peptide ions were

excluded from repeat analysis for 20 s. Top 5 fragmentions were chosen for synchronous precursor selection and fragmented with higher energy CID (HCD:1.3 Da isolation, 65 % collision energy) for detection of reporter ions in the Orbitrap analyzer (resolution 50,000, maximum fill time 86 ms, target 100,000). Peptides from tritosome samples were separated on an easy-nLC1000 nano HPLC system (ThermoFisher Scientific). Peptides were dissolved in 5 % ACN, 5 % FA. 5 µl were injected onto a C18 analytical column as above and separated during a linear gradient from 1 % to 35 % solvent B within 90 min at 400 nl/min. The nanoHPLC was coupled online to an LTQ Orbitrap Velos mass spectrometer (Thermo Fisher Scientific). Peptide ions between 400 and 1200 m/z were scanned in the Orbitrapdetector (resolution 30,000, maximum fill time 300 ms, AGC target 106). m/z 401.922718 was used for internal calibration. Top 10 most intense precursor ions were subjected to collision induced dissociation with higher energy (HCD: 2.0 Da isolation, threshold intensity 5000, normalized energy 42 %) and fragments analyzed in the Orbitrap with target 50,000, maximum fill time 250 ms, and resolution 7,500. Fragmented peptide ions were excluded from repeat analysis for 30 s.

3.2.26.8 Data analysis and statistical evaluation for 20,000 g liver pellet and tritosome dataset

Raw data processing was performed with Proteome Discoverer software 2.4.0.305 (Thermo Fisher Scientific). Peptide identification was done with an in-house Mascot server version 2.6.1 (Matrix Science Ltd). MS data were searched against Mus musculus sequences from SwissProt. Precursor ion m/z tolerance was 10 ppm, fragment ion tolerance 0.5 Da (CID). Tryptic peptides with up to two missed cleavages were searched. Propionamide on cysteines and TMT10-plex (20.000 x g pellets) or TMT6-plex (tritosomes) on N-termini and lysines were set as static modifications. Oxidation of methionine and phosphorylation on Ser, Thr and Tyr were allowed as dynamic modifications. Mascot results were evaluated by the percolator algorithm (Kall et al. 2008) version 3.02.1 as implemented in Proteome Discoverer. Spectra with identifications below 1 % q-value were sent to a second round of database search with semitryptic enzyme specificity (one missed cleavage allowed). Protein N-terminal acetylation, methionine oxidation, phosphorylations, and N-terminal TMT were then set

as dynamic modifications. Reporter ion intensities were extracted from the MS3 level (most confident centroid). Actual FDR values were typically ≤0.8 % (peptide spectrum matches), ≤1.0 % (peptides), and 1.0 % (proteins) for both datasets. Peptide abundances were normalized by the sum of peptide abundances per sample. Peptide and protein ratios were determined using the pairwise ratio approach and p-values were obtained by a background-based t-test as implemented in PD. First, peptide ratios were calculated by forming all possible ratio combinations of the peptide abundances and with an uneven number of ratios taking the median or in case of an even number of ratios, the geometric median of the two middle values. Accordingly, the protein ratio was calculated as the median or the geometric median of all peptide ratios. These protein ratios were subjected to a background-based t-test. For the background 200 proteins with their maximum intensity being closest to the target protein and having similar protein ratios were selected. These feature the non-regulated proteins, which were compared to the protein of interest. This approach was chosen because of its robustness in the case of missing values and big variance variations in the proteomic data set (Navarro et al. 2014). P-values were adjusted with the Benjamini-Hochberg correction. The mass spectrometry proteomics data have been deposited to the ProteomeXchange Consortium via the PRIDE(Perez-Riverol et al. 2019) partner repository with the dataset identifier PXD016599.

3.2.26.9 LC-MS measurement for BioID samples

OffGel-fractionated peptides were on a Dionex Ultimate 3000 RSLC nano HPLC system (Dionex GmbH). The autosampler was operated in µl-pickup mode. Peptides were dissolved in 10 µl 5 % FA, 5 % ACN. 3 µl were injected onto a C18 trap column made in-house (100 mm length, 100 µm inner diameter, ReproSil-Pur 120 C18-AQ, 5 µm) equilibrated with solvent A (0.1 % FA). Peptides were separated during a linear gradient from 5 % to 35 % solvent B (90 % ACN, 0.1 % FA) within 30 min at 300 nl/min on a column with 300 mm length, 100 µm inner diameter, and 3 µm C18-AQ particles made in-house. The nanoHPLC was coupled online to an Orbitrap Velos mass spectrometer (Thermo Fisher Scientific). Peptide ions between 330 and 1600 m/z were scanned in the Orbitrap with a resolution of 30,000. Polysiloxane (445.12002 Da) was used for internal calibration (typical mass error ≤1.5 ppm). Top 20 most intense

peptide ions were subjected to collision induced dissociation (CID: 1.1 Da isolation, threshold intensity 3000, normalized energy 35 %) and fragments analyzed in the linear ion trap. Fragmented peptide ions were excluded from repeat analysis for 13 s.

SAX-fractionated peptides were separated on an easy-nLC1000 nano HPLC system (ThermoFisher Scientific). Peptides were dissolved in 20 µL 5 % ACN, 5 % FA. 5 µL were injected onto an analytical column (300 mm length, 100 µm inner diameter, 3 µm C18-AQ particle) made in-house. The column was equilibrated with solvent A (5 % DMSO, 0.1 % FA). Peptides were separated during a linear gradient from 1 to 35 % solvent B (90 % ACN, 0.1 % FA, 5 % DMSO) and analyzed on an Orbitrap Velos mass spectrometer. Peptide ions with 400-1200 m/z were analyzed in the Orbitrap detector with R=60.000. 401.9227 m/z was used as lock mass. Top 10 most intense Ions were isolated with 2 Da width and fragmented in the linear ion trap by CID (35 % CE).

3.2.26.10 Data analysis for BioID samples

Raw data processing was performed with Proteome Discoverer software 2.2.0.388 (Thermo Fisher Scientific). Peptide identification was done with an in-house Mascot server version 2.6.1 (Matrix Science Ltd). MS data were searched against Homo sapiens sequences from SwissProt, the sequence of the biotin ligase BirA* from Escherichia coli (strain K12) and contaminant sequences (cRAP) (Mellacheruvu et al. 2013). Precursor ion m/z tolerance was 10 ppm, fragment ion tolerance 0.6 Da (CID). Tryptic peptides with up to two missed cleavages were searched. Propionamide on cysteines was set as a fixed modification. Isotopic labeling of arginine ($^{13}C_6$,$^{14}N_4$; $^{13}C_6$,$^{15}N_4$) and lysine ($^{2}H_4$; $^{13}C_6$,$^{15}N_2$), oxidation of methionine and protein N-terminal acetylation were set as dynamic modifications. Mascot results were evaluated by the percolator algorithm (Kall, Storey et al. 2008) version 3.00 as implemented in Proteome Discoverer. Spectra with identifications below 1 % q-value were sent to a second round of database search with semitryptic enzyme specificity (one missed cleavage allowed) and in which isotopic labeling of arginine ($^{13}C_6$,$^{14}N_4$; $^{13}C_6$,$^{15}N_4$) and lysine ($^{2}H_4$; $^{13}C_6$,$^{15}N_2$), propionamide on cysteines, protein N-terminal acetylation and methionine oxidation were set as dynamic modifications. SILAC 3plex was used as quantification method. Actual FDR values were typically ≤0.8 % (peptide spectrum matches), ≤1.0 %

(peptides), and 1.0 % (proteins) for all datasets. Peptide and protein ratios were calculated based on the summed peptide and protein abundances.

4 Results

4.1 Investigation of the lysosomal proteome in CLN6 deficiency

One objective of this thesis is to determine the effects of the devastating NCL disease caused by CLN6 deficiency on a molecular level. To elucidate which cellular components are altered and in which biological pathway CLN6 functions, samples from *nclf* mice that have no functional Cln6 protein (Bronson et al. 1998) were compared with wt control samples in various experiments. Because NCL is a lysosomal storage disease and it has been shown that the biochemical composition of lysosomes in NCL differs from lysosomes in healthy cells (Seehafer et al. 2006), the lysosome obviously presents the most interesting cellular compartment for the detection of relevant molecular changes. Proteins are the most relevant biological molecule class for lysosomal integrity and health. For instance, lysosomal storage diseases are typically caused by deficiencies of distinct lysosomal proteins (Cox et al. 2012). Consequently, it is expected that changes due to NCL can be found most likely on the protein level in the lysosome and therefore, the lysosomal proteome was analyzed.

Two main research questions should be answered by these investigations. First, are there any significant alterations of the lysosomal proteome detectable, which could explain the phenotype of the NCL6 disease and lysosomal dysfunction? And second, do these alterations suggest a possible pathway or function of CLN6 or are related to CLN6 in any other way? How these questions were addressed in detail and which results were obtained is explained in the following chapters.

4.1.1 Comparing the lysosomal proteome of wt and *nclf* mice

To investigate and compare the lysosomal proteome of wt and NCL6 diseased samples a mouse model was utilized. The *nclf* mice display a c.316dupC mutation causing a frame shift in their *CLN6* gene, which leads to a stop codon after another 25 amino acids and to the expression of truncated Cln6 proteins that are rapidly degraded (Kurze et al. 2010). The pathology of *nclf* mice includes rear limb paresis at approximately the age of 8 months, which deteriorates gradually and is followed by paralysis and death in

the next months. Furthermore, retinal degeneration, inclusion of storage material mainly in the brain and spinal cord, but also in other tissues like for instance in Kupffer cells of the liver, pathological changes of the brain and neurodegeneration were observed in *nclf* mice (Bronson et al. 1998, Wheeler et al. 2002, Thelen et al. 2012). Thus, these mice show similar symptoms as NCL patients and are a suitable model organism to investigate the proteomic changes in the NCL6 disease. To obtain the lysosomal fraction of wt and *nclf* mice two methods were used resulting in either the highly pure tritosomes or the cruder 20.000 g pellets.

4.1.1.1 Analysis of tritosomes from wt and *nclf* mice by mass spectrometry

Tritosomes present highly purified lysosomal fractions from the liver. They were obtained by several centrifugation steps including a final density gradient centrifugation. Under normal physiological conditions the similar density of lysosomes and other organelles, particularly mitochondria, complicates the enrichment of lysosomes by density gradient-based methods and leads to many contaminants. However, the injection of Triton-WR1339 affects the density of hepatic lysosomes and facilitates the separation of lysosomes from other cellular components in the purification process (Wattiaux et al. 1963). But as Triton-WR1339 only affects the density of hepatic lysosomes, tritosomes cannot be obtained from other tissues. Although NCL6 is a neurodegenerative disease and induces mainly neurological symptoms, also different tissues and peripheral organs including the liver are affected by CLN6 deficiency and show pathological changes (Bronson et al. 1998). Therefore, liver also presents a suitable tissue source for the analysis of proteomic changes in NCL6. Moreover, tritosomes are also an ideal sample source for mass spectrometric analysis, because of their low complexity and little contaminants from other organelles.

After the tritosomes were obtained from wt and *nclf* mice, western blots were performed to verify the comparability, to determine the purification efficiency and to examine the presence of contaminants from the ER and mitochondria (Figure 4.1). Western blots of the lysosomal membrane protein lysosomal-associated membrane protein 1 (Lamp1) and the soluble Ctsz from every purification step showed a similar enrichment between wt and *nclf* samples of the respective proteins. The Lamp1 signal was 10-fold higher in the tritosomes than in the liver homogenate giving an approximate enrichment

efficiency. Moreover, no significant amount of Pdi and carnitine o-palmitoyltransferase 2 (Cpt2), marker for the ER and mitochondria respectively, could be detected in wt and *nclf* tritosomes by western blot, suggesting no considerable contamination by other organelles. These western blot experiments characterize the quality of the tritosomes and show their usability for quantitative measurements.

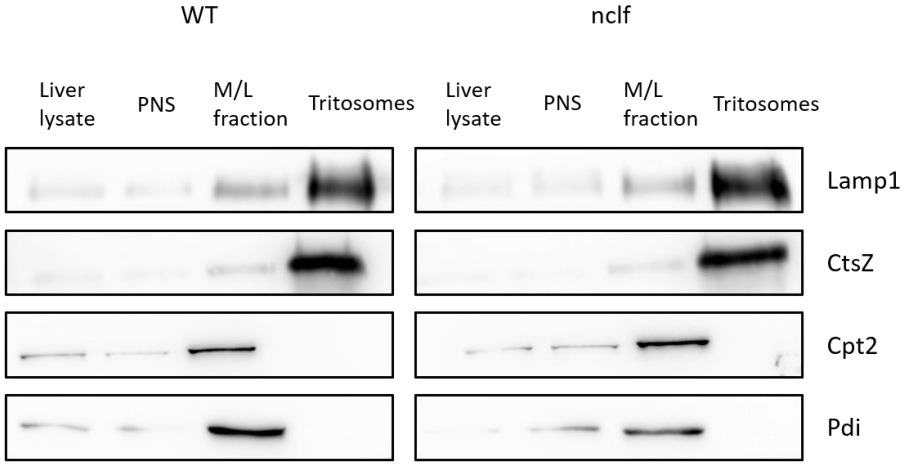

Figure 4.1: Characterization of tritosomes obtained from wt and *nclf* mice by western blots of selected marker proteins
10 µg of protein from *nclf* and wt samples of liver lysate, PNS, the mitochondrial/lysosomal (M/L) fraction and the tritosome fraction were separated by SDS-PAGE, blotted onto PVDF membranes and probed against Lamp1, Ctsz, Cpt2 and Pdi antibodies. The blots show the comparative protein amounts of the four marker proteins for the lysosome, mitochondria and the ER in each stage of the tritosome generation.

The main experiment was the mass spectrometry analysis. After tritosomes from three wt and three *nclf* mice were prepared for mass spectrometry, TMT-labeled and measured, the received data was evaluated carefully regarding any differences between the proteome of lysosomes enriched from normal or nclf mouse liver. In the tritosome samples a total of 1691 proteins could be identified by mass spectrometry and 237 proteins thereof were annotated to the lysosomal compartment according to the protein center database from Protein Discoverer (Figure 4.4). In total 1556 proteins and 227 lysosomal proteins could be quantified. For visualizing the results, a volcano plot was created, in which all quantified proteins were depicted displaying their respective *nclf*/wt $\log_2$ abundance ratios and corrected p-values (Figure 4.2). To sort the data set for the most relevant alterations between *nclf* and wt mice in the proteome, proteins also were listed with respect to their *nclf*/wt abundance ratios and corrected p-values. Proteins displaying a *nclf*/wt log2 fold change of at least -0,75 or 0,75 and a corrected p-

value of less than 0,05 are shown in the table 4.1 on page 63. The most significantly reduced protein in *nclf* tritosomes is sphingomyelin phosphodiesterase (Smpd1), followed by acid ceramidase (Asah1) and N-acylethanolamine-hydrolyzing acid amidase (Naaa), which all constitute lysosomal hydrolases. Overall, 11 lysosomal proteins of the tritosome data set meet the set criteria and therefore, were found in the *nclf* samples at least 50 % less abundant than in the wt samples with a confidence of more than 95 %. Strikingly, eight of these proteins are soluble hydrolases. Only two of the eleven proteins, phosphatidylinositol 4,5-bisphosphate 4-phosphatase and probable phospholipid-transporting ATPase are membrane proteins. Furthermore, the last protein is associated with the lysosomal protein, nucleoporin Seh1 (Seh1). The data set also contains non-regulated lysosomal proteins, for example membrane protein Lamp1 and soluble protein β-hexosaminidase, which show no different protein amounts between healthy and pathological lysosomes. No lysosomal protein was present more abundantly in the *nclf* tritosomes than in the wt tritosomes having a p-value of 0,05. Therefore, the data set shows the tendency for lysosomal proteins being less abundant in the liver samples obtained from mice with Cln6 deficiency when compared to samples from wt mice, which is already visible in the volcano plot as a lop-sided distribution. The data set shows also proteins significantly increased or reduced proteins, which are not annotated to lysosomal compartment. However, solely based on this study it is not apparent, if the regulation of these proteins is in any way linked to the deficiency of Cln6 and might be relevant for the development and understanding of NCL6. Furthermore, it is not clear, which proteins are upregulated due to the diminished degradation capacity and are part of the accumulating storage material. The most reduced non-lysosomal protein is the transmembrane protein 106C and the most increased one is the NAD(P) transhydrogenase.

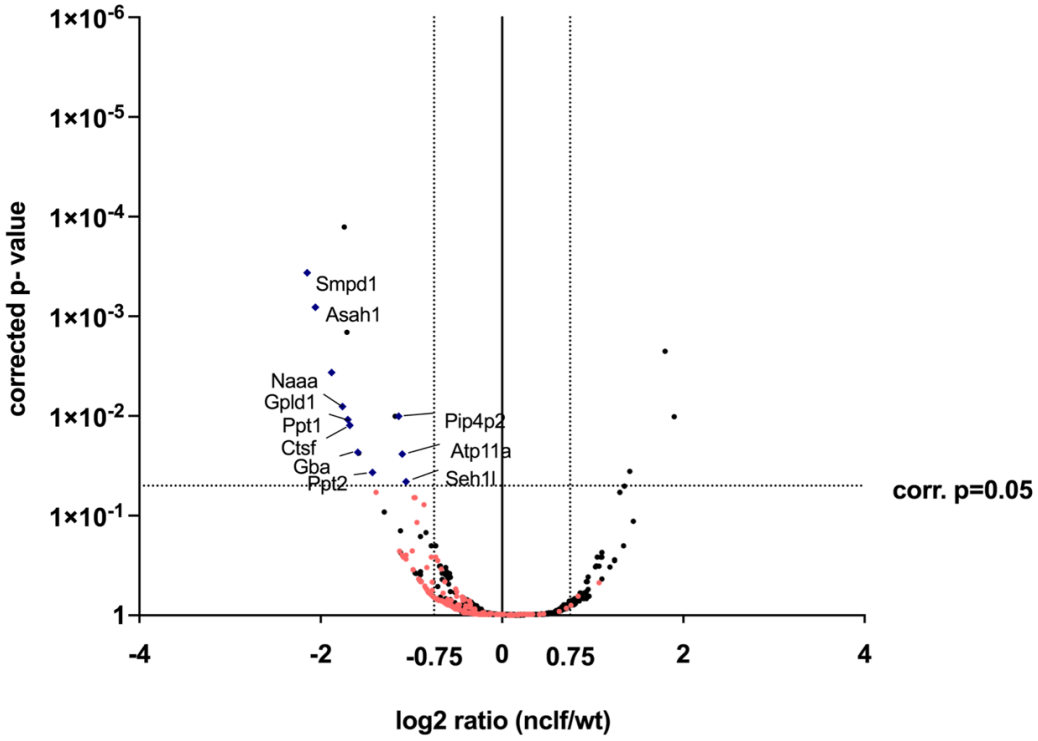

Figure 4.2: Volcano plot of identified and quantified proteins in the tritosome data set
For each protein the corrected p-value is shown on the y-axis and plotted against the log2 *nclf*/wt abundance ratio on the x-axis. Lysosomal proteins significantly reduced at least by 50 % are highlighted (red squares) and labeled with their respective gene names. One outlier, NAD(P) transhydrogenase, was excluded from the graph for purposes of presentation. N=3 biological replicates.

4.1.1.2 Analysis of 20.000 g pellets from wt and *nclf* mice by mass spectrometry

For a valid comparison of wt and *nclf* samples it is a necessary requirement that both are treated uniformly. However, differences between wt and *nclf* mice in the biophysical and biochemical properties of lysosomes for example due to the big variation in storage material could possibly lead to differences in the metabolization of Triton-WR1339 or in the purification of the lysosomal fraction and affect the comparability of tritosomes coming from wt and *nclf* mice. Therefore, the tritosome results have to be validated with a second purification method, which does not rely on a density shift in lysosomes and a density gradient centrifugation. To ensure the validity of the tritosome data set 20.000 g pellets from wt and *nclf* mouse liver tissue were analyzed by mass spectrometry. The generation of 20.000 g pellets is a very simple and fast method to enrich for lysosomal proteins. In this method the post nuclear supernatant is centrifuged

at 20.000 g to sediment the lysosomal fraction. This purification procedure is expected to be less affected by biophysical and biochemical differences in lysosomes and therefore serves as validation for the tritosome data set. However, besides lysosomes, 20.000 g pellets contain also other organelles with a similar density and size, especially mitochondria and peroxisomes and are not as pure as tritosomes (Graham 2002).

After 20.000 g pellets were obtained from wt and *nclf* mice, they were examined by western blot and mass spectrometry in the same way as the tritosomes. Western blots of Lamp1 and Ctsz from liver homogenate and 20.000 g pellets show a similar enrichment between *nclf* and wt samples. However, a much lower enrichment efficiency could be achieved by this method compared to the tritosome enrichment, as the 2,5-fold increase of the Lamp1 signal from homogenates to the final fractions indicates. Furthermore, the marker proteins Pdi and Ctp2 were clearly detected by western blot in the 20.000 g pellets. Thus, these pellets include substantial contaminations of the ER and mitochondria. In summary, the western blots confirm the expected quality and validate the comparability of wt and *nclf* 20.000 g pellets (Figure 4.3).

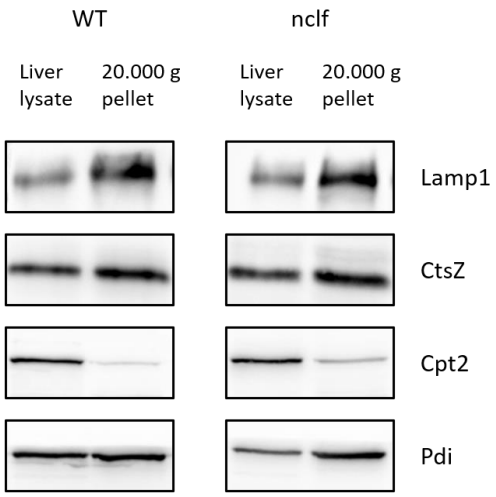

Figure 4.3: Western blots of selected lysosomal, mitochondrial and ER proteins showing their enrichment in wt and *nclf* 20.000 g pellets
10 µg of protein from wt and *nclf* samples of liver lysate and 20.000 g pellets were separated by SDS-PAGE, blotted onto PVDF membranes and probed against Lamp1, Ctsz, Cpt2 and Pdi antibodies. The blots show the comparative protein amounts of the four marker proteins for the lysosome, mitochondria and the ER in the whole liver lysate and the 20.000 g pellet sample.

Alkylated, reduced, trypsinated and TMT-labeled 20.000 g pellets of four wt and four *nclf* mice were measured by mass spectrometry. These results were evaluated regarding relevant proteomic changes and compared to the tritosome data set. As expected, a lot

more proteins, however less proteins annotated to the lysosome were measured in 20.000 g pellets than in tritosomes. In total 2530 proteins, which are 569 more than in the tritosomes and 167 lysosomal proteins, which are 70 less than in the tritosomes were identified. Overall, 2207 proteins and 150 lysosomal proteins could be quantified. Comparing the two purification methods 1257 proteins could be found in both data sets, which equals 50 % and 74 % of all proteins measured in 20.000 g pellets and tritosomes, respectively. Both data sets contain 147 identical lysosomal proteins. 88 % of all lysosomal proteins found in 20.000 g pellets were also measured in tritosomes, but only 62 % of lysosomal proteins detected in tritosomes were present also in 20.000 g pellets (Figure 4.4). The two mass spectrometry proteomics data sets have been deposited to the ProteomeXchange Consortium via the PRIDE (Perez-Riverol et al. 2019) partner repository with the dataset identifier PXD016599.

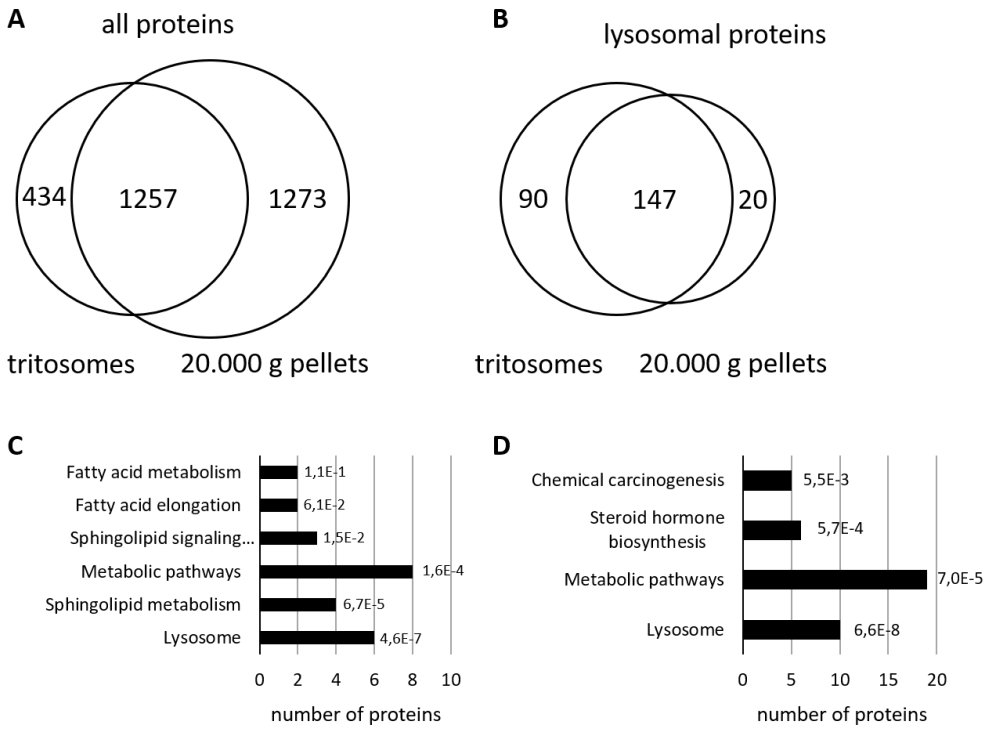

Figure 4.4: Analysis of proteins in mass spectrometry data sets of tritosomes and 20.000 g pellets

Venn diagrams show the overlap of the tritosome and the 20.000 g pellet data set in respect to all identified proteins (A) and the lysosomal proteins (B). KEGG pathway analyses are presented of proteins showing at least a *nclf*/wt fold change of 0,5 and a p-value of < 0,05 in the tritosome data set (C) and the 20.000 g pellet data set (D). For the KEGG pathway analysis of the proteins from the 20.000 g pellets only pathways with at least 5 proteins were included. Benjamini-Hochberg corrected p-values are given next to the respective bars (Huang da et al. 2009).

For visualizing the data of the 20.000 g pellets another volcano plot was created (Figure 4.5). Again, the results were sorted and proteins with a *nclf*/wt log2 fold change of at least -0,75 or 0,75 and a corrected p-value < 0,05 are listed in table 4.1 altogether with the proteins from the tritosome data set. In total, there are 16 lysosomal proteins, which meet these criteria in the 20.000 g pellet mass spectrometry data set. Both data sets have four lysosomal proteins, namely **Asah1**, **Ppt1**, **Ctsf** and **Gba** in common with the chosen cut-off criteria. Table 4.1 displays overall comparability between the purification methods used for obtaining tritosomes and 20.000 g pellets. Interestingly, again soluble hydrolases account for the majority of these 16 proteins. There is only one exception, the lysosomal membrane protein Lamp2. The overall observations are completely in line with the previous findings in the mass spectrometry results of wt and *nclf* tritosomes and the general remarks from the tritosome data set apply here as well. Therefore, the 20.000 g pellet data set gives no new insights in the alterations of the wt and *nclf* proteome, however it verifies the results obtained with tritosomes. In contrast to the tritosome data set, in which no lysosomal protein could be measured with a *nclf*/wt log2 abundance ratio > 0,75 and a corrected p-value of 0,05 two lysosomal proteins in the 20.000 g pellet data set meet these criteria, namely progranulin and transmembrane protein 106B with an abundance ratio of 1,98 and 2,23 respectively. The abundance ratios of many more non-lysosomal proteins are reduced or increased in the 20.000 g pellet data set compared to the tritosome results, which is not surprising as the entire protein count is also substantially higher. Alpha-1-antitrypsin 1-5 shows the lowest ratio and Cytochrome P450 3A16 the highest, both with corrected p-values of at least 0,05.

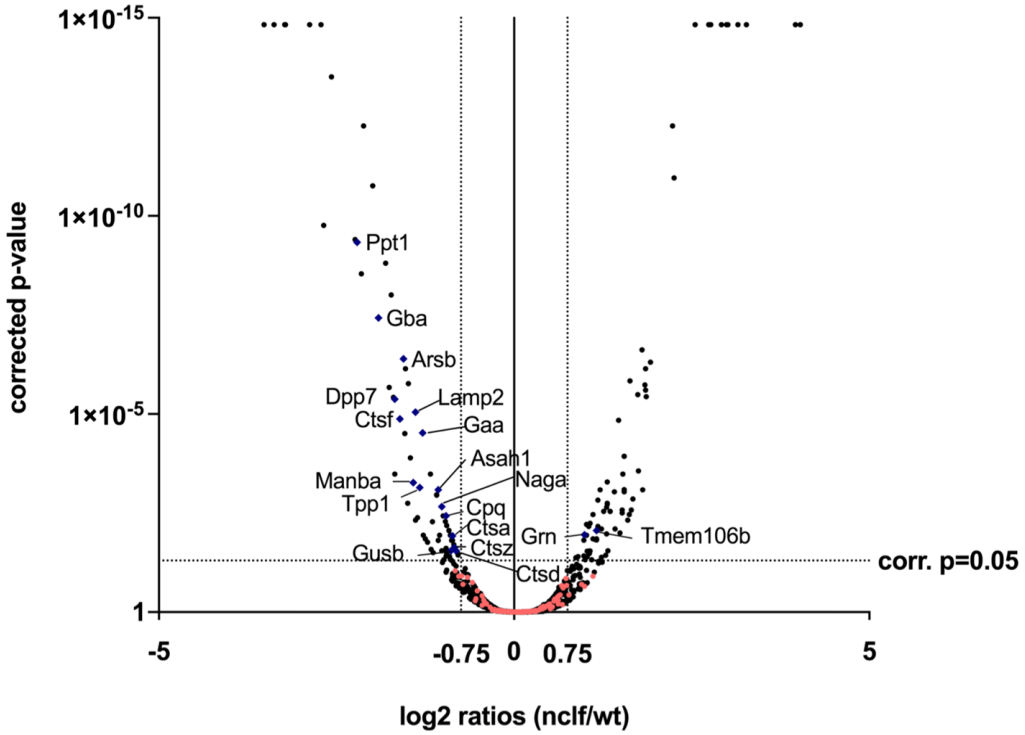

Figure 4.5: Volcano plot of identified and quantified proteins of the 20.000 g pellet data set
For each protein the corrected p-value is shown on the y-axis and plotted against the log2 nclf/wt abundance ratio on the x-axis. Lysosomal proteins significantly reduced at least by 50 % are highlighted (red squares) and labeled with their respective gene names. N=4 biological replicates.

Table 4.1: Regulated proteins in the tritosome and 20.000 g pellet data sets
Proteins with a log2 wt/nclf abundance ratio lower than -0,75 or greater than 0,75 and a corrected p-value of at least 0,05 are listed and the abundance ratios of the two data sets are compared. Proteins, which are significantly regulated in both data sets are highlighted.

Accession	Protein name	Gene Symbol	Log2 Tritosomes	Corrected p-value	Log2 20.000 g pellets	Corrected p-value
O35448	Lysosomal thioesterase PPT2	Ppt2	-1,43	3,68E-02	-0,83	9,08E-02
O70362	Phosphatidylinositol-glycan-specific phospholipase	Gpld1	-1,76	8,04E-03	-0,72	1,99E-01
O88531	Palmitoyl-protein thioesterase 1	Ppt1	-1,7	1,08E-02	-2,21	4,63E-10
O89023	Tripeptidyl-peptidase 1	Tpp1	-1,13	2,27E-01	-1,33	7,18E-04
P12265	Beta-glucuronidase	Gusb	-0,6	7,83E-01	-0,89	2,83E-02
P16675	Lysosomal protective protein	Ctsa	-0,61	7,69E-01	-0,87	1,20E-02
P17047	Lysosome-associated membrane glycoprotein 2	Lamp2	-0,89	4,60E-01	-1,39	9,02E-06
P17439	Lysosomal acid	Gba	-1,59	2,31E-02	-1,91	3,77E-08

	glucosylceramidase					
P18242	Cathepsin D	Ctsd	-1,08	2,60E-01	-0,82	2,82E-02
P28798	Progranulin	Grn	-0,03	9,76E-01	0,99	1,12E-02
P50429	Arylsulfatase B	Arsb	-0,74	6,70E-01	-1,56	4,05E-07
P70699	Lysosomal alpha-glucosidase	Gaa	-0,72	6,89E-01	-1,29	3,00E-05
P98197	Probable phospholipid-transporting ATPase	Atp11a	-1,1	2,40E-02	nd	nd
Q04519	Sphingomyelin phosphodiesterase	Smpd1	-2,15	3,65E-04	nd	nd
Q80X71	Transmembrane protein 106B	Tmem106b	-0,68	7,10E-01	1,16	8,76E-03
Q8K2I4	Beta-mannosidase	Manba	-0,58	7,90E-01	-1,42	5,38E-04
Q8R2U0	Nucleoporin	Seh1l	-1,06	4,56E-02	nd	nd
Q9CZX7	Type 2 phosphatidylinositol 4,5-bisphosphate 4-phosphatase	Tmem55a	-1,14	1,01E-02	nd	nd
Q9D7V9	N-acylethanolamine-hydrolyzing acid amidase	Naaa	-1,88	3,66E-03	nd	nd
Q9ET22	Dipeptidyl peptidase 2	Dpp7	-0,72	6,89E-01	-1,68	4,20E-06
Q9QWR8	Alpha-N-acetylgalactosaminidase	Naga	-0,59	7,83E-01	-1,02	2,19E-03
Q9R013	Cathepsin F	Ctsf	-1,68	1,24E-02	-1,61	1,34E-05
Q9WUU7	Cathepsin Z	Ctsz	-0,66	7,16E-01	-0,84	2,37E-02
Q9WV54	Acid ceramidase	Asah1	-2,06	8,13E-04	-1,07	8,23E-04
Q9WVJ3	Carboxypeptidase Q	Cpq	-0,6	7,83E-01	-0,96	3,73E-03

4.1.1.3 Western blot analysis of selected proteins from the mass spectrometry data sets

The differences of specific proteins in the proteome between wt and *nclf* tritosomes was determined by western blot to assure that the obtained results are method independent and not affected by the mass spectrometry analysis. Ctsd, Ctsz, Ppt1 and Tpp1 were selected, showing *nclf*/wt abundance ratios of 0,472; 0,631; 0,456 and 0,307 in the tritosome data set, respectively. Ctsd, Ppt1 and Tpp1 were chosen, due to their relation to NCL, as their deficiency causes other NCL subtypes and due to their proposed interaction with CLN6 in a recent publication. These previously published data also show a significant reduction of Ctsd, Ppt1 and Tpp1 in *nclf* mouse liver, however do not indicate that Ctsz is significantly reduced in *nclf* samples (Bajaj et al. 2020). Therefore, Ctsz was selected to validate the mass spectrometry data set also with a lysosomal

hydrolase, which is, in contrast, neither known to interact with CLN6 nor to be related to NCLs. Western blots were performed using equal protein amounts of wt and *nclf* samples. Proteins were separated by SDS-PAGE and transferred to PTFE membranes. After developing the blots and generating the images, the bands were quantified and statistically evaluated by an unpaired student's t-test (Figure 4.6). For the quantification of Ctsd the bands of the mature, the heavy and light chain were used and a 69 % reduction of Ctsd in tritosomes of *nclf* mice was determined. Ctsz, Ppt1 and Tpp1 were found 24 %, 79 % and 70 % reduced, respectively. The reduction of all proteins besides Ctsz was significant. Importantly, the results show similar reductions of the selected proteins compared to the mass spectrometry data set. Sorted by their abundance ratios these proteins are listed in the same order in both analyzes, as Ppt1 displays the greatest and Ctsz the lowest reduction. Because one *nclf* sample seems to be an outlier, the quantifications were normalized to Lamp1, which was not regulated in the mass spectrometry data sets. Due to insufficient sample material and that the incubation with Lamp1 on the same blot was not possible anymore, a separate blot was used for Lamp1. The results are given in Fig. 4.6 (C) and show no substantial difference to the quantification without normalization. However, the standard deviations are apparently lower, which leads to Ctsz being also significant reduced in *nclf* tritosomes.

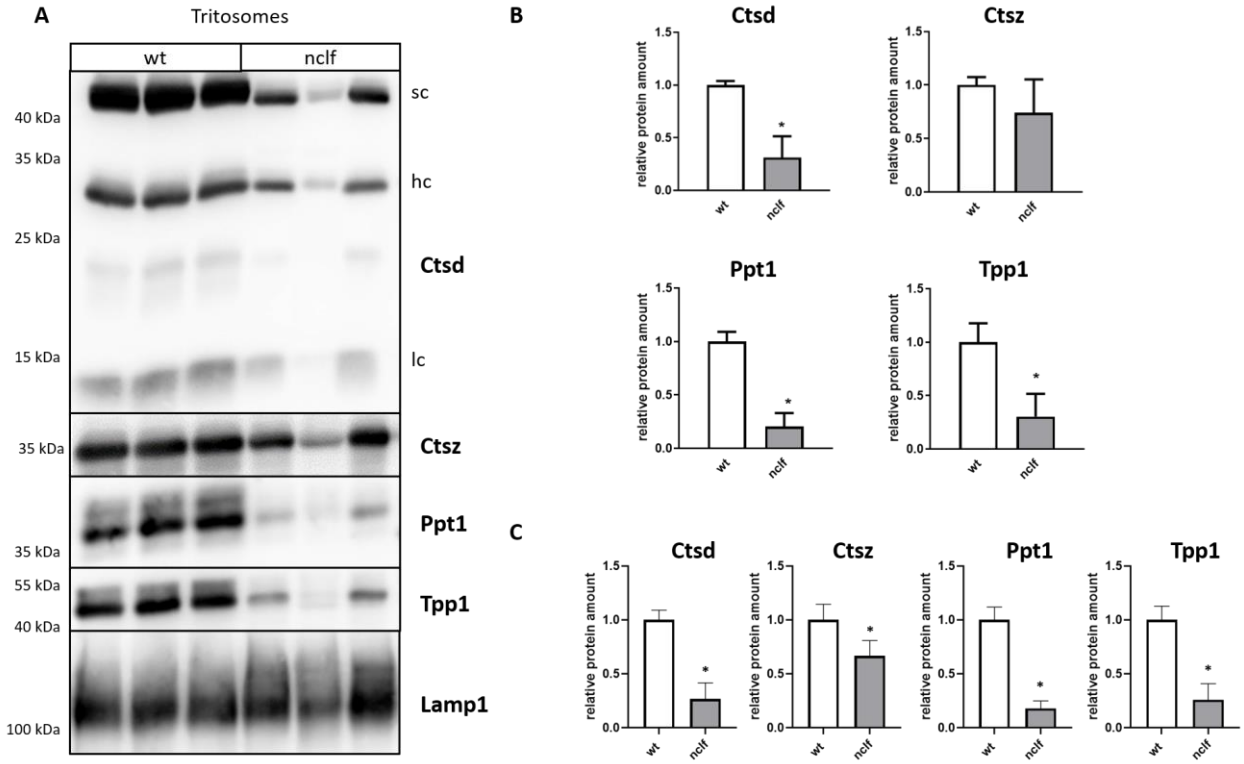

Figure 4.6: Quantitative comparison of protein abundances from selected proteins in wt and *nclf* tritosomes by western blot
(A) Equal protein amounts of wt and *nclf* tritosome fractions were separated by SDS-Page, blotted onto a PVDF membrane and probed with antibodies against Ctsd, Ctsz, Ppt1 and Tpp1, respectively. Shown are three biological replicates each. sc = single chain, hc = heavy chain, lc = light chain of fully mature Cathepsin D. (B) Densitometric quantifications of Ctsd, Ctsz, Ppt1 and Tpp1 are depicted in bar graphs showing the relative protein amount in *nclf* tritosomes as the protein amount of wt control samples was set to 1. (C) The relative protein amounts of Ctsd, Ctsz, Ppt1 and Tpp1 in wt and *nclf* tritosomes were normalized to Lamp1, which was blotted on a separate membrane. An unpaired student's t-test was performed and significant differences were indicated. * = p-value < 0,05. N = 3.

4.1.1.4 Western blot analysis of whole liver lysates from wt and *nclf* mice

Subcellular fractions like tritosomes and 20.000 g pellets present the advantage for proteomic analyses that many proteins of non-lysosomal subcellular location are depleted and therefore, the identification and quantification of the lysosomal proteins are facilitated. However, the fractionation can lead to wrong conclusions about the overall abundance of a lysosomal protein. If CLN6 deficiency causes redistribution of proteins from the lysosomes to for example the endoplasmic reticulum or misdirection of proteins their abundances in fractionated lysosomes are reduced but overall abundances remain unchanged. To determine the if a redistribution or misdirected transport of the proteins is the cause of the detected proteomic changes, tritosomes and 20.000 g pellets were further analyzed in whole mouse liver tissue by western blot. As western blots of Tpp1 were not usable for quantification due to excessive unspecific binding, only Ppt1, Ctsz and Ctsd were quantified after being normalized to actin. While Ppt1 and Ctsd were reduced by 70 and 89 %, respectively, the protein amount of Ctsz, however, was increased by 30 %. The differences in the protein amount of Ppt1 and Ctsz were significant. As shown in figure 4.7 in the western blots of Ppt1 and Ctsd a lot more protein bands apart from those corresponding to their specific mature isoforms are present. In the case of Ppt1, there is a protein band closely above the 25 kDa marker, which is much fainter in the *nclf* samples similar as the signal of the canonical Ppt1 at 34 kDa. Furthermore, the blot of Ctsd shows, besides the mature heavy chain other bands resulting from unspecific binding, also the bands of procathepsin D and preprocathepsin D, which appear fainter in *nclf* samples compared

to the wt control samples. However, the difference between wt and *nclf* samples is not as pronounced as it is for the heavy chain of mature Ctsd.

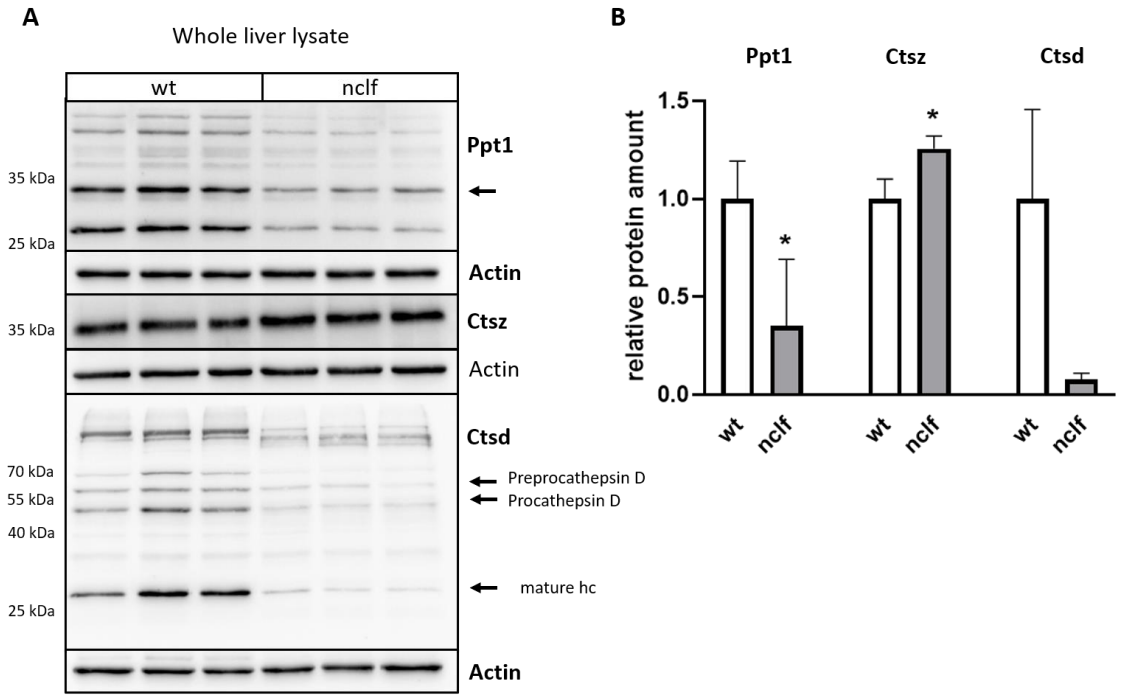

Figure 4.7: Quantitative comparison of protein abundances from selected proteins in whole liver lysates from wt and *nclf* mice by western blot
(A) Equal protein amounts of whole liver lysates from wt and *nclf* mice were separated by SDS-Page, blotted onto a PVDF membrane and probed with antibodies against Ppt1, Ctsz and Ctsd, respectively. Shown are three biological replicates each. hc = mature heavy chain of cathepsin D. (B) Densitometric quantifications of Ppt1, Ctsz and Ctsd are depicted in a bar graph showing the relative protein amounts in whole liver lysates of *nclf* mice as the protein amount of wt control samples was set to 1. The mature heavy chain of cathepsin D and the canonical 34 kDa isoform of Ppt1 were used for quantification. Protein amounts were normalized to actin. An unpaired student's t-test was performed and significant differences were indicated. * = p-value < 0,05. N = 3.

4.1.1.5 Western blot analysis from brain tissue of selected proteins from the mass spectrometry data sets

Since NCL is a neurodegenerative disease, it impacts in particular the neural system (Anderson et al. 2013). For this reason, 20.000 g brain pellets and whole brain lysates of wt and *nclf* mice were also analyzed by western blot to test if the proteomic changes observed in liver tissue are present also in the brain and could potentially be a general pathological effect. The protein amounts of Ctsz, Ppt1 and Tpp1 were determined in wt and *nclf* samples. However, it was not possible to quantify Ctsd in the mouse brain samples, because the antibody exhibited too much unspecific binding. Actin was used as a loading control. The results showed for all three proteins a reduction in 20.000 g pellets obtained from *nclf* mice compared to the wt samples. Ppt1 was detected 68 %,

Tpp1 40 % and Ctsz 25 % less abundant in these samples. Interestingly, in the brain homogenate only Ppt1 was reduced by 31 %. However, Tpp1 and Ctsz were found increased by 44 and 78 % in brain lysates from *nclf* mice compared to the wt samples.

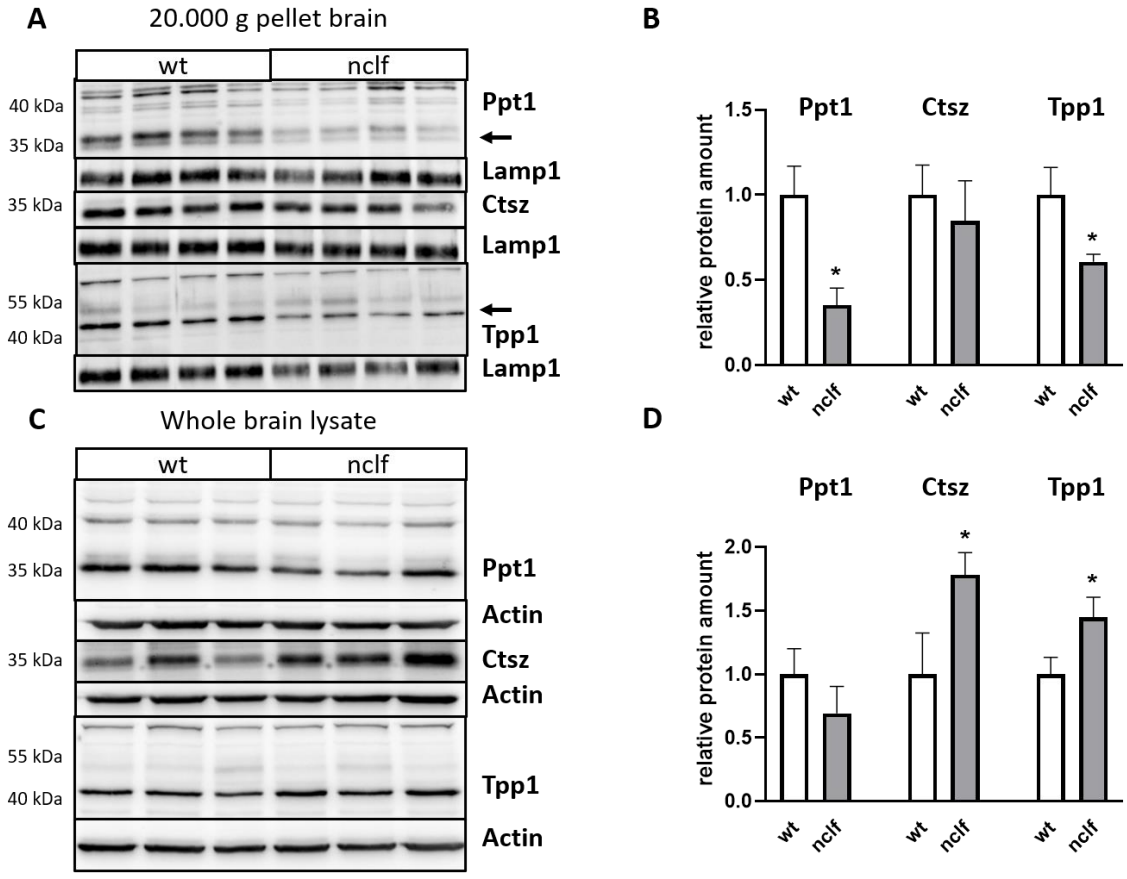

Figure 4.8: Quantitative comparison of protein abundances from selected proteins in 20.000 g pellets and whole lysates from wt and *nclf* mouse brain by western blot
Equal protein amounts of (A) 20.000 g brain pellets or (C) whole brain lysates from wt and *nclf* mice were separated by SDS-Page, blotted onto a PVDF membrane and probed with antibodies against Ppt1, Ctsz and Tpp1, respectively. Shown are four biological replicates for the 20.000 g pellet samples and three replicates for the whole brain lysates. (B and D) Densitometric quantifications of Ppt1, Ctsz and Tpp1 are depicted in bar graphs showing the relative protein amounts in 20.000 g pellets and whole brain lysates of *nclf* mice as the protein amount of wt control samples was set to 1. Protein amounts were normalized to actin. An unpaired student's t-test was performed and significant differences were indicated. * = p-value < 0,05. N = 3

4.1.1.6 Ezyme activity assays of three lysosomal hydrolases selected from the mass spectrometry data sets

Various hydrolases were found to be substantially less abundant in *nclf* tritosomes and 20.000 g pellets of the mass spectrometry data sets. To verify, if the reduced protein amount also leads to a decreased enzyme activity, enzyme activities of Ctsd, Ppt1 and Gba were determined in wt and *nclf* samples (Figure 4.9). The reduction of Gba in the mass spectrometry data set is very interesting, as Gba is known to be transported to the Golgi by LIMP2 and independently of CLN8. Thus, its depletion suggests that the function of CLN6 is not exclusively linked to CLN8 and the EGRESS complex. However, the protein amount in tritosome and 20.000 g pellets of Gba could not be quantified by western blot due to various polypeptide signals, which do not correspond to the mature Gba isoform and have a higher intensity than the specific signal of Gba (data not shown). Therefore, the Gba activity assay was performed to validate the significant depletion of Gba detected by the mass spectrometric analyses. The enzyme activity assays of all three hydrolases, Ctsd, Gba and Ppt1, show a significant reduction in enzyme activity of *nclf* samples compared to the wt control. The activities of Ctsd and Gba were measured in tritosomes, whereas the activity of Ppt1 was determined in whole liver lysates.

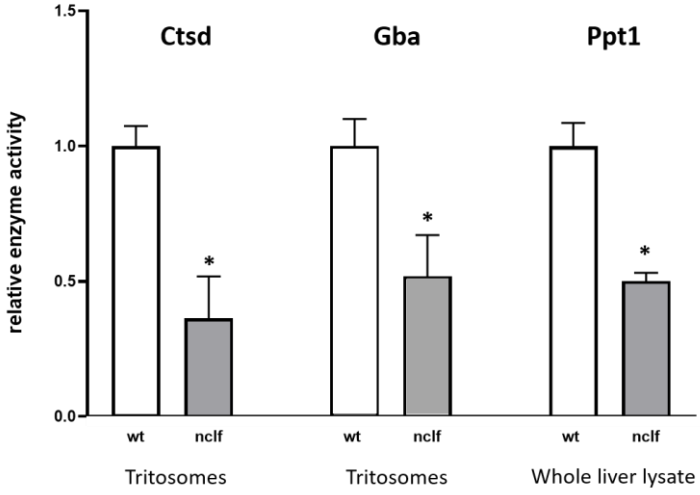

Figure 4.9: Enzyme assays show decreased activities of Ctsd, Gba and Ppt1 in *nclf* samples
Fluorometric enzyme activity measurements for Ctsd and Gba in tritosome samples and for Ppt1 in whole liver lysates. Equal protein amounts were applied to fluorogenic substrates and after the incubation time the reaction was terminated and the fluorescence intensities were determined and compared. Significance was determined by unpaired student's t-test, * = $p < 0.05$, N=3

4.2 Identifying novel interaction partners of CLN6

Besides analyzing the lysosomal proteome of cells with CLN6 deficiency, this study deals with CLN6's direct interaction partners as the second major research subject. At the beginning of this study not many interaction partners of CLN6 had been discovered and also there were no functional relation of proteins with CLN6 known that explained its crucial role for lysosomal homeostasis, although various experiments have already been conducted to address this issue. In this study the BioID approach was utilized, which has not yet been applied in the context of CLN6 (Li et al. 2017). Subsequently several candidate proteins were further evaluated regarding their interaction with CLN6 by the BiFC assay. The aim of finding novel interaction partners is to gain more insight about CLN6, as its interaction partners could point towards its function and contribute to a better understanding of the NCL disease.

4.2.1 Utilizing the BioID approach to determine CLN6´s interactome

The concept of the BioID approach is to label and identify proteins, which are located in close proximity with a distance of about 10 nm from the protein of interest (Roux et al. 2012). More specifically, a cDNA construct is created containing a biotin ligase fused to the protein of interest. After transfection and expression of this fusion protein, the ligase biotinylates proteins nearby in the presence of biotin and ATP. As interaction partners are located in close proximity of each other, using the BioID approach it is expected that especially these interacting proteins are labeled. Adding the biotin ligase to CLN6 can potentially affect how it is being processed, its location, structure and function. CLN6 retaining its normal physiological state however is essential for finding relevant interaction partners. Fortunately, the topology of CLN6 is suitable for this approach, as CLN6 having its N-terminus in the cytoplasm and its C-terminus in the ER lumen. Therefore, both compartments can be examined in respect to potential interaction partners by fusing the ligase either at the N-terminus or at the C-terminus to CLN6.

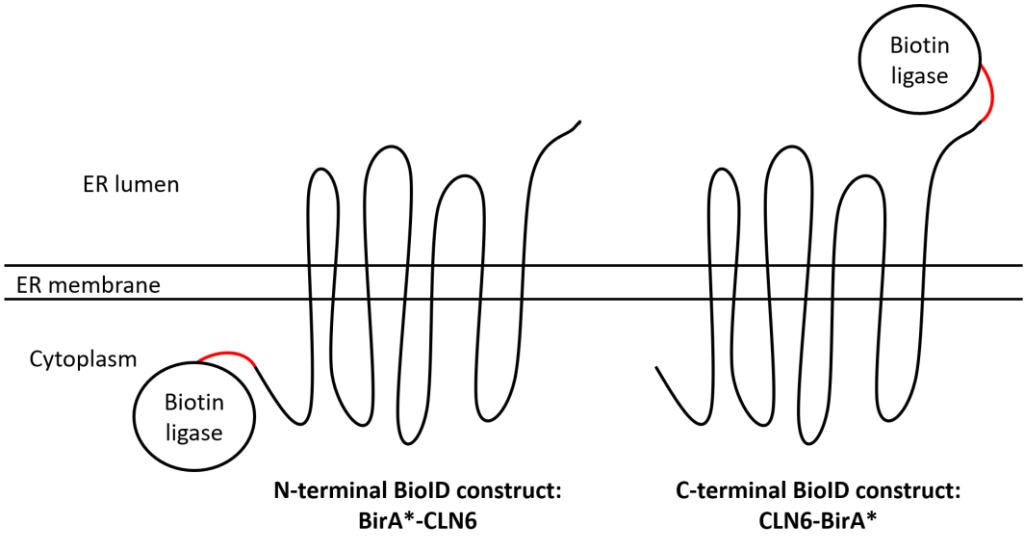

Figure 4.10: Schematic representation of the BioID constructs
Shown are the BioID constructs, in which the biotin ligase BirA* is fused by a linker to the N- and the C-terminus of CLN6, respectively. In case of the N-terminal BioID construct, the biotin ligase is present in the cytoplasm, whereas in the C-terminal construct it is located in the ER lumen.

Coupling the BioID approach with mass spectrometry enables the identification of the labeled proteins in a relatively simple and straightforward way. Before the mass spectrometric measurements, the samples were validated by western blot in regard to their proper transfection and biotinylation. Besides the sample with biotinylated proteins the experiment included two controls. In control 1 no biotin was added to the media and control 2 lacked the fusion protein. To distinguish between the sample and the two controls the cells were SILAC labeled before treatment (Thelen et al. 2017). As label switch experiments with three differently SILAC labeled cells were performed one experiment included three samples with biotinylated proteins, three times the control 1 and three times the control 2. Samples, controls 1 and controls 2 were labeled light, medium or heavy respectively and resulting in overall six sample/control abundance ratios. For example, the sample, which was labeled light was compared to the controls with a medium and heavy label. The arbitrary cut off for the sample/control 1 and sample/control 2 abundance ratios, which should point out reliable biotinylation was set at 2. Proteins were classified as potentially relevant, if they meet this cut off in four out of six possible abundance ratios. Several experiments were conducted and the results were compared to obtain reliable data. Based on this data candidate proteins were chosen, which potentially interact with CLN6.

4.2.1.1 Assessment of the expression of the BirA*-CLN6 and CLN6-BirA* fusion proteins and the biotinylation by western blot

After the HEK cells were transfected with the BioID constructs and biotin was added to the media after 24 h of transfection, the cells as well as the control cells were harvested and lysed. The lysates were analyzed by western blots confirming the proper expression of the BirA*-CLN6 and CLN6-BirA* fusion proteins and the biotinylation to ensure only samples containing a sufficient number of biotinylated proteins were used for further time- and cost-consuming mass spectrometric analysis. In figure 4.11 exemplary western blot images of one label switch experiment show the expression of BirA*-CLN6, the N-terminal BioID construct, and the extent of biotinylation of the sample as well as the two negative controls for all SILAC labels. The expression of the N-terminal BioID construct was validated by probing against a CLN6 and an α-myc antibody, as it contains a myc-tag at the C-terminus. The first blot (Figure 4.11A) was incubated with an α-myc antibody. In the SILAC labeled samples (lanes 9-11) and controls (lanes 3-5), which were transfected with BirA*-CLN6, the antibody identified polypeptides with a mass corresponding to the fusion protein slightly underneath the 70 kDa marker, as CLN6 and BirA* have a molecular weight of 36 and of 35 kDa, respectively. Moreover, in lane 12 (Figure 4.11A) there is an unexpected signal visible. HEK cells were transfected with CLN6-myc, lysed and included as positive control. Besides the identified polypeptide signal corresponding to CLN6-myc, there is another protein band underneath, which might indicate a degradation product of CLN6-myc.

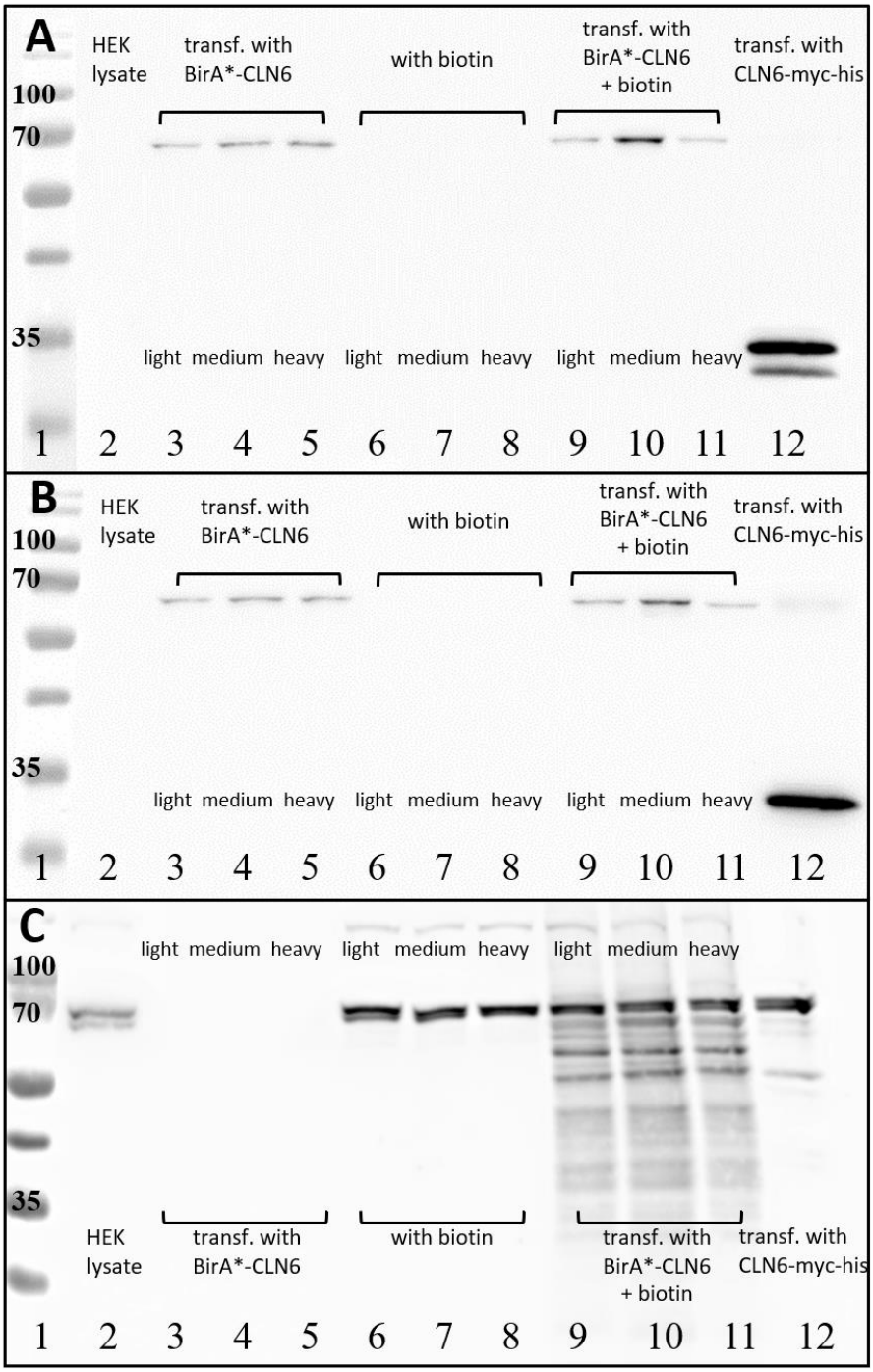

Figure 4.11: Expression of BirA*-CLN6 and biotinylation in HEK cells were evaluated by western blot images

The expression of the BirA*-CLN6 fusion protein in transfected HEK cells was verified by (A) a α-myc and (B) α-CLN6 antibody. (C) Biotinylation was determined by incubating the blot with HRP-streptavidin. Each blot shows the marker (lane 1), lysate of untreated HEK cells as a negative control, lysates of HEK cells, which were transfected with the BioID construct (control 1; lanes 3-5), lysates of HEK cells, which were treated with biotin (control 2; lanes 6-8), lysates of HEK cells, which were treated with biotin and transfected with the BioID construct (sample; lanes 9-11) and lysate of HEK cells transfected with a myc- and his-tagged CLN6 as positive control (lane12). Sample and controls are labeled light, medium and heavy, respectively.

The blot in figure 4.11B was incubated with antibody raised against CLN6 and verifies the result of the first blot (Figure 4.11A) showing the same polypeptide signals except that the second polypeptide signal in lane 12 is not present. This also suggest that the second signal might be a degradation product, which lacks a N-terminal part of CLN6-myc, as the CLN6 antibody was obtained by an immunization using a peptide containing CLN6's amino acids 2-20. In both blots (4.11. A and B) in the various lanes there are differences in the intensities of the signals, which can be easily observed by the naked eye and indicate also differences in the abundances of the transfected fusion protein. Finally, the last blot in the image (Figure 4.11C) was probed against Steptavidin-HRP and therefore, indicates biotinylated proteins. It gives evidence on the biotinylation of proteins from transfected and with biotin treated HEK cells (lanes 9-11). There seems to be no notable difference in the extent of biotinylation between the differently SILAC labeled samples. Interestingly, also the varying protein expressions of the fusion protein do not affect the number of biotinylated proteins drastically as lane 10 depicts the most intense signal for the fusion protein (Figure 4.11A+B) but does not display the same intensity variations in the biotinylation blot (Figure 4.11C). As expected, no extensive biotinylation occurs in HEK cell, which were not treated with biotin (control 1; lanes 3-5) or which did not express the BioID construct (control 2; lanes 6-8). There are only two unspecific polypeptide signals detectable in control 2 (Figure 4.11 lanes 6-8), which are also produced by the lysate of untreated HEK cells (lane 2) and therefore they cannot be induced by the addition of biotin.

After expression of the N-terminal fusion protein and its biotinylation was assessed, the CLN6-BirA* construct with the biotin ligase attached at the C-terminus was examined accordingly. The respective western blots are depicted in figure 4.12, which verify the expression and biotinylation. The expression level of the fusion protein was determined with an α-his antibody, what is depicted in the first blot (Figure 4.12A lanes 3-5 and 9-11). Although the antibody causes an unspecific band in all lanes, the fusion protein can be visualized clearly by a signal located between the 70 kDa and 55 kDa marker and therefore lies approximately in the same range as the N-terminal BioID construct. Again, the proper expression was validated in the second blot (Figure 4.12B) with the CLN6 antibody. In the third blot (Figure 4.12C) the proper biotinylation of the sample is validated as the lanes 9-11 show biotinylated proteins.

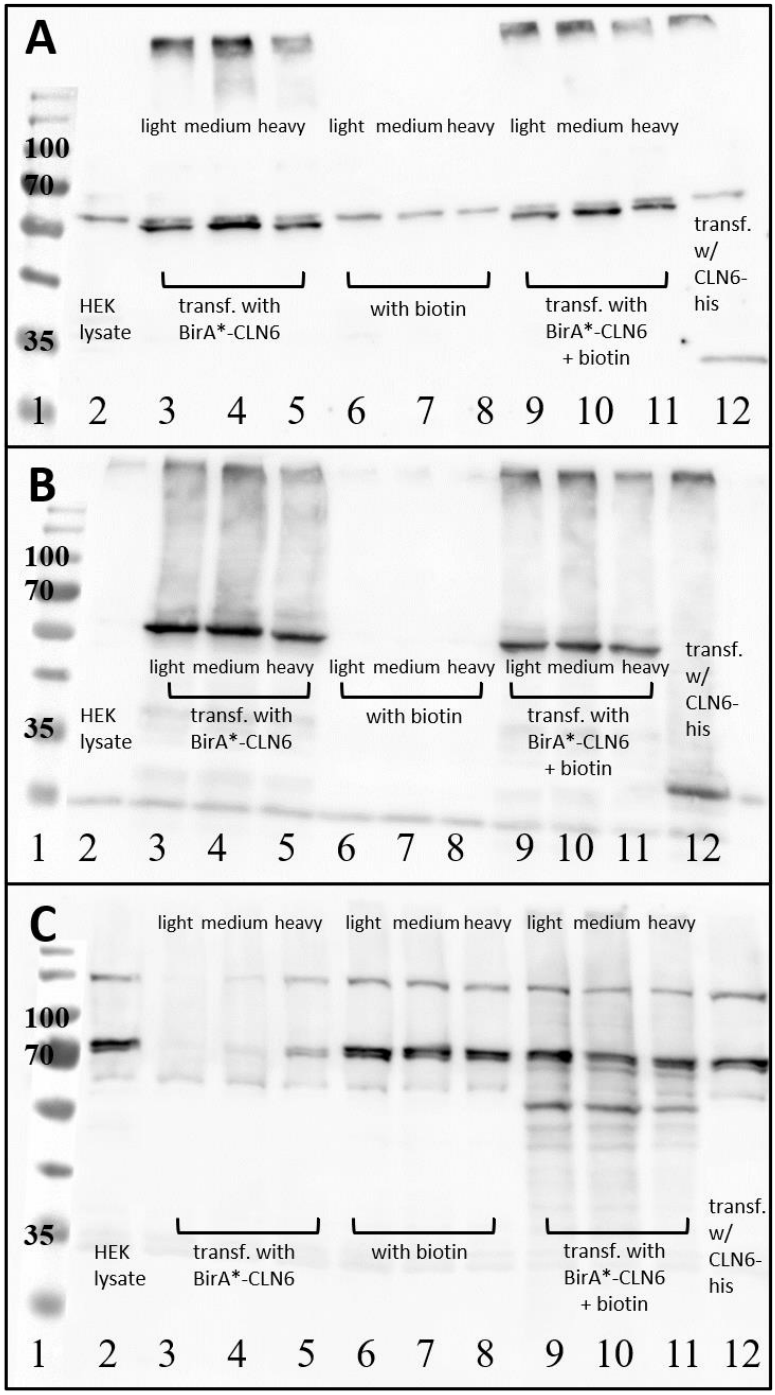

Figure 4.12: Expression of CLN6-BirA* and biotinylation in HEK cells were evaluated by western blot images

The expression of the CLN6-BirA* fusion protein in transfected HEK cells was verified by (A) a α-myc and (B) α-CLN6 antibody. (C) Biotinylation was determined by incubating the blot with HRP-streptavidin. Each blot shows the marker (lane 1), lysate of untreated HEK cells as a negative control, lysates of HEK cells, which were transfected with the BioID construct (control 1; lanes 3-5), lysates of HEK cells, which were treated with biotin (control 2; lanes 6-8), lysates of HEK cells, which were treated with biotin and transfected with the BioID construct (sample; lanes 9-11) and lysate of HEK cells transfected with a myc- and his-tagged CLN6 as positive control (lane12). Sample and controls are labeled light, medium and heavy, respectively.

The controls show no notable biotinylation as signals in the respective lanes are most probable caused by unspecific binding or aggregated proteins not running correctly in the SDS-PAGE. Comparing western blot images of biotinylated proteins generated by the N- and C-terminal BioID construct, the band patterns seem to be slightly different. This is not surprising, as the constructs are located in different compartments containing a different set of proteins. Overall, western blot is a useful and crucial method to assess the expression of the fusion proteins consisting of CLN6 and BirA* as well as the extent of biotinylation in HEK cells before further investigations.

4.2.1.2 The influence of different incubation times with biotin on biotinylation

After the addition of biotin, the number of biotinylated proteins in a cell containing a biotin ligase increases over time and is expected to reach its maximum when degradation and secretion of biotinylated proteins and their formation are in balance. In case the biotin ligase is linked to another protein, the biotinylation is affected by the location and lifecycle of this protein. The extent of biotinylation at different incubation times with biotin was evaluated by western blot to select an appropriate incubation time for the identification of biotinylated proteins by mass spectrometry. Therefore, HEK cells were transfected with the BirA*-CLN6 fusion protein and harvested 48 h after transfection. Biotin was added to the cell culture media 15 min, 1, 3, 6, 12 or 24 h before the cells were harvested. Afterwards cells were lysed and subjected to western blot (Figure 4.13).

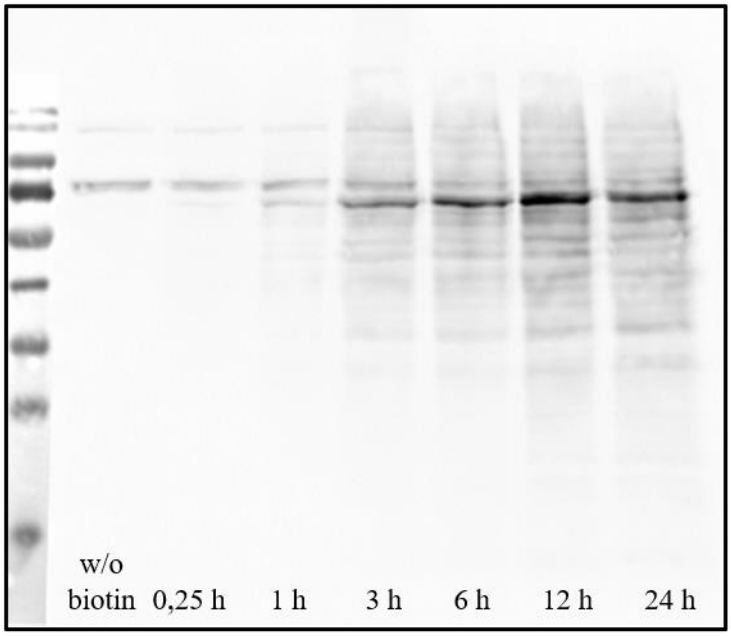

Figure 4.13: Extent of biotinylation after different incubation times with biotin
HEK cells were transfected with the BirA*-CLN6 fusion protein. Then biotin was added either 15 min, 1, 3, 6, 12 or 24 hours before the cells were harvested and lysed. Also, a negative control was included with no addition of biotin. All samples were evaluated by western blot using Streptavidin-HRP to show biotinylated proteins.

The result shows a continuous increase in biotinylated proteins. Biotinylation for 1 h or less leads to no clearly visible signals of biotinylated proteins on the western blot. However, after 3 h of biotinylation numerous proteins can be detected, as a large extent of the lane is stained. The intensity of the polypeptide signals increases until the incubation time of 12 h notably. Between 12 and 24 hours there is no major difference in the extent of biotinylation observable anymore. As below the detection limit of the mass spectrometer no identification of biotinylated proteins is achievable and very complex protein samples can also lead to proteins being not identified due to the measuring capacity of the mass spectrometer two extreme contrary incubation times, 2 h and 24 h, were chosen for initial testing their suitability in mass spectrometry experiments.

4.2.1.3 Comparison of identified biotinylated proteins by mass spectrometry obtained with biotin incubation times of 2 and 24 h

Two BioID label switch experiments with the N-terminal construct and either 2 h or 24 h of biotin incubation were performed. One label switch experiment results in 6 sample/control abundance ratios. The incubation time of 2 h yielded 413 proteins, of

which 18 met the cut off criteria of 2 in at least 4 out of 6 abundance ratios, whereas 24 h of biotin incubation resulted in 953 total proteins and 123 thereof meeting the cut off. As expected, a longer biotinylation time leads to more proteins, namely double as much total proteins and even about 5 times more proteins meeting the arbitrary cut off criteria comparing the two BioID experiments with 2 and 24 h. Thus, not only the protein number but also the ratio between biotinylated and not biotinylated proteins increases with the biotin incubation time. When taking the proteins fulfilling the cut off requirements, only 6 proteins were shown in the 2 h data set, which are not included in the 24 h data set, however vice versa 111 proteins were not identified in the 2 h data set, which were present in the 24 h data set. This means that only 6 proteins were not identified due to longer incubation with biotin and the resulting greater number of biotinylated proteins in the BioID experiment with 24 h biotin incubation. Half of the proteins, which are exclusively determined in the data set with a 2 h biotin incubation, are directly related to the translation process and suggest that the biotinylation started prior to CLN6 reaching its natural location. As the biotin ligase is translated before CLN6, it is able to biotinylate proteins immediately after its proper folding and potentially also before CLN6 is completely expressed. The other 3 proteins do normally not reside in the ER or the cytoplasm. The protein IDs of both data sets are listed in the annex. Considering the result of the comparison between 2 h and 24 h biotin incubation, the longer incubation time was chosen for further BioID experiments, mostly because only a comparatively small number of proteins is lost in mass spectrometric analyses due to the increase in biotinylation time and in the sample complexity.

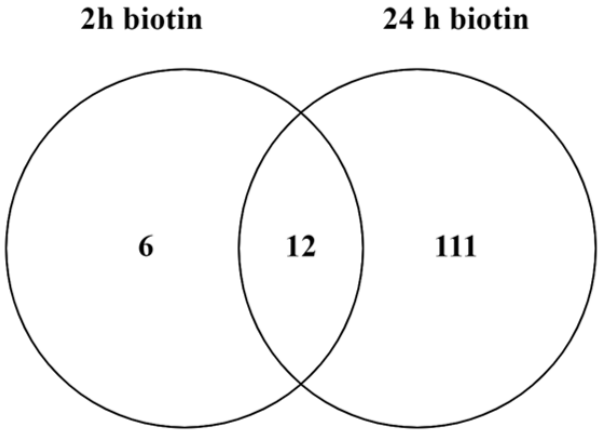

Figure 4.14: Venn diagram of proteins identified by mass spectrometry in two label switch experiments with different biotin incubation times, which meet the cut-off in 4 out of 6 sample/control abundance ratios
Shown is the intersection of two mass spectrometry data sets, which were generated with the N-terminal BioID construct adding biotin either 2 h or 24 h before the cells were harvested.

4.2.1.4 Comparison of mass spectrometric results from BioID experiments with BirA*-CLN6 and BirA*-mFA2H

For further evaluation of the BirA*-CLN6 mass spectrometry data set a murine fatty acid 2-hydroxylase (mFA2H) was used as another bait protein. The BirA*-mFA2H construct was kindly provided by Dr. Matthias Eckhardt (Hardt et al. 2018). This control fusion protein was chosen, as mFA2H is also a membrane protein, which is assigned to the ER membrane and the BirA* is fused to its N-terminus, which is located in the Cytosol. Thus, its subcellular location and assembly is similar to the BirA-CLN6 fusion protein. In total 942 proteins were identified expressing in the HEK cells mFA2H coupled to BirA*. This number is very similar to the overall amount of 953 in the BirA*-CLN6 data set. However, 66 and 123 proteins meeting the cut off criteria with mFA2H and CLN6 as bait protein respectively, of which 51 proteins are included in both data sets, 15 are exclusively contained in the FA2H data set and 72 are only identified in the CLN6 data set. The proteins identified in the FA2H data set meeting the arbitrary cut-off are also indicated in the table 4.2 and table 4.3, listing the proteins included in all three or at least in 2 label switch experiment data sets with the N-terminal CLN6 BioID construct. Even if it cannot be excluded that specific interactors of CLN6 are also biotinylated by BirA*-mFA2H, comparison with the mFA2H data set gives additional information, which might be useful for selecting interaction partner

candidates for CLN6. Another BioID experiment with the biotin ligase located in the ER lumen was not performed, as there was no suitable fusion protein construct available.

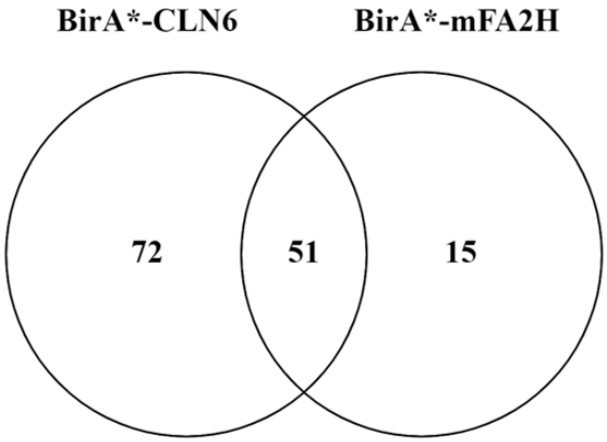

Figure 4.15: Venn diagram of proteins identified by mass spectrometry in two label switch experiments with different bait proteins, CLN6 and FA2H, which meet the cut-off of 2 in 4 out of 6 sample/control abundance ratios
Shown is the intersection of two mass spectrometry data sets, which were generated with either the N-terminal BioID or the BirA*-FA2H construct.

4.2.1.5 Identified proteins biotinylated by the BirA*-CLN6 fusion protein

In this experiment the biotin ligase was coupled to the N-terminus of CLN6 and utilized to find proteins potentially interacting with CLN6`s cytosolic parts. As the fusion protein consisting of CLN6 and BirA* is expected to biotinylate itself, CLN6 and BirA* were used as positive controls for quality assessment. If the mass spectrometry measurement results include either CLN6 or BirA* with 4 out of 6 sample/abundance ratios above 2 the data set was considered as valid. One successful label switch experiment has already been performed with the N-terminal BioID construct and compared to a shorter biotin incubation time and another bait protein. This experiment was reproduced with the same parameters as biotin was incubated for 24 h and peptides were fractioned by SAX for mass spectrometric measurements. Another experiment was performed with a slight modification. Peptides were fractioned by Offgel instead of SAX. Overall, three valid data sets with a biotin incubation of 24 h were generated and analyzed in terms of their biotinylated proteins. Data set one, two and three contain 953, 407 and 1414 total proteins and 123, 129 and 229 proteins having a cut off value above 2 in 4 out of 6 sample/control abundance ratios, respectively. Data set three shows a

higher overall and biotinylated protein number, presumably due to a better peptide separation by Offgel compared to SAX. Both of the other data sets show a very similar number for biotinylated proteins, however a huge discrepancy in the total protein number. Identified proteins of the three experiments meeting the cut off criterion were included in a Venn diagram (Figure 4.16), which illustrates that the three data sets have 57 proteins in common.

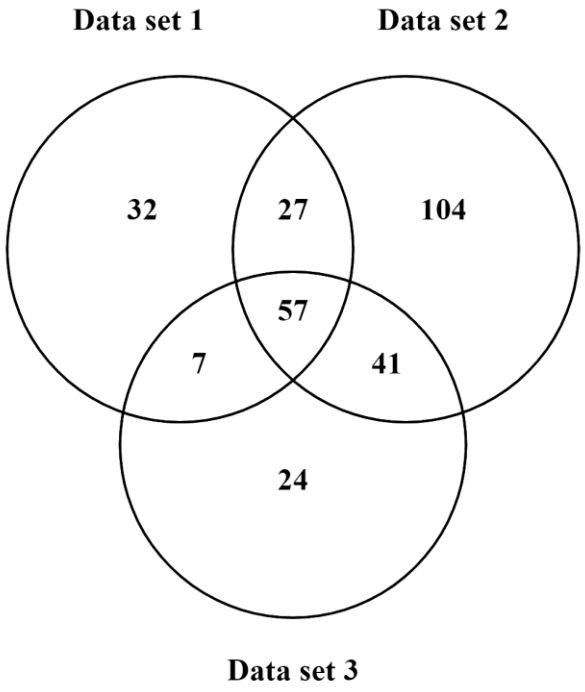

Figure 4.16: Venn diagram of identified proteins in the three mass spectrometry data sets generated by using the N-terminal BioID construct
Diagram shows how many proteins, which have at least 4 out of 6 sample/control ratios above 2, are present in all three, in two data sets or only in one data set. One data set resembles the result of one label switch experiment, which includes biotinylated samples with light, medium and heavy isotopic labeling. These samples were measured separately on the mass spectrometer with their respective controls, which were differently labeled. The first control lacks the addition of biotin and the second control the transfection of the fusion protein.

Table 4.2: List of proteins, which are contained in all three data sets of the N-terminal BioID construct

Proteins are listed, which meet the cut-off criterion in at least 4 out of 6 sample/control abundance ratios in all three label switch experiments generated by using the BirA*-CLN6 construct. Proteins, which are also identified in the mFA2H data set were labeled green. Proteins are labeled yellow, if they were identified in the mFA2H and the BioID N-terminal data set with 2 h biotin incubation time. No proteins were determined exclusively in the latter.

Acession	Protein name	Gene symbol	Acession	Protein name	Gene symbol
P51572	B-cell receptor-associated protein 31	BCAP31	Q04721	Neurogenic locus notch homolog protein 2	NOTCH2
P11717	Cation-independent mannose-6-phosphate receptor	IGF2R	Q15758	Neutral amino acid transporter B(0)	SLC1A5
Q96JB5	CDK5 regulatory subunit-associated protein 3	CDK5RAP3	O75694	Nuclear pore complex protein Nup155	NUP155
Q9UBF2	Coatomer subunit gamma-2	COPG2	P0CG47	Polyubiquitin-B	UBB
Q96A33	Coiled-coil domain-containing protein 47	CCDC47	P0CG48	Polyubiquitin-C	UBC
Q07065	Cytoskeleton-associated protein 4	CKAP4	Q8WYP5	Protein ELYS	AHCTF1
Q8TCJ2	Dolichyl-diphosphooligo-saccharide--protein glycosyl-transferase subunit	STT3B	Q86UE4	Protein LYRIC	MTDH
P49959	Double-strand break repair protein MRE11	MRE11	O15027	Protein transport protein Sec16A	SEC16A
P49792	E3 SUMO-protein ligase RanBP2	RANBP2	Q5HYI8	Rab-like protein 3	RABL3
P50402	Emerin	EMD	P0DJD0	RANBP2-like and GRIP domain-containing protein 1	RGPD1
Q04637	Eukaryotic translation initiation factor 4 gamma 1	EIF4G1	P0DJD1	RANBP2-like and GRIP domain-containing protein 2	RGPD2
Q9BSJ8	Extended synaptotagmin-1	ESYT1	A6NKT7	RanBP2-like and GRIP domain-containing protein 3	RGPD3
P49327	Fatty acid synthase	FASN	Q7Z3J3	RanBP2-like and GRIP domain-containing protein 4	RGPD4
P21333	Filamin-A	FLNA	P51149	Ras-related protein Rab-7a	RAB7A
Q86UL3	Glycerol-3-phosphate acyltransferase 4	GPAT4	Q9NQC3	Reticulon-4	RTN4
Q14789	Golgin subfamily B member 1	GOLGB1	Q9P2E9	Ribosome-binding protein 1	RRBP1
Q6Y7W6	GRB10-interacting GYF protein 2	GIGYF2	Q9Y265	RuvB-like 1	RUVBL1
P30519	Heme oxygenase 2	HMOX2	P08240	Signal recognition particle receptor subunit alpha	SRPRA
Q9Y2U8	Inner nuclear membrane protein Man1	LEMD3	Q9UHB9	Signal recognition particle subunit SRP68	SRP68
Q86UP2	Kinectin	KTN1	Q9H3N1	Thioredoxin-related transmembrane protein 1	TMX1
P42167	Lamina-associated polypeptide 2, isoforms beta/gamma	TMPO	Q5JTV8	Torsin-1A-interacting protein 1	TOR1AIP1
Q14739	Lamin-B receptor	LBR	P37802	Transgelin-2	TAGLN2
P20700	Lamin-B1	LMNB1	Q9UGP8	Translocation protein SEC63 homolog	SEC63
Q9H089	Large subunit GTPase 1 homolog	LSG1	Q5JRA6	Transport and Golgi organization protein 1 homolog	MIA3
O95573	Long-chain-fatty-acid--CoA ligase 3	ACSL3	P18031	Tyrosine-protein phosphatase non-receptor type 1	PTPN1
P84157	Matrix-remodeling-associated protein 7	MXRA7	P62987	Ubiquitin-60S ribosomal protein L40	UBA52

O15173	Membrane-associated progesterone receptor component 2	PGRMC2	Q9Y5A9	YTH domain-containing family protein 2	YTHDF2
Q8TCT9	Minor histocompatibility antigen	HM13	Q7Z2W4	Zinc finger CCCH-type antiviral protein 1	ZC3HAV1
Q8WXH0	Nesprin-2	SYNE2			

These 57 proteins were biotinylated with great certainty by the biotin ligase coupled to the N-terminus of CLN6 and are listed in table 4.2. Evaluating the proteins, they are a heterogenous group with different locations and functions in the cell, containing all sorts of modifications and including membrane as well as soluble proteins. As expected, the table includes a number of cytosolic proteins. The nuclear envelope/lamina is another location, where a relatively large number of identified proteins are from. Furthermore, also several ER membrane proteins of different subcompartments were purified and measured due to biotinylation of their cytosolic parts. Two examples are the translocation protein SEC63 homolog and a subunit of the OST complex, which both function at the site of protein biosynthesis (Gemmer et al. 2020). In contrast, the identified protein transport protein SEC16A and transport and Golgi organization protein 1 homolg function at the ER exits sites (Watson et al. 2006, Zanetti et al. 2012). However, soluble ER proteins are not listed in the table. Remarkably, only one protein annotated to the lysosome is among the 57 proteins, the cation-independent mannose-6-phosphate receptor. Moreover, the proteins included in the mFA2H and the 2 h biotin incubation data sets are highlighted in different colors. This gives additional information on the biotinylation specificity.

Table 4.3: List of proteins, which are contained in two of the three data sets of the N-terminal BioID construct

In contrast to table 4.2, which contains proteins, which were identified in all three data sets, this table shows proteins, which are present in two data sets. Therefore, proteins are listed, which meet the cut-off criterion in at least 4 out of 6 sample/control abundance ratios in two label switch experiments generated by using the BirA*-CLN6 construct. Proteins, which are also identified in the mFA2H data set, were labeled green. Protein, which were identified in the BioID N-terminal data set with 2 h biotin incubation time, were labeled red. Proteins are labeled yellow, if they were identified additionally in both data sets.

Acession	Protein name	Gene symbol	Acession	Protein name	Gene symbol
Q9UBM7	7-dehydrocholesterol reductase	DHCR7	P00167	Cytochrome b5	CYB5A
O00400	Acetyl-coenzyme A transporter 1	SLC33A1	Q96HY6	DDRGK domain-containing protein 1	DDRGK1
Q8IWZ3	Ankyrin repeat and KH domain-containing protein 1	ANKHD1	P51648	Fatty aldehyde dehydrogenase	ALDH3A2
Q14126	Desmoglein-2	DSG2	Q9Y2H6	Fibronectin type-III domain-	FNDC3A

				containing protein 3A	
Q9C0E8	Endoplasmic reticulum junction formation protein lunapark	LNPK	P0DMV8	Heat shock 70 kDa protein 1A	HSPA1A
P42566	Epidermal growth factor receptor substrate 15	EPS15	P11142	Heat shock cognate 71 kDa protein	HSPA8
P58107	Epiplakin	EPPK1	P08238	Heat shock protein HSP 90-beta	HSP90AB1
P52292	Importin subunit alpha-1	KPNA2	P04264	Keratin, type II cytoskeletal 1	KRT1
Q9HDC5	Junctophilin-1	JPH1	O00264	Membrane-associated progesterone receptor component 1	PGRMC1
Q96AG4	Leucine-rich repeat-containing protein 59	LRRC59	P35579	Myosin-9	MYH9
Q9HD20	Manganese-transporting ATPase 13A1	ATP13A1	P16435	NADPH--cytochrome P450 reductase	POR
Q9ULH7	MKL/myocardin-like protein 2	MKL2	Q09666	Neuroblast differentiation-associated protein AHNAK	AHNAK
A2RRP1	Neuroblastoma-amplified sequence	NBAS	P07197	Neurofilament medium polypeptide	NEFM
P52948	Nuclear pore complex protein Nup98-Nup96	NUP98	Q9HCU5	Prolactin regulatory element-binding protein	PREB
P12270	Nucleoprotein TPR	TPR	P49257	Protein ERGIC-53	LMAN1
Q93008	Probable ubiquitin carboxyl-terminal hydrolase FAF-X	USP9X	P48741	Putative heat shock 70 kDa protein 7	HSPA7
P46060	Ran GTPase-activating protein 1	RANGAP1	Q58FF7	Putative heat shock protein HSP 90-beta-3	HSP90AB3P
Q99666	RANBP2-like and GRIP domain-containing protein 5/6	RGPD5	Q92928	Putative Ras-related protein Rab-1C	RAB1C
O14715	RANBP2-like and GRIP domain-containing protein 8	RGPD8	Q9H2J7	Sodium-dependent neutral amino acid transporter B(0)AT2	SLC6A15
P62491	Ras-related protein Rab-11A	RAB11A	Q13586	Stromal interaction molecule 1	STIM1
Q15907	Ras-related protein Rab-11B	RAB11B	Q96A49	Synapse-associated protein 1	SYAP1
P61011	Signal recognition particle 54 kDa protein	SRP54	O15498	Synaptobrevin homolog YKT6	YKT6
Q13435	Splicing factor 3B subunit 2	SF3B2	P50990	T-complex protein 1 subunit theta	CCT8
P43307	Translocon-associated protein subunit alpha	SSR1	Q5VV42	Threonylcarbamoyladenosine tRNA methylthiotransferase	CDKAL1
Q8N511	Transmembrane protein 199	TMEM199	Q8NFQ8	Torsin-1A-interacting protein 2	TOR1AIP2
Q92575	UBX domain-containing protein 4	UBXN4	P17706	Tyrosine-protein phosphatase non-receptor type 2	PTPN2
Q00341	Vigilin	HDLBP	Q9Y385	Ubiquitin-conjugating enzyme E2 J1	UBE2J1
P55036	26S proteasome non-ATPase regulatory subunit 4	PSMD4	Q9P0L0	Vesicle-associated membrane protein-associated protein A	VAPA
P46108	Adapter molecule crk	CRK	O95292	Vesicle-associated membrane protein-associated protein B/C	VAPB
O60503	Adenylate cyclase type 9	ADCY9	Q9HBM0	Vezatin	VEZT
Q02952	A-kinase anchor protein 12	AKAP12	P27797	Calreticulin	CALR
Q9Y679	Ancient ubiquitous protein 1	AUP1	Q14315	Filamin-C	FLNC
Q8WWM7	Ataxin-2-like protein	ATXN2L	Q9Y6M1	Insulin-like growth factor 2 mRNA-binding protein 2	IGF2BP2
Q9Y2J2	Band 4.1-like protein 3	EPB41L3	O00425	Insulin-like growth factor 2 mRNA-binding protein 3	IGF2BP3
P27824	Calnexin	CANX	P42166	Lamina-associated polypeptide 2, isoform alpha	TMPO
Q9NWW5	Ceroid-lipofuscinosis neuronal	CLN6	Q14157	Ubiquitin-associated protein 2-	UBAP2L

	protein 6			like	
Q96S66	Chloride channel CLIC-like protein 1	CLCC1	Q9NZC7	WW domain-containing oxidoreductase	WWOX
Q14677	Clathrin interactor 1	CLINT1			

The proteins listed in table 4.3 were also biotinylated by the BioID fusion protein with a very high confidence, as they are included in two out of three data sets meeting the cut off criteria in 4 out 6 sample/control abundance ratios. The proteins in this table like in the previous one show also different locations and functions with no obvious priority. Furthermore, there is no protein present, which is annotated to the lysosomal compartment. However, in table 4.3 there are proteins involved in synthesizing and processing lysosomal proteins and also being part of the calnexin cycle, in particular CALR and CANX. Besides, any functional relation to CLN6 of the various other proteins is not apparent or known as of yet. Again, proteins being present in the FA2H and the 2 h biotin incubation data sets are highlighted in different colors indicating the biotinylation specificity of the N-terminal CLN6 BioID construct.

4.2.1.6 Identified proteins biotinylated by the CLN6-BirA* fusion protein

After potential interaction partners of CLN6 were determined in the cytosol using the BioID approach, proteins were biotinylated and identified in the ER lumen with the C-terminal BioID construct accordingly to find proteins potentially interacting with the domains of CLN6 located in the ER lumen. Label switch experiments were conducted in the same way as with the N-terminal construct, except this time only SAX fractionation was applied and three valid data sets were generated. Results were filtered for proteins, which have 4 out of 6 sample/control abundance ratios above 2 as they are considered to be biotinylated. Mass spectrometric measurements yielded 1461, 348 and 349 total proteins and 36, 138 and 139 biotinylated proteins in data set 1, 2 and 3 respectively. To compare the three data sets with respect to their biotinylated proteins, a Venn diagram was created (Figure 4.17).

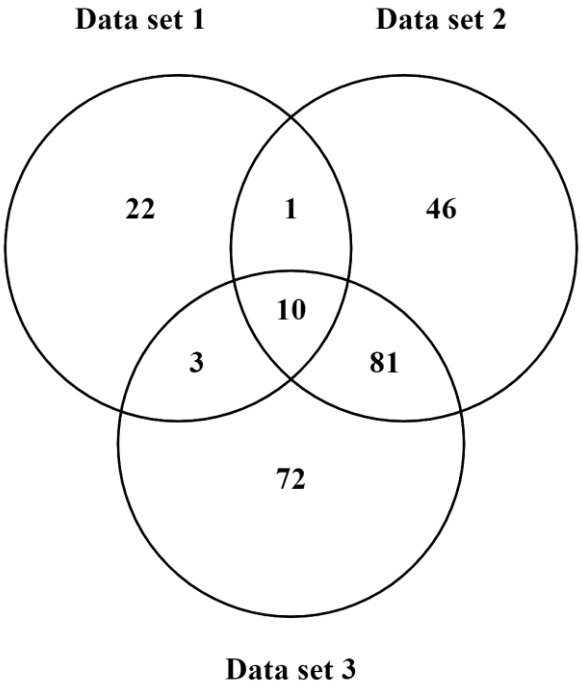

Figure 4.17: Venn diagram of identified proteins in the three mass spectrometry data sets generated by using the C-terminal BioID construct
The diagram shows how many proteins, which have at least 4 out of 6 sample/control ratios above 2, are present in all three, in two data sets or only in one data set. One data set resembles the result of one label switch experiment, which includes biotinylated samples with light, medium and heavy isotopic labeling. These samples were measured separately on the mass spectrometer with their respective controls, which were differently labeled. The first control lacks the addition of biotin and the second control the transfection of the fusion protein.

Table 4.4: List of proteins, which are contained in all three data sets of the C-terminal BioID construct
Proteins are listed, which meet the cut-off criterion in at least 4 out of 6 sample/control abundance ratios in all three data sets generated by using the CLN6-BirA* construct

Acession	Protein name	Gene symbol
P06709	Bifunctional ligase/repressor BirA	birA
Q96A33	Coiled-coil domain-containing protein 47	CCDC47
Q8TCJ2	Dolichyl-diphosphooligosaccharide--protein glycosyltransferase subunit STT3B	STT3B
Q6Y7W6	GRB10-interacting GYF protein 2	GIGYF2
P42167	Lamina-associated polypeptide 2, isoforms beta/gamma	TMPO
Q09666	Neuroblast differentiation-associated protein AHNAK	AHNAK
P48634	Protein PRRC2A	PRRC2A
Q9Y265	RuvB-like 1	RUVBL1

Q14157	Ubiquitin-associated protein 2-like	UBAP2L
Q9Y5A9	YTH domain-containing family protein 2	YTHDF2

First of all, the diagram displays the relatively big variations between the three data sets and a big number of proteins present only in one data set, which is also different compared to the previous results with the N-terminal construct. Furthermore, the diagram shows that 10 proteins, which meet the cut off criterion, are present in all three data sets. Consequently, these 10 proteins are most likely not biotinylated randomly by the C-terminal BioID construct, but are generally in close proximity to CLN6. Compared to the previous Venn diagram less proteins are included in all three data sets, caused by a higher variability between the data sets and not a lower number of total identified proteins. The 10 overlapping proteins were listed and further assessed (Table 4.4). Besides two ER membrane proteins, surprisingly, the table lacks other proteins purely located in the ER lumen. Instead, many listed proteins are closely related to the ER either spatially or functionally. For example, GRB10-interacting GYF protein 2 is a component of a complex, which acts as repressor of translation initiation and lamina-associated polypeptide 2 resides in the nucleus membrane (Morita et al. 2012). Overall, 6 of the 10 proteins can also be found in table 4.2. Proper procedure of the experiment, biotinylation and mass spectrometric measurements in all three label switch experiments were validated by the biotin ligase being biotinylated and meeting the arbitrary cut off in all three cases. Strikingly, no lysosomal protein is included in the table, what would have indicated a direct connection between CLN6 and the lysosome.

Table 4.5: List of proteins, which are contained in two of the three data sets of the C-terminal BioID construct

In contrast to table 4.4, which contains proteins, which were identified in all three data sets, this table shows proteins, which are present in two data sets. Therefore, proteins are listed, which meet the cut-off criterion in at least 4 out of 6 sample/control abundance ratios in two data sets generated by using the CLN6-BirA* construct.

Acession	Protein name	Gene symbol	Acession	Protein name	Gene symbol
P62913	60S ribosomal protein L11	RPL11	Q15233	Non-POU domain-containing octamer-binding protein	ONO
P46108	Adapter molecule crk	CRK	Q7Z417	Nuclear fragile X mental retardation-interacting protein 2	UFIP2
Q8WWM7	Ataxin-2-like protein	ATXN2L	Q99733	Nucleosome assembly protein 1-like 4	AP1L4
Q08211	ATP-dependent RNA helicase A	DHX9	O95613	Pericentrin	PCNT
O00571	ATP-dependent RNA helicase DDX3X	DDX3X	Q15154	Pericentriolar material 1 protein	PCM1

O15523	ATP-dependent RNA helicase DDX3Y	DDX3Y	Q9H307	Pinin	PNN
P51572	B-cell receptor-associated protein 31	BCAP31	P09874	Poly [ADP-ribose] polymerase 1	PARP1
P27824	Calnexin	CANX	Q15365	Poly(rC)-binding protein 1	PCBP1
P27797	Calreticulin	CALR	Q15366	Poly(rC)-binding protein 2	PCBP2
Q9NWW5	Ceroid-lipofuscinosis neuronal protein 6	CLN6	P0CG47	Polyubiquitin-B	UBB
Q96S66	Chloride channel CLIC-like protein 1	CLCC1	P0CG48	Polyubiquitin-C	UBC
O75534	Cold shock domain-containing protein E1	CSDE1	Q93008	Probable ubiquitin carboxyl-terminal hydrolase FAF-X	USP9X
O60884	DnaJ homolog subfamily A member 2	DNAJA2	P30101	Protein disulfide-isomerase A3	PDIA3
Q8IXB1	DnaJ homolog subfamily C member 10	DNAJC10	P13667	Protein disulfide-isomerase A4	PDIA4
P49792	E3 SUMO-protein ligase RanBP2	RANBP2	P49257	Protein ERGIC-53	LMAN1
P13639	Elongation factor 2	EEF2	P18583	Protein SON	SON
P50402	Emerin	EMD	Q58FF3	Putative endoplasmin-like protein	HSP90B2P
P11021	Endoplasmic reticulum chaperone BiP	HSPA5	Q58FF8	Putative heat shock protein HSP 90-beta 2	HSP90AB2P
P14625	Endoplasmin	HSP90B1	Q58FF7	Putative heat shock protein HSP 90-beta-3	HSP90AB3P
Q9NPA0	ER membrane protein complex subunit 7	EMC7	P0DJD0	RANBP2-like and GRIP domain-containing protein 1	RGPD1
P60842	Eukaryotic initiation factor 4A-I	EIF4A1	P0DJD1	RANBP2-like and GRIP domain-containing protein 2	RGPD2
Q04637	Eukaryotic translation initiation factor 4 gamma 1	EIF4G1	A6NKT7	RanBP2-like and GRIP domain-containing protein 3	RGPD3
P21333	Filamin-A	FLNA	Q7Z3J3	RanBP2-like and GRIP domain-containing protein 4	RGPD4
Q14315	Filamin-C	FLNC	Q99666	RANBP2-like and GRIP domain-containing protein 5/6	RGPD5
P14314	Glucosidase 2 subunit beta	PRKCSH	O14715	RANBP2-like and GRIP domain-containing protein 8	RGPD8
P0DMV8	Heat shock 70 kDa protein 1A	HSPA1A	P16615	Sarcoplasmic/endoplasmic reticulum calcium ATPase 2	ATP2A2
P34931	Heat shock 70 kDa protein 1-like	HSPA1L	P61011	Signal recognition particle 54 kDa protein	SRP54
P11142	Heat shock cognate 71 kDa protein	HSPA8	P50990	T-complex protein 1 subunit theta	CCT8
P07900	Heat shock protein HSP 90-alpha	HSP90AA1	Q8NBS9	Thioredoxin domain-containing protein 5	TXNDC5
Q14568	Heat shock protein HSP 90-alpha A2	HSP90AA2P	Q9H3N1	Thioredoxin-related transmembrane protein 1	TMX1
P08238	Heat shock protein HSP 90-beta	HSP90AB1	Q5JTV8	Torsin-1A-interacting protein 1	TOR1AIP1
P54652	Heat shock-related 70 kDa protein 2	HSPA2	Q13263	Transcription intermediary factor 1-beta	TRIM28
P09651	Heterogeneous nuclear ribonucleoprotein A1	HNRNPA1	P37802	Transgelin-2	TAGLN2
P61978	Heterogeneous nuclear ribonucleoprotein K	HNRNPK	P43307	Translocon-associated protein subunit alpha	SSR1
P52272	Heterogeneous nuclear ribonucleoprotein M	HNRNPM	Q9UPQ9	Trinucleotide repeat-containing gene 6B protein	TNRC6B
Q9NZI8	Insulin-like growth factor 2 mRNA-binding protein 1	IGF2BP1	Q13885	Tubulin beta-2A chain	TUBB2A
Q9Y6M1	Insulin-like growth factor 2 mRNA-binding protein 2	IGF2BP2	Q9BVA1	Tubulin beta-2B chain	TUBB2B

Q8N1G4	Leucine-rich repeat-containing protein 47	LRRC47	P68371	Tubulin beta-4B chain	TUBB4B
P43243	Matrin-3	MATR3	P62987	Ubiquitin-60S ribosomal protein L40	UBA52
O15173	Membrane-associated progesterone receptor component 2	PGRMC2	Q9NZC7	WW domain-containing oxidoreductase	WWOX
Q8TCT9	Minor histocompatibility antigen H13	HM13	Q7Z739	YTH domain-containing family protein 3	YTHDF3
P07197	Neurofilament medium polypeptide	EFM	Q7Z2W4	Zinc finger CCCH-type antiviral protein 1	ZC3HAV1
Q14697	Neutral alpha-glucosidase AB	ANAB			

While only few proteins are present in all three data sets of the C-terminal BioID construct, with 85 proteins there are many more meeting the cut off criterion in 4 out of 6 sample/control abundance ratios in two of the three data sets (Table 4.5). As suggested proteins in table 4.5 mostly reside in the ER, from which several are part of the calnexin cycle including CALR, CANX, the subunits of glucosidase II and protein disulfide isomerases. Furthermore, there is no lysosomal protein included, which could give a direct link to the contribution of CLN6 to lysosomal function. Interestingly, the proteins, which were significantly reduced in the nclf tritosomes and 20.000 g pellets or newly discovered interaction partners of CLN6, namely CLN8, CTSD, PPT1, TPP1 and GALNS are also not found here or in any other BioID data set (Bajaj et al. 2020).

4.2.1.7 Selection of biotinylated proteins from the BioID data sets possibly functionally related to CLN6

The BioID experiments yieled in an enormous number of identified proteins, which are presumably located in close proximity of CLN6. Among these proteins there are potentially proteins, with which CLN6 has a functional relation. To determine these proteins is one aim of this study. The most obvious candidates are certainly the proteins in the tables 4.2 and 4.4 due to their rich and repeated biotinylation following by the proteins in table 4.3 and 4.5, still showing relatively high extent of biotinylation by the BioID. However, for many proteins no functional relation to CLN6 is apparent and it is more likely that they are included in the tables because of their high abundancy and favorable biotinylation sites. As CLN6 deficiency leads to a lysosomal storage disease, proteins annotated to the lysosome would be likely to have a functional relation to CLN6. However, in the data sets almost no lysosomal proteins and no lysosomal proteins, which were found significantly reduced in *nclf* tritosomes and 20.000 g pellets

were detected. Furthermore, also newly discovered interaction partners of CLN6, in particular CLN8, are not included in the BioID data sets (Bajaj et al. 2020). The next protein group worth considering are proteins interacting, transporting or processing lysosomal proteins. Most lysosomal proteins are glycosylated and therefore pass the calnexin cycle, in which many proteins are involved in folding, transporting, processing or the quality control of glycosylated proteins. Remarkably, a substantial number of these proteins are present in the BioID data sets. Three proteins, CANX, CALR and glucosidase 2, are very crucial for the development of glycosylated proteins and key players in the calnexin cycle (Caramelo et al. 2008). Even though they are not listed in table 4.2 or table 4.4, they were identified in all of the six label switch experiments and just barely missed the criteria for being listed in one or both tables. More precisely, CANX, CALR meet the cut off criteria in two of three data sets for both BioID constructs. The catalytic alpha subunit of glucosidase 2 (GANAB) meets the cut off criteria in two of three data sets of the C-terminal BioID construct. However, it is not included in any data set of the N-terminal construct with the designated sample/control abundance ratios. This was expected, as glucosidase 2 is a soluble protein residing exclusively in the ER lumen (Pelletier et al. 2000). Due to their potential biological relevancy in relation to CLN6 and their close proximity to CLN6 validated by the BioID data sets, these three proteins were selected for further investigations.

4.2.2 Using the bimolecular fluorescence complementation assay to verify interaction partner candidates of CLN6

As the BioID approach only identifies proteins in close proximity but does not indicate interactions, the candidate proteins were assessed by the BiFC assay. This assay utilizes fluorescent proteins, which are split in two fragments. These fragments do not fluoresce on their own and are fused to two proteins. If these proteins interact, they will stay in really close proximity for a certain period, what enables the reconstitution of the fluorescent protein fragments. Reconstituted fluorescent proteins again emit fluorescence, which can be quantified and indicates the interaction of the analyzed proteins (Kerppola 2009). Besides the BioID approach, also the literature and the investigation of the lysosomal proteome of wt and *nclf* mice provided a big number of proteins potentially related to CLN6. From the BioID data sets CANX, CALR and

glucosidase 2 were selected to be further assessed by the BiFC assay. By comparing the lysosomal proteome of wt and *nclf* samples a correlation between CLN6's function and the abundance of various hydrolases in the lysosome was observed. Even though none of these hydrolases were shown to be in close proximity of CLN6 by the BioID approach, it was checked by the BiFC assay, if affected hydrolases CTSD, CTSZ and PPT1 interact directly with CLN6. In a recent investigation CTSD and PPT1 were also identified as interaction partners of CLN6 after overexpression by co-immunoprecipitation (Co-IP). As in Co-IPs the actual *in vivo* conditions are not entirely reflected and they are prone to unspecific binding especially in the case of overexpression, the BiFC assay was used to validate the previous results with a method, which in contrast detects proteins interacting *in vivo*. Moreover, the same investigation has discovered CLN8 as a novel interaction partner of CLN6 with the BiFC assay (Bajaj et al. 2020). Therefore, CLN8 was also included in the BiFC assay to validate the newly discovered interaction and as a potential positive control. Another positive control was the interaction of Ergic-53 and MCFD, two well-known interaction partners identified by this assay (Nyfeler et al. 2005). In addition, CLN6 itself was used as a positive control, because its dimerization should also lead to a YFP signal (Heine et al. 2007). As negative controls BHK cells transfected with an empty vector to subtract the autofluorescence of the cells and cells transfected with YFP constructs of CLN6 or CLN8, respectively, and Ergic53, which are not known to interact with each other, were used.

4.2.2.1 Exclusion of interaction partner candidates CTSD, CTSZ, GANAB and PPT1 by preliminary studies with the BiFC assay

To determine interaction of specific proteins with CLN6, YFP constructs of these proteins were created, co-transfected in BHK cells, which were harvested after two days, washed and measured to determine their fluorescence signal. In the first place, the fluorescence measurements were performed with the Tecan reader instead of using FACS analysis. In these experiments all interaction partner candidates were included except PPT1, as the YFP-constructs were generated at a later stage. Due to massive variations between the experiments and only small or no differences between samples and negative controls with the Tecan reader this experimental set up was not feasible to

obtain valid results. However, the results have already given some first tendencies. CANX, CALR and CLN8 showed at least a slightly higher fluorescence signal compared to the negative controls when YFP1 was fused to CLN6, but the differences were not significant and not always reproducible. All other proteins tested for CLN6 interaction displayed no apparent differences to the negative controls (Figure 4.18). After these results the protocol was adjusted and the fluorescence measurements were performed by FACS to increase measurement sensitivity and reproducibility. With this change the experiments were repeated and the previous results were clearly confirmed by FACS. Measured fluorescence intensities showed no indication that CTSD, CTSZ or GANAB interact with CLN6. Meanwhile the YFP constructs of PPT1 have been cloned and also showed no interaction in the BiFC assay. Therefore, these candidates were not further analyzed (data not shown). However, CLN6-YFP constructs expressed with CANX, CALR or CLN8 having the corresponding YFP fragment resulted in higher fluorescence intensities than the negative control at least in one of both possible YFP combination. Therefore, two more replicates for these proteins were produced to get statistically evaluable data.

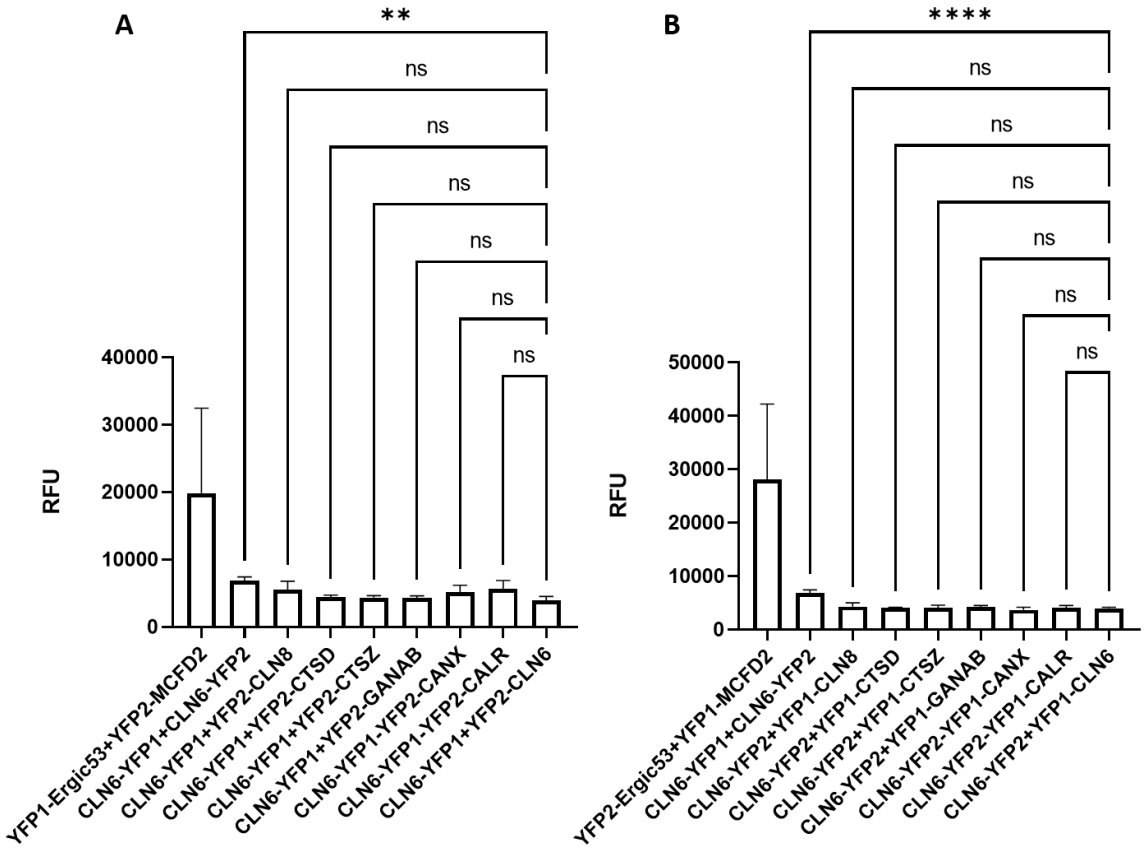

Figure 4.18: The interactions of CLN8, CTSD, CTSZ, GANAB, CANX and CALR with CLN6 were analyzed by the BiFC assay
Shown are the fluorescence signals of cells co-transfected with the indicated YFP-constructs measured by the Tecan reader. The experiments were conducted with (A) YFP1 and (B) YFP2 being linked to CLN6, while the interaction partner candidates were fused to the corresponding YFP fragment. The known protein interaction of Ergic-53 and MCFD2 and the dimerization of CLN6 YFP-fragments were used as a positive control. The intensities were compared to the negative control consisting of CLN6-YFP constructs, in which YFP1 and YFP2 were separated by the ER membrane, by an ordinary one-way ANOVA. Significant differences are indicated as follows: **** = p-value < 0,0001; *** = p-value < 0,001; ** = p-value < 0,01; * = p-value < 0,05; ns = not significant. N = 3.

4.2.2.2 Evaluation of CLN6's interaction partner candidates CANX, CALR and CLN8 with the BiFC assay by FACS

After three replicates were prepared, the measured data was statistically analyzed. In dot blots of every FACS measurement the cell population was gated with forward (FSC) and side scatter (SCC) shown as axes and the mean fluorescence intensities were determined of the cells emitting a higher fluorescence signal than the negative control. The means of these values for the three replicates and their standard deviation were

calculated. Furthermore, statistically significant difference between samples and the negative control were analyzed by an ordinary one-way ANOVA (Figure 4.19).

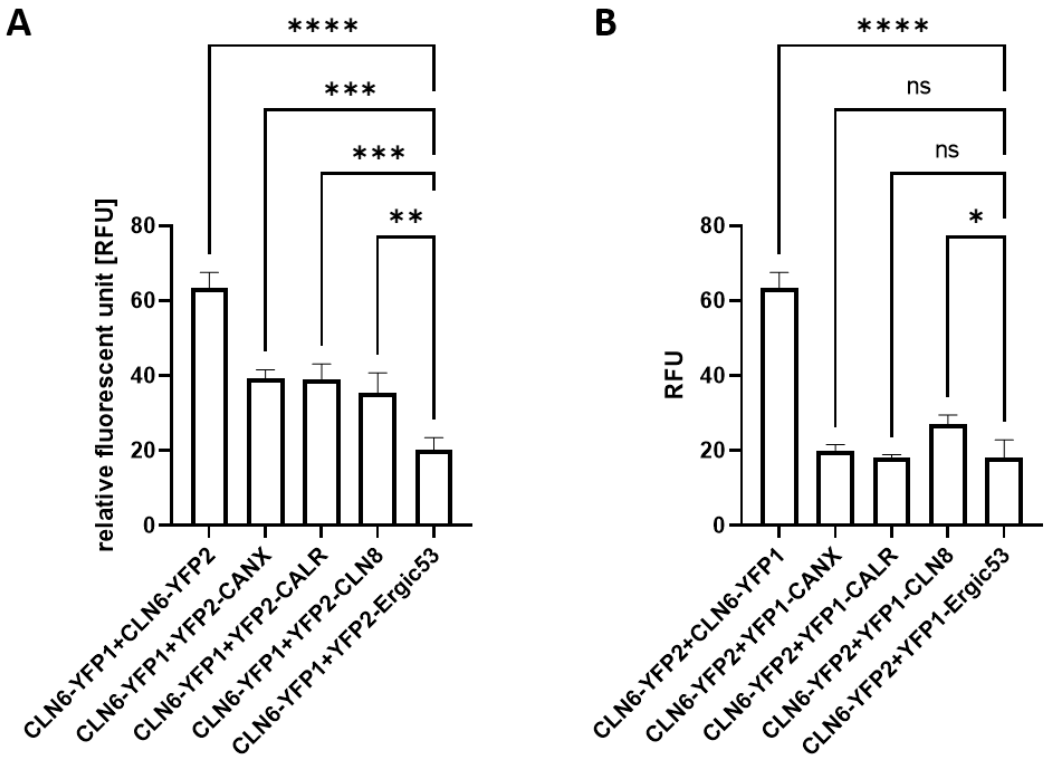

Figure 4.19: The interaction of CANX, CALR and CLN8 with CLN6 was analyzed by the BiFC assay

Depicted are the means of measured fluorescence intensities emitted by cells transfected with (A) CLN6-YFP1 or (B) CLN6-YFP2, respectively, and the corresponding YFP constructs of CANX, CALR and CLN8. The dimerization of CLN6 YPF-fragments was used as a positive control. The intensities were compared to the negative control consisting of the respective YFP constructs of CLN6 and Ergic53 by an ordinary one-way ANOVA. Significant differences are indicated as follows: **** = p-value < 0,0001; *** = p-value < 0,001; ** = p-value < 0,01; * = p-value < 0,05; ns = not significant. N = 3.

As there are two different YFP fragments and every protein has got a N- and a C-terminus, for every tested protein pair there are various possible combinations to attach the fragments to the proteins. For every protein in this experiment the YFP fragments are present inside the ER lumen. Therefore, they were fused to the N-terminus of CANX, CALR and CLN8 and the C-terminus of CLN6. For every tested protein-protein interaction both possible YFP combinations were evaluated. As shown in figure 4.19 the interaction of CLN8 and CLN6 could be confirmed. Although the graph shows no big elevation of the fluorescence, for both YFP combinations the fluorescence intensity is significantly higher compared to the negative control. The proteins CANX and CALR

show similar results, if YFP1 was attached to CLN6 and the corresponding YFP2 was expressed together with CANX or CALR, as a significant difference compared to negative control is determined that is even slightly bigger than that of CLN6-YFP1 co-transfected with YFP2-CLN8. However, if the YFP fragments are exchanged, the significant difference to the negative control is lost, as the measured fluorescence intensity of the CANX and CALR YFP1-constructs with CLN6-YFP2 is similar to the intensity of negative control.

4.2.2.3 Influence of CLN6's second loop and C-terminus on the interaction with CANX, CALR and CLN8

As potential interactions of CLN6 with CANX, CALR and CLN8 were determined by the BiFC assay further experiments were conducted to identify CLN6's domains involved in these interactions. For this purpose, the biggest domain, the second loop (amino acids 135-175) of CLN6 was deleted in the YFP constructs. These CLN6 YFP constructs devoid of CLN6's second loop were used in a BiFC assay with YFP constructs of CANX, CALR and CLN8. Again, three replicates were produced and the data was statistically analyzed (Fig. 4.20). In case of CLN6Δ2Loop-YFP1 and YFP2-CLN8 the significant difference between sample and negative control was lost due to the deletion of the second loop. However, there is only a slight decrease in intensity detected and the fluorescence signal is still relatively high, so that a significant difference was missed very closely. Furthermore, the CLN6Δ2Loop-YFP2 and YFP1-CLN8 combination shows even a little higher fluorescence compared to the same constructs with the wt CLN6 sequence. For all other protein-protein combinations the lack of CLN6's second loop has no massive and clear influence on the result of the BiFC assay and the protein interactions.

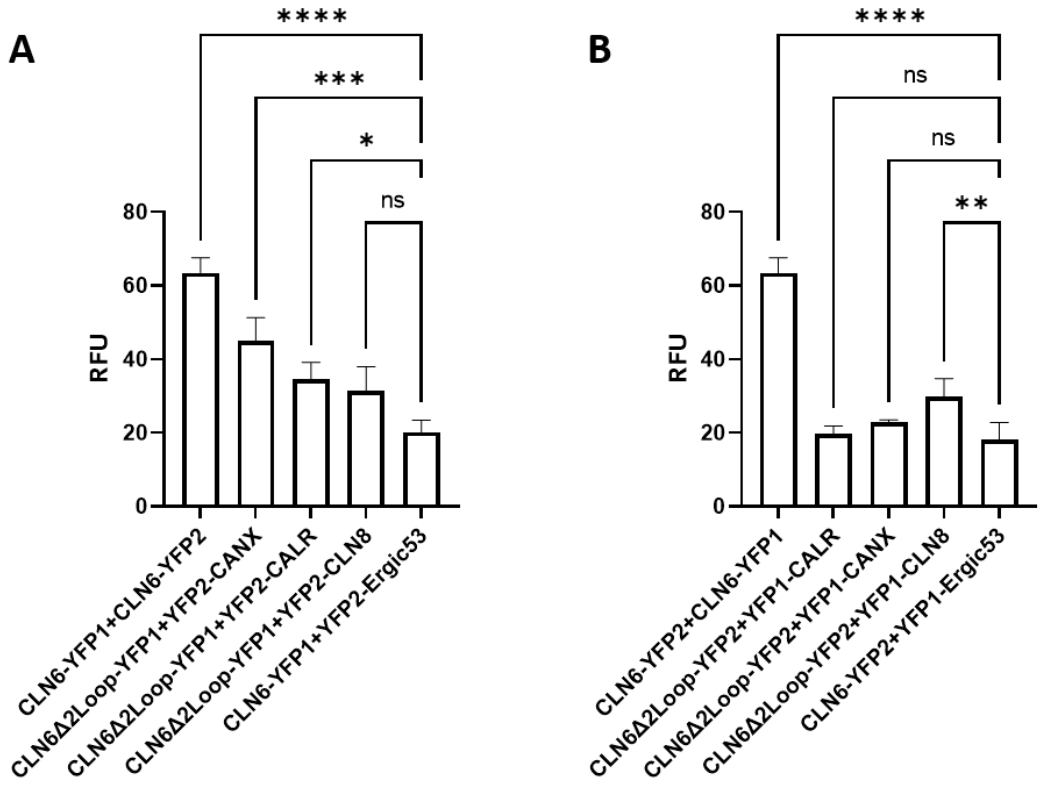

Figure 4.20: The interaction of CANX, CALR and CLN8 with CLN6 devoid of its second loop was analyzed by the BiFC assay
Depicted are the means of measured fluorescence intensities emitted by cells transfected with (A) CLN6Δ2Loop-YFP1 or (B) CLN6Δ2Loop-YFP2, respectively, and the corresponding YFP constructs of CANX, CALR and CLN8. The dimerization of CLN6 YPF-fragments was used as a positive control. The intensities were compared to the negative control consisting of the respective YFP constructs of CLN6 and Ergic53 by an ordinary one-way ANOVA. Significant differences are indicated as follows: **** = p-value < 0,0001; *** = p-value < 0,001; ** = p-value < 0,01; * = p-value < 0,05; ns = not significant. N = 3.

The means of the fluorescence intensities change slightly, but without any consistent tendency and stay in relatively the same range. Therefore, the absence of the second loop does not change the significance of differences between samples and negative control in general. However, in some cases the level of significance was altered. After obtaining these results two more YFP constructs with a mutated CLN6 were prepared. Firstly, CLN6's C-terminus was replaced by a glycine linker and secondly, both mutations were combined, so that CLN6's second loop and C-terminus were deleted. For these constructs only one BiFC assay was performed, which however showed no fluorescence reduction, if they were tested together with YFP-constructs of CANX and CALR (data not shown).

4.2.2.4 Analyzing the interaction of CLN8 with CANX and CALR by the BiFC assay

Besides investigating potential interactions of CLN6 with several candidates, also the protein interaction among some candidates was evaluated. As CLN8 is related to another subtype of NCL its interaction with CANX and CALR was of special interest and was also tested by the BiFC assay. The same YFP-constructs of CANX, CALR and CLN8 previously used also were used for these experiments, which were performed as described in the previous sections. Three replicates were prepared and statistically analyzed (Fig. 4.21).

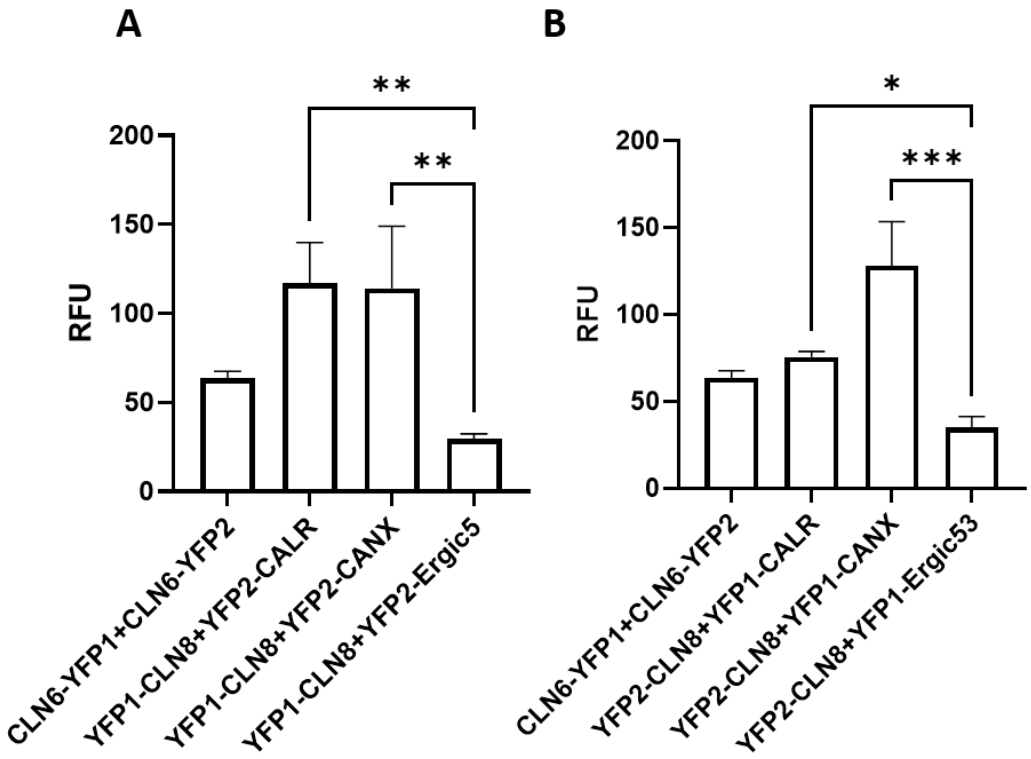

Figure 4.21: The interaction of CANX and CALR with CLN8 was analyzed by the BiFC assay

Depicted are the means of measured fluorescence intensities emitted by cells transfected with (A) CLN8-YFP1 or (B) CLN8-YFP2, respectively, and the corresponding YFP constructs of CANX and CALR. The fluorescence intensity of dimerizing CLN6-YPF fragments was included as a reference value of an already known interaction. The intensities were compared to the negative control consisting of the respective YFP constructs of CLN8 and Ergic53 by an ordinary one-way ANOVA. Significant differences are indicated as follows: **** = p-value < 0,0001; *** = p-value < 0,001; ** = p-value < 0,01; * = p-value < 0,05; ns = not significant. N = 3.

The results show significantly higher fluorescence signals as the negative control for both YFP combinations indicating a protein interaction of CLN8 with CANX and CALR. Interestingly, the measured fluorescence intensities are immensely higher compared to intensities, which were determined in any BiFC experiment including the positive control of CLN6's dimerization.

5 Discussion

Even though NCL diseases are relatively rare, for those people affected, they have very serious and drastic consequences, also because for most NCL forms there is no cure available. One reason for lacking successful therapeutic approaches is that the pathomechanisms of NCLs and the functions of CLN proteins are poorly understood, which in particular applies to CLN6, the subject of this study. This project had the aim to provide new valuable insights in regard to CLN6's molecular biology. The conducted investigations are divided into two main parts focusing on different aspects of CLN6's molecular biology. On the one hand, the lysosome was examined in respect to proteomic changes in CLN6 deficiency using mass spectrometry and western blotting. On the other hand, CLN6's interactome in the ER was explored by the BioID approach and the BiFC assay.

5.1 Analysis of the lysosomal proteome in CLN6 deficiency

The lysosomal storage disease NCL6 indicates the relationship between CLN6 deficiency and lysosomal dysfunction. However, which exact lysosomal functions are impaired and why have not been discovered yet. CLN6 resides in the ER and is not directly involved in lysosomal degradation. Consequently, CLN6 contributes indirectly to lysosomal function and homeostasis. To determine the type of lysosomal dysfunction caused by CLN6 deficiency, the proteomes of healthy and diseased lysosomes were compared and examined regarding alterations in the lysosomal composition. Differing compositions could give a conceivable explanation for lysosomal dysfunction in NCL6. Furthermore, proteomic changes of the lysosome caused by CLN6 deficiency could also give indications on possible interaction partners and the function of CLN6.

5.1.1 The comparison of tritosomes obtained from wt and *nclf* mice reveals characteristic proteomic changes due to CLN6 deficiency

Tritosomes were isolated from liver tissue of wt and *nclf* mice and analyzed to determine proteomic changes of the lysosome in NCL6. Western blot images indicated a similar enrichment of lysosomes in tritosomes of wt and *nclf* mice, as in both the

protein amount of lysosomal membrane protein Lamp1 is relatively increased by about 10-fold compared to the liver homogenate. The enrichment of the lysosomal soluble protein Ctsz validates the Lamp1 blots and points out the intactness of tritosomes from wt or *nclf* mice. The absence of the marker proteins Pdi and Ctp2 show that tritosomes are not considerably contaminated by the ER and the mitochondria. After the characterization of the tritosome fractions from wt and *nclf* mice confirmed their purity and comparability, mass spectrometric analysis was performed. The volcano plot displaying the *nclf*/wt log2 abundance ratios and the p-values of all identified and quantifiable proteins already suggests a significant reduction of several lysosomal proteins in Cln6 deficiency. Indeed, filtering the data set for proteins with at least a *nclf*/wt abundance ratio of 0,5 and a corrected p-value of 0,05 yielded 11 lysosomal proteins (Table 4.1). Interestingly, eight of these proteins are soluble hydrolases. Two proteins are integral membrane proteins and one protein is associated with the lysosomal membrane in the cytoplasm. First, this result clearly indicates that Cln6 deficiency leads to proteomic changes in the lysosomal composition and second, that mainly the reduction of soluble proteins accounts for these differences. The hydrolases, which are decreased more than 2-fold in tritosomes from *nclf* mice, all contain signal peptides present at the N-terminus, which are required for targeting proteins to the Sec61 complex and ER translocation (Janda et al. 2010). Furthermore, they are all N-glycosylated and except for Phosphatidylinositol-glycan-specific phospholipase D (Gpld1) form disulfide bonds. These two modifications take place right after or during protein translation in the ER (Feige et al. 2011, Aebi 2013). ER localization during translocation and processing provides the possibility for a direct interaction of these hydrolases with Cln6. However, the transport of these most affected hydrolases from the ER to the lysosomes follows no common pathway. While most hydrolases were shown to be transported by CLN8 from the ER to the Golgi and via the M6P-dependent pathway to the lysosome, GBA for instance is targeted to the lysosome solely by its receptor LIMP2 (Reczek et al. 2007, di Ronza et al. 2018). Moreover, the reduced hydrolases do not function in a common degradation pathway and are involved in the cleavage of different protein and lipid substrates. Smpd1 (Jenkins et al. 2010), Asah1 (Li et al. 1998) and Gba (Akiyama et al. 2013) play a role in sphingolipid metabolism. Naaa, which shares homologies with Asah1, cleaves fatty acid amides to their

corresponding acids (Tsuboi et al. 2005). Ppt1 (Camp et al. 1994) and Ppt2 (Gupta et al. 2003) are members of the palmitoyl thioesterase family. Ctsf (Tang et al. 2006) is a protease and Gpld1 (LeBoeuf et al. 1998) hydrolyzes the inositol phosphate linkage in proteins anchored by phosphatidylinositol glycans. Notably, the data set also includes soluble hydrolases, like ß-hexosaminidase (Yamanaka et al. 1994), which show no substantial changes in their abundancy. This poses the question, what are the decisive differences in affected and unaffected soluble hydrolases. Besides soluble proteins, also two membrane proteins, phosphatidylinositol 4,5-bisphosphate 4-phosphatase (Ungewickell et al. 2005) and probable phospholipid-transporting ATPase (Wang et al. 2018), are significantly reduced at least 2-fold in *nclf* tritosmes. Being involved in degradation and lysosomal export, their depletion might contribute to the disease phenotype. However, as membrane and soluble proteins use distinct processing and transport machineries in the ER, it remains to be determined, where they both require CLN6's function. Interestingly, several in *nclf* tritosomes drastically reduced soluble hydrolases are associated with other NCL subtypes. Deficiency of these hydrolases namely, Ppt1, Tpp1, Cln5, Ctsd and Ctsf causes NCL1, NCL2, NCL5, NCL10 and NCL13 respectively (Platt et al. 2018). Therefore, this finding provides a plausible explanation for lysosomal dysfunction and the development of the NCL phenotype due to CLN6 deficiency, as substrates of heavily reduced hydrolases cannot be sufficiently degraded and accumulate in the lysosomal lumen. For instance, the main accumulating substrate in NCL6 is subunit c of the mitochondrial ATPase synthase, which accounts for at least 50 % of storage material (Palmer et al. 1989) and is degraded, among others, by CTSD (Koike et al. 2000) and TPP1 (Ezaki et al. 2000), which are substantially depleted in the tritosome data set. Also, in other NCL subtypes like NCL3, NCL7 and NCL8 depletion of specific CLN proteins in the lysosome, which function as hydrolases was detected (Danyukova et al. 2018, di Ronza et al. 2018, Schmidtke et al. 2019). Besides by the primary effect of CLN6 deficiency, the changes in the protein composition of the lysosome may be also caused by its secondary effects. Massive accumulation of storage material in LSDs leads to the impairment of the fusion between lysosomes and autophagosomes as well as endosomes (Platt et al. 2012). Without the formation of endolysosomes, first, endosomes are not able to dispose their internal substrates and accumulate in the cytoplasm and, second, lysosomes are not supplied

with new lysosomal proteins, what might affect lysosomal homeostasis and cause the depletion of lysosomal proteins. However, secondary effects of LSDs usually emerge and become relevant in later stages of the disease. As the mice used for this investigation were 6 months of age, the presence of secondary effects influencing the lysosomal composition is certainly possible. Therefore, the reduction of proteins in *nclf* mouse liver tissue cannot exclusively be traced back to the absence of CLN6's primary function. Seh1 was significantly decreased with an abundance ratio of 0,479 in *nclf* tritosomes possibly due to another secondary effect, as it does not colocalize with Cln6 in the ER lumen. Seh1 is a cytosolic protein and is associated with the lysosomal membrane as part of the GATOR2 complex, which regulates lysosomal signaling. Under physiological conditions GATOR1 and GATOR2 form a complex. However, under stress conditions like a lysosomal storage disease this complex dissociates, which activates eventually the coordinated lysosomal expression and regulation (CLEAR) of 471 genes (Ho et al. 2016). The corresponding gene products elevate the lysosomal degradation capacity with the aim to remove cellular stress inducing agents (Sardiello et al. 2009, Palmieri et al. 2011). Lower mTOR activity levels in the brain of CLN3-deficient mice suggest the activation of the CLEAR pathway also in NCL diseases (Cao et al. 2006). Therefore, the stress-induced dissociation of the GATOR2 complex might be a plausible explanation for the depletion of Seh1 in the *nclf* tritosomes. Apart from secondary effects, the primary reason for the proteomic changes in *nclf* mice lies presumably in the absence of Cln6's function. In general, there are three plausible explanations for the depletion of proteins in the *nclf* lysosomes. The first one is a reduction in rate of protein biosynthesis of lysosomal proteins, as lesser proteins would be transported to the lysosome. Protein synthesis can be lowered, for instance, by downregulated gene transcription or protein translation. As CLN6 resides in the ER, where protein synthesis of lysosomal proteins takes place, principally a role in the regulation of the translation process is possible. However, so far there are no sufficient indications that CLN6 affects the translation rate. The second explanation is a decreased stability of lysosomal proteins due to Cln6 deficiency. As a consequence, they would be degraded more rapidly in the lysosomal lumen, which also results in a lesser protein amount compared to wt lysosomes. For example, increased degradation rates were shown for deglycosylated LAMP1 and 2, as glycosylation protects the lysosomal

membrane proteins from the enzymatic degradation of hydrolases (Kundra et al. 1999). Modulating proteins by protein engineering the stability and half-life time of therapeutic enzymes including lysosomal hydrolases were increased (Mumtaz et al. 1992, Dellas et al. 2021). A function of Cln6 in ER protein processing, which affects the physiological stability of proteins in the lysosome, is also feasible. Lastly, another explanation for the obtained results is an impaired transport or sorting of lysosomal proteins, which would consequently not reach the lysosome in sufficient numbers. In fact, there are several LSDs known, in which deficient transport or sorting is the cause of the disease. For instance, in mucolipidosis II and III due to GNTP deficiency the attachment of M6P-residues and, therefore, M6P-dependent transport are inhibited (Coutinho et al. 2012). Another example is the deficiency of the receptor CLN8, which disrupts the ER to Golgi transport and causes NCL8 (di Ronza et al. 2018). Likewise, for CLN6 a role in transport or sorting is possible and could explain the depletion of lysosomal proteins. In fact, the discrepancies in the western blots of the lysosomal fraction and whole tissue from wt and *nclf* mouse liver could possibly indicate such a defect. Examining the significantly reduced lysosomal proteins, none of these three possibilities for their reduction appears more likely than the other as each of these proteins depends on proper translation, processing and transport/sorting to be present in the lysosome in physiological healthy numbers. Overall, the results of the tritosome data set show a drastic reduction of specific, mostly soluble lysosomal proteins in mouse liver due to CLN6 deficiency. The function of these proteins in various degradation pathways, which are partly associated with other NCL subtypes, explains the development of an LSD and the NCL phenotype. However, the results give no clear indication on CLN6's function, as the reduced proteins are a heterogenous group, including soluble and membrane proteins, which rely on many different processing and transport pathways. Furthermore, differentiation between primary and secondary effects of CLN6's deficiency as the main cause for the depletion of these proteins in each case is not clear.

5.1.2 Investigation of 20.000 g pellets obtained from wt and *nclf* mice verify the mass spectrometric measurements of tritosomes

As the purification procedure for tritosomes is a multistep process and relies on an induced density shift and gradient centrifugation, it might be possible that lysosomes

from wt and *nclf* mice are not enriched in the same way due to biophysical and biochemical variations. To exclude this possibility, the proteomic lysosomal comparison of wt and *nclf* mice was repeated with 20.000 g liver pellets, which are obtained by only two centrifugation steps and, therefore, are not such a pure lysosomal fraction as tritosomes. Besides the lysosomal fraction, 20.000g pellets generally include other organelles like mostly mitochondria and peroxisomes, but also Golgi membranes and some ER (Graham 2002). Consequently, the western blot analysis displayed a lower enrichment of Lamp1 and Cstz compared to tritosomes and the contamination of mitochondria and ER in 20.000 g pellets of wt and *nclf* mouse liver tissue. The contaminations are indicated by the marker proteins CPT2 and PDI. However, the lysosomal enrichment is sufficient and appears to be comparable between wt and *nclf* samples and, therefore, the 20.000 g pellet fractions are usable for further mass spectrometric analysis. Except the sample purification, the mass spectrometric analysis of tritosome and 20.000 g pellet samples were conducted and analyzed identically. As expected, due to differences in the level of purity the two data sets differ in the total number of identified proteins. While in 20.000 g pellets 2530 proteins were detected, in tritosomes only 1691 proteins were identified. However, the tritosome data set contains with 237 proteins more lysosomal proteins compared to the 167 lysosomal proteins found in the 20.000 g pellets. Despite the discrepancy the data sets show a big overlap and have 1257 total proteins and 147 lysosomal proteins in common. Sharing 88 % of the lysosomal fraction is sufficient to compare the tritosome and the 20.000 g pellet data sets in respect of their lysosomal proteome. Furthermore, the lysosome is the second most abundant result in KEGG pathway analysis of at least 2-fold significantly reduced proteins from the tritosome and 20.000 g pellet data set, respectively. In contrary to the volcano plot of the tritosome data set, the volcano plot of the 20.000 g pellet data set indicates no clear lopsided distribution, because the number of proteins is drastically increased, which are not lysosomal. The table 4.2 with proteins, which are reduced at least by 50 % and with a 0,05 p-value, contains 11 lysosomal proteins, although only 4 of them are identical with the significantly reduced proteins in the tritosome data set. However, the composition of these lysosomal proteins is similar, as 10 of them are soluble hydrolases and only one, Lamp2, is a membrane protein. Again, these hydrolases all contain signal peptides, which indicate their translocation into the ER.

Furthermore, they are N-glycosylated and except for dipeptidyl peptidase 2 form disulfide bonds. Similar to the significantly reduced hydrolases found in *nclf* tritosomes they do not act in any particular degradation pathway or are transported to the lysosome in one and the same way. Consequently, these results are in line with the findings in the tritosome data set, as they verify the reduction of lysosomal proteins upon CLN6 deficiency, which include mainly soluble hydrolases. NCL related soluble proteins, CLN1, CLN2, CLN10 and CLN13 are also found substantially depleted in *nclf* 20.000 g pellets as in *nclf* tritosomes. However, CLN5 was not identified. Moreover, there were also soluble hydrolases in the data set, like again ß-hexosaminidase, which show no substantial differences between wt and *nclf* samples. In contrast to the tritosome data set, in which no lysosomal protein was significantly increased, two lysosomal proteins, progranulin and transmembrane protein 106B, were found increased at least by 50 % and a 0,05 p-value in the 20.000 g pellets from *nclf* mice. The increase of both proteins is associated with the inhibition of vacuolar H^+-ATPases (Lang et al. 2012). In multiple LSDs including NCLs dysregulation of acidification and an elevated pH were observed, which indicates the inhibition of H^+-ATPases (Holopainen et al. 2001, Bagh et al. 2017). Therefore, the upregulation of progranulin and transmembrane protein 106B is most likely caused by this secondary effect of CLN6 deficiency. Interestingly, impairment of progranulin leads to NCL11 and its function is closely related to the development, survival and function of neurons and microglia (Rhinn et al. 2022). Therefore, the upregulation of progranulin might also present a compensatory response to the aggravating neurodegeneration. As the localization of both proteins is not exclusively the lysosome, this difference compared to the tritosome data set might be due to the inclusion of other cellular fractions in 20.000 g pellets containing these proteins. In contrary to the tritosomes, where only lysosomes are supposed to be purified, in 20.000 g pellets additional enrichment of mitochondria, peroxisomes, Golgi and ER is method-dependent. Consequently, in the 20.000 g pellet data set, besides lysosomal proteins, there are also a substantial number of proteins from other cellular organelles significantly decreased or elevated. Among these proteins there are certainly interesting candidates, which might play a role in the pathology of NCL6. However, solely by the mass spectrometric analysis, it is not possible to differentiate, if proteins were primarily affected by CLN6 deficiency or by another of various disease related

secondary effects. For instance, in knock-out models the depletion of a distinct protein is often compensated by adaptive proteomic changes (Periquet et al. 2005). Furthermore, the accumulation of storage material in NCL6 is another potential secondary effect for the increase of proteins like several subunits of the mitochondrial membrane protein ATP synthase as well as the TIM and the TOM complexes in *nclf* 20.000 g pellets. Therefore, this study focuses solely on changes in known bona fide lysosomal proteins.

5.1.3 Western blot analysis of selected hydrolases in tritosomes and whole liver lysates from wt and *nclf* mice

As the lysosomal proteome of wt and *nclf* mice was only investigated by mass spectrometry so far, the results could have been influenced by mass spectrometric sample preparation and measurements. Therefore, the reduction of selected hydrolases in the tritosome data set was confirmed by western blot to ensure the results are method independent. Equal protein amounts of wt and *nclf* tritosomes were separated by SDS-PAGE, blotted on a PVDF membrane and probed with antibodies against Ctsd, Ctsz, Ppt1 and Tpp1. The quantification of these proteins showed a very similar reduction of the protein amount in *nclf* samples compared to the tritosome data set providing further validation. In addition, also whole liver lysates were tested for the protein amount of Ctsd, Ctsz and Ppt1 by western blot. While Ctsd and Ppt1 were reduced in unfractionated liver lysates of *nclf* mice similar as in tritosomes, Ctsz was significantly increased. This might indicate a role for CLN6 in sorting and transport. Beside the heavy chain, the western blot of Ctsd also displays its precursors. Ctsd with its signal peptide and propeptide is present as inactive preprocathepsin in the ER. As the signal peptide is cleaved preprocathepsin D is converted to procathepsin D, which is finally processed in endosomes and lysosomes to its mature and active form by removing the propeptide and being split to its light and heavy chain (Gieselmann et al. 1985, Zaidi et al. 2008). Interestingly, the differences of these three Ctsd forms between wt and *nclf* samples do not appear to be proportional. While the protein amount of immature Ctsd forms is already clearly decreased in *nclf* samples, the protein amount of mature Ctsd is found to be even more decreased, what might be another indication for sorting and transport defects in CLN6 deficiency. A recent proteomic investigation of secretome

changes in CLN6 deficient cells has revealed an increased secretion of various soluble hydrolases including Ctsd, which was also shown to be reduced intracellularly (Best et al. 2021). This finding is in line with the results of these study and also points to a possible transport aberration of specific hydrolases in CLN6 deficiency.

5.1.4 Western blot analysis of selected hydrolases in 20.000 g brain pellets and whole brain lysates from wt and *nclf* mice

NCL6 is a neurodegenerative disease and shows mainly neurological symptoms (Morgan et al. 2013, Sawiak et al. 2015, Rus et al. 2022). As the highly purified lysosomal tritosome fraction can be only obtained from liver tissue, this method is not suitable to investigate proteomic changes in neuronal tissue. Therefore, selected hydrolases were compared in 20.000 brain pellets from wt and *nclf* mice by western blot to determine if the reduction of specific lysosomal proteins in mouse liver tissue is also present in the brain. Ppt1 and Tpp1 showed a significant protein amount reduction in *nclf* brain samples similar to their reduction in liver tissue. The reduction of Ctsz was not as big and did not reach significance. These results suggest, that the proteomic changes determined in liver tissue by mass spectrometric measurements are not tissue specific and also present in neuronal tissue as it was shown for Ppt1, Tpp1 and Ctsz in the brain. Therefore, the reduction of soluble hydrolases, including NCL related proteins Ppt1, Tpp1 and Ctsd, in brain tissue might give a plausible explanation for the development of the neurological pathology in NCL6. Furthermore, the same three proteins were analyzed and quantified in whole brain lysates of wt and *nclf* mice. Interestingly, for Ctsz and Tpp1 the protein amount was significantly increased in *nclf* mouse brain tissue. In the case of Ppt1, the protein amount was still reduced, however not significantly anymore. These findings along with comparable results in whole liver lysates might indicate an aberrant transport or sorting of specific soluble proteins in CLN6 deficiency. Potentially, the transport of these proteins is inhibited and they do not reach the lysosome but clog in other cellular compartments. That still some hydrolases show a reduction in the whole brain lysate, like Ppt1, might be explained by increased secretion of these proteins, as elevated secretion levels of specific proteins in CLN6 deficiency have been shown by a recent study (Best et al. 2021).

5.1.5 The reduction of protein amount correlates with the enzyme activities of Ctsd, Gba and Ppt1

To identify the reduction from protein amount of various different soluble hydrolases as reason for the lysosomal dysfunction, enzyme activity assays were conducted of selected substantially decreased hydrolases. Activities of Ctsd and Gba in *nclf* tritosomes and Ppt1 activity in *nclf* whole liver tissue were drastically reduced compared to the wt controls. The extent of reduction corresponds approximately to the reduction in protein amount. Therefore, it can be assumed that the decreased abundancies of the lysosomal hydrolases in CLN6 deficiency leads to a functional impairment and is the reason for the development of NCL6.

5.2 Exploration of CLN6's interactome in the ER

Besides the investigations of proteomic changes in the lysosome due to CLN6 deficiency, the second objective of this study was to determine novel interaction partners of CLN6. The identification of CLN6's interactome could give important functional information about CLN6. For instance, protein-protein interaction data has been used to predict protein function in silico (Letovsky et al. 2003). Furthermore, identifying proteins interacting with CLN6 would enable further functional investigations including CLN6 and these proteins. As this study along with many more previous research on CLN6 has revealed various insights on CLN6 biology, the determined interaction partners can be evaluated with respect to whether their interaction with CLN6 is coherent with or even explains the previous findings. In that regard proteins, which are associated with lysosomal hydrolases and their synthesis, processing or transport to the lysosome, are of special interest, as they might indicate the relation between CLN6 deficiency and the reduction of soluble hydrolases. To determine candidate proteins for the interaction with CLN6, the BioID approach was applied, which provides proteins in close proximity of the target protein (Varnaitė et al. 2016). Afterwards the interaction of selected candidates and CLN6 was tested by the BiFC assay, which is a suitable method to indicate protein-protein interactions (Kerppola 2009).

5.2.1 Identification of proteins in the vicinity of CLN6 using the BioID approach

HEK cells were transfected with the fusion proteins of CLN6 and the BioID. The biotinylation by a biotin ligase attached to either the N- or C-terminus of CLN6 enabled the purification and identification of soluble proteins in the cytoplasm or the ER lumen and membrane proteins integrated in the ER membrane, which are in close proximity of CLN6. Cells, which were either not transfected with the CLN6-BioID fusion protein or not incubated with biotin, served as internal controls and could be differentiated from the sample as they were differently SILAC labeled before treatment. Finally, proteins were purified and analyzed by mass spectrometry. If proteins showed a 2-fold change compared to the controls, they were considered as biotinylated and, therefore, had to be in the vicinity of CLN6. As biotinylation is a very rare post-translational modification most proteins are biotinylated by the BioID (Chapman-Smith et al. 1999). Furthermore, proteins biotinylated by endogenous biotin ligases are supposed to show similar protein amounts in the control samples and, therefore, should be not included in the data sets. Three data sets obtained by using the BioID fused on the N-terminus of CLN6 were created and displayed 57 common proteins. Apart from ER localization, these proteins reside in the nucleus, the nuclear envelope, the cytoplasm, the Golgi and the lysosome. Biotinylation of proteins from so many different intracellular locations is not surprising, as the ER membrane is adjacent to the cytoplasm, the nucleus and the nuclear envelope. In addition, it shares contact sites to the Golgi, mitochondria and the endosomal-lysosomal system (Raiborg et al. 2015). Apart from potentially relevant proteins for CLN6 biology, the three data sets include also many structural and ubiquitous proteins like lamina-associated polypeptide 2 or filamin-A and randomly biotinylated proteins, which give no insights of CLN6's interactions or functions. Considering the relevancy of CLN6 for lysosomal homeostasis only one protein, the CI-M6P receptor, is labeled by the BioID approach, which is localized at the lysosome. In fact, CI-MPR is crucial for the transport of lysosomal proteins, however the receptor first binds its ligands in the trans-Golgi after they received M6P residues and transport them from there to endosomes, which later fuse with lysosomes (Bajaj et al. 2019). Therefore, a function of CLN6 linked to CI-MPR is limited to its synthesis or processing. As also soluble hydrolases for example Gba are affected by Cln6 deficiency, which are transported via M6P independent pathways, this correlation is rather unlikely. The presence of

eukaryotic translation initiation factor 4 gamma 1 (eIF-4G1) in all N-terminal BioID data sets indicates CLN6's proximity to the site of protein biosynthesis. The eIF-4G1 subunit acts as scaffold for further subunits of the eukaryotic initiation factor 4 complex, which recruits ribosomes to mRNA by binding to its 5' cap structure (Jaiswal et al. 2019). Inhibition of eIF-4G1 is associated with reduced cap-dependent translation (Moerke et al. 2007). Even though eIF-4G1 is of cytoplasmic location, it can be biotinylated by the N-terminal BioID construct as the N-terminus is present in the cytoplasm. Most presumably eIF-4G1 and CLN6 come close to each other at the Sec63 translocons, where recruited ribosomes translate mRNA into the ER lumen and their close proximity consequently opens up a potential role for CLN6 in the regulation of mRNA translation. Studies have yet to be conducted to investigate and clearly determine the effect of CLN6 on translation, as so far there are no sufficient indications for a possible correlation. Two subunits of the signal recognition particle and dolichyl-diphosphooligosaccharide--protein glycosyltransferase subunit STT3B (STT3B) were also found in all three data sets confirming CLN6's vicinity to the site of protein biosynthesis. STT3B is the catalytic subunit of the OST complex, which transfers N-glycans onto newly translocated nascent polypeptides and modifies also a large set of lysosomal proteins, as all soluble hydrolases, which were significantly reduced by at least 50 %, are N-glycosylated (Ramírez et al. 2019). The previous findings and the results of this investigation are not sufficient to clarify the role of CLN6 in glycosylation. Certainly, CLN6 deficiency does not lead to a full impairment of glycosylation, as soluble hydrolases dependent on N-glycans for their transport still reach the lysosome. However, an involvement of CLN6 in glycosylation cannot be excluded on the basis of the spatial proximity between CLN6 and OST. Besides proteins playing a role in translation or early protein modification at the translocon complex, there are also two proteins found in all three N-terminal BioID data sets, protein transport protein Sec16A (SEC16A) and transport and golgi organization protein 1 homolog (TANGO1), which suggest that CLN6's localization is not limited to the site of biosynthesis. These two proteins both function at the ERESs. While SEC16A presumably plays a key role in the establishment of COPII vesicles, TANGO1 is required for the loading of specific larger cargoes into COPII vesicles (Hughes et al. 2010, Raote et al. 2021). These proteins most likely do not play a role in NCL6

pathogenesis and are not directly related to the reduced hydrolases in the lysosome, however, it is interesting that CLN6 seems to show mobility across the ER membrane and is at least localized at two distinct sites, the site of protein biosynthesis and the ERES, which are passed by lysosomal proteins on the secretory pathway to the lysosome. The BioID experiment was also conducted with the biotin ligase being fused to the C-terminus of CLN6 to label proteins close to CLN6 in the ER lumen. As the greatest proportion of CLN6 is located in the ER lumen and also the most of the pathological mutations leading to NCL6 are found there (https://www.ucl.ac.uk/ncl-disease/mutation-and-patient-database/mutation-and-patient-datasheets-human-ncl-genes/cln6), it is thought to be more likely to contain relevant interaction partners of CLN6 than the cytoplasm. Again, three data sets were generated, which have 10 proteins in common, which are a lot less compared to the 57 proteins contained in all three data sets of the N-terminal BioID construct. Comparing table 4.3 and 4.4, 6 proteins are identical and only 4 proteins are found additionally using the C-terminal BioID construct, which appear not to be relevant for CLN6's function. Furthermore, the 10 proteins are not mainly ER resident proteins, but their localization is mostly predicted to be nuclear. As nuclear proteins in general do not reside in the ER lumen, it is remarkable that so many nuclear proteins and comparatively only few ER resident or secretory proteins were labeled by the biotin ligase. This fact could point to technical issues of the BioID approach. Proteins, which were not biotinylated like abundant nuclear proteins, might be included in the analysis due to unspecific binding to the streptavidin beads. Mechanistic variability could also be an explanation for the big variations between the three data sets. The ER is a very crowded environment with a protein concentration of more than 100 mg/mL (Kleizen et al. 2004). Therefore, random biotinylation in such an environment with an enormous protein amount might partly account for the differences in the three data sets. As a recent study shows the interaction of CLN6 with several lysosomal hydrolases including CTSD and PPT1 as well as CLN8, it raises the question why these proteins are not included in any of the obtained data sets (Bajaj et al. 2020). One possible explanation is that the biotinylation sites of these proteins are not accessible for the BioID constructs. The lysosomal hydrolases are processed and modified by an enormous number of proteins, which might block the access of the biotin ligase. Moreover, the newly synthesized proteins like the lysosomal

hydrolases are greatly outnumbered by these abundant chaperones and folding enzymes forming a gel-like protein matrix in the ER lumen and, therefore, the amount of biotinylated newly synthesized proteins might be not sufficient to surpass the detection limit in the mass spectrometric measurements (Kleizen et al. 2004). Additionally in case of membrane protein CLN8, low solubilization in the BioID lysis buffer could be another reason that it was not purified and identified by mass spectrometry.

5.2.2 Evaluation of interactions between CLN6 and selected candidate proteins by the BiFC assay

The BioID data sets, the investigation of the lysosomal proteome in CLN6 deficiency and the literature provided many proteins, which could potentially interact with CLN6. The candidate proteins PPT1, CTSD, CTSZ, GANAB, CANX, CALR and CLN8 were selected and their interaction with CLN6 was evaluated by the BiFC assay. The method relies on the reconstitution of YFP fragments fused to the investigated proteins. This assay has already been successfully applied for the identification of interactions between proteins in the early secretory pathway and poses a useful and promising method for this purpose (Nyfeler et al. 2005). Furthermore, as only few interaction partners of CLN6 were identified so far, it is beneficial that also transient and weak interactions can be detected by the BiFC assay, as the YFP reconstitution is irreversible and stabilizes the protein-protein interaction (Kerppola 2008). The candidate proteins include significantly reduced hydrolases, key components of the calnexin cycle and CLN8, a receptor for various soluble lysosomal proteins and, therefore, are all linked to the lysosomal biogenesis. After preliminary experiments interaction of the proteins PPT1, CTSD, CTSZ and GANAB with CLN6 could be excluded according to the BiFC assay. However, a recent study verified the interaction of PPT1 and CTSD with CLN6 by Co-IP and suggested that CLN6 acts as adaptor protein and plays a role in the transport of specific soluble lysosomal hydrolases (Bajaj et al. 2020). There are various potential reasons for the contradictory results obtained by Co-IP and BiFC. The size of the interacting proteins and the type and length of the linker affect the spatial orientation and the freedom of the YFP fragments, what presumably prevent a YFP reconstitution despite an actual interaction. Another reason might be again the crowded environment around newly synthesized proteins in the ER (Kleizen et al. 2004). On the contrary, Co-

IP experiments are also prone for false positive results especially in case of overexpression. As the preliminary BiFC studies suggested higher fluorescent intensities for combinations of CANX, CALR or CLN8 with CLN6 compared to the negative control, further BiFC experiments were conducted, measured by FACS and replicated three times. The most suited and stringent negative control for the BiFC assay consists of a combination of the two potentially interacting proteins, while one contains a mutation in the domain relevant for the protein-protein interaction. However, in most cases it is not possible to include this negative control, because the interacting domain is not known previously or due to instability of the mutated protein. Another good negative control for the BiFC assay is a closely related protein (Kudla et al. 2016). However, the domains of CLN6, which are binding to its interaction partners, are not identified and there are also no homologues of CLN6 known. Therefore, Ergic53, which resides in the ER and is hypothetically able to interact with CLN6, was chosen as the negative control. However, this control is not optimal, as protein structures of Ergic53 and the investigated proteins greatly vary. Because of these structural differences it is not necessarily possible to conclude a protein-protein interaction from significantly different fluorescence values, as the protein structure might affect random YFP reconstitution. In the previously mentioned study, the interaction of CLN6 with CLN8 has already been shown in BiFC assays and was confirmed by Co-IP analysis (Bajaj et al. 2020). Therefore, CLN8 was included in the assay as positive control and to validate the previous results. The dimerization between CLN6 proteins was used as another positive control. The evaluated CLN6-CLN8 results display a slightly but significantly higher fluorescent signal compared to the negative control for both YFP combinations. However, the fluorescence intensity is much lower compared to the CLN6 positive control. This result validates the previous finding and a possible association of CLN6 and CLN8 is very interesting, as both proteins are related to NCL and, therefore, might give new insights in relevant pathomechanisms. The BiFC results for CLN6 and CANX or CALR are also showing significant higher fluorescence signals when the YFP1 fragment was fused to CLN6. If the YFP2 signal was fused to CLN6, these differences to the negative control are lost possibly due to steric constraints. However, one combination of YFP fragments, which shows a YFP reconstitution and includes valid controls, is sufficient to indicate a protein-protein interaction by the BiFC assay

(Kerppola 2008). So far, a possible interaction of CANX and CALR with CLN6 has not been reported yet and might also give new important information for the development of NCL6. In a further BiFC experiment, the exact same proteins were investigated with a mutated CLN6 devoid of its second loop, which accounts for the majority of CLN6's part in the ER lumen. This experiment was conducted to determine, if the second loop of CLN6 includes the binding domain for the interactions to CLN8, CANX or CALR. The results of three replicates obtained with the mutated CLN6 and the canonical CLN6 show no significant differences and, therefore, give no clear evidence, if the second loop plays any role in a potential protein-protein interaction between CLN6 and the investigated proteins. To assess if the C-terminus of CLN6 is responsible for the interaction of CLN6 with CANX or CARL, this region was also deleted. However, only one replicate was generated for the YFP construct combinations with CLN6 devoid of its C-terminus. As FACS measurements display great reproducibility also one experiment gives already a good impression. The result does not show a reduction of the fluorescence intensities compared to the results with the full-length CLN6 constructs and, therefore, does not indicate an involvement of the C-terminus in the protein-protein interaction. To determine and validate if the detected YFP reconstitution is actually based on a protein-protein interaction in the ER lumen both mutations were combined, which resulted in a CLN6 almost completely devoid of its ER luminal parts. With YFP constructs containing the double mutated CLN6 the BiFC experiments with CANX and CALR were repeated. However, again only one replicate was generated. Interestingly, also with this construct a fluorescence signal could be detected, which was even higher than the one with the full-length CLN6. As CANX and CLN6 both are membrane proteins, they might still interact through their transmembrane domains. However, CALR's interaction with CLN6 without its ER luminal parts is unclear. Possibly, the structure of the mutated CLN6 is altered or leads to misfolding and CANX and CALR act as chaperones for the mutated CLN6. In general, CANX and CALR bind to N-glycans of glycosylated proteins. However, CANX and CALR also contain a binding site for protein-protein interactions. Therefore, they are also capable to bind proteins, which have no glycosylation site like CLN6 (Saito et al. 1999, Danilczyk et al. 2001). Finally, the interaction of CLN8 with CANX and CALR was investigated in three BiFC assays and statistically analyzed, as CLN8 presumably interacts with CLN6 and is

related to NCL. The negative control for these experiments was a combination of CLN8- and Erig53-YFP constructs. The results clearly show an increased YFP reconstitution for both proteins compared to the negative control, which was also significant and indicates an interaction of CLN8 with CANX and CALR. This finding supports a close functional relation between CLN6, CLN8, CANX and CALR. However, to truly validate all these investigated protein-protein interactions, the results have to be repeated by at least another independent method (Kudla et al. 2016). Still, the BiFC assay on its own certainly verifies the very close proximity between CLN6, CLN8, CANX and CALR, which is necessary for a functional relation. The study, which showed protein-protein interactions between CLN6 and CLN8 as well as CLN6 and specific hydrolases, indicated also an impaired transport of respective hydrolases to the Golgi in CLN6 deficient cells (Bajaj et al. 2020). These findings are in line with the results of the lysosomal proteome analysis, the BioID approach and the BiFC assay. According to the BioID results CLN6 could act as an adapter protein and bind lysosomal hydrolases right after their translocation into the ER, mediate the association between CLN8 and the hydrolases and guide them towards the ERES, where CLN6 dissociates from CLN8 and the hydrolases before they are packed into COPII vesicles. This hypothesis is also supported by new findings about the goal-keeper protein UGGT, which reglycosylates mis- or unfolded glycoproteins in the ER to allow further rounds of binding to CALR and CANX in the calnexin cycle. Lysosomal proteins, which were found to interact with CLN6 and CLN8 are not reglycosylated by UGGT1 or 2 (Adams et al. 2020). Due to the proposed close attachment to the ER membrane through CANX, CALR, CLN6 and CLN8 lysosomal proteins possibly are prevented from coming into contact with the UGGT, which is a soluble protein and resides inside the ER lumen. This would require that lysosomal proteins are correctly folded during a one binding event in the calnexin cycle and are therefore processed independently of UGGT1 activity, which was shown for exemplary proteins by deleting UGGT1 (Solda et al. 2007). In the lysosomal proteome of *nclf* mice also at least one hydrolase, GBA, was found significantly reduced, which is not transported to the Golgi by the CLN8 receptor but by LIMP2. Consequently, according to this hypothesis CLN6 has to act also as an adaptor protein for GBA and LIMP2. In this model, however, the binding sites between CLN6, the set of hydrolases and CLN8 or LIMP2 and the exact underlying molecular

mechanism is still to be determined. The proposed interactions of lysosomal hydrolases and CLN6, which were not validated in this study, could also indicate an indirect interaction between CLN6 and CANX as well as CALR, as both, the chaperones and CLN6, were shown to bind glycosylated hydrolases. Therefore, the YFP reconstitution in the BiFC assay might be caused by the formation of a complex consisting of CLN6, CLN8, CANX, CALR and a lysosomal hydrolase and not by a direct interaction between CLN6 with CANX and CALR. According to this model CLN6 enhances the association of hydrolases to the ER membrane and increases the percentage of hydrolases, which are transported in a receptor-mediated manner compared to the ones, which are transported by bulk flow. Although, the bulk flow can also show rapid transport rates, the receptor-mediated transport is overall more efficient and targeted. Therefore, this suggested model for CLN6's function as adaptor protein is conceivable and explains the reduction of soluble hydrolases in the lysosome as CLN6 deficiency impairs their proper trafficking in the early secretory pathway.

6 Outlook

In this study the NCL subtype, which is caused by CLN6 deficiency was closely investigated. Previously the connection between CLN6 dysfunction and NCL was largely unknown. The results of this study indicate a substantial decrease in protein amount and activity of many soluble hydrolases in *nclf* lysosomes as reason for the development of an LSD. Furthermore, the BioID approach identified CLN6 to be in close proximity of proteins of the protein synthesis and ERES and investigations by the BiFC assay showed the glycoprotein chaperones CANX and CALR are potential interaction partners of CLN6. The obtained results contribute to the knowledge about the molecular biology of CLN6 and raise new questions. As reduced lysosomal hydrolases in NCL6 are transported by different pathways it is up to future investigations to elucidate how in detail CLN6 affects these various different proteins. Since the interaction partner studies contained also subunits of the OST, another valid research question would be if CLN6 deficiency impacts the glycosylation process and structure. Further scientific effort will also be needed to verify the proposed hypothesis, that the function of CLN6 might be to ensure membrane association of newly synthesized lysosomal proteins until they sufficiently folded and processed to bind to their membrane-anchored receptors and chaperones like CLN8, LIMP2 and CANX. Especially, the binding domain and mechanism of CLN6 is of high interest as hydrolases with such different protein structures are affected. Indications to this hypothesis and the function of CLN6 could also be provided by examination of the route and destination of lysosomal proteins in CLN6 deficiency, which are not reaching the lysosome. Progress in CLN6 research in the areas mentioned above could also lead to an improvement in therapy and treatment of NCL6.

7 List of references

. "CLN6 mutation database." from https://www.ucl.ac.uk/ncl-disease/mutation-and-patient-database/mutation-and-patient-datasheets-human-ncl-genes/cln6.

Abeijon, C. and C. B. Hirschberg (1992). "Topography of glycosylation reactions in the endoplasmic reticulum." Trends Biochem Sci **17**(1): 32-36.

Adams, B. M., N. P. Canniff, K. P. Guay, I. S. B. Larsen and D. N. Hebert (2020). "Quantitative glycoproteomics reveals cellular substrate selectivity of the ER protein quality control sensors UGGT1 and UGGT2." Elife **9**.

Aebi, M. (2013). "N-linked protein glycosylation in the ER." Biochimica et Biophysica Acta (BBA) - Molecular Cell Research **1833**(11): 2430-2437.

Akiyama, H., S. Kobayashi, Y. Hirabayashi and K. Murakami-Murofushi (2013). "Cholesterol glucosylation is catalyzed by transglucosylation reaction of β-glucosidase 1." Biochem Biophys Res Commun **441**(4): 838-843.

Anderson, G. W., H. H. Goebel and A. Simonati (2013). "Human pathology in NCL." Biochim Biophys Acta **1832**(11): 1807-1826.

Appenzeller, C., H. Andersson, F. Kappeler and H. P. Hauri (1999). "The lectin ERGIC-53 is a cargo transport receptor for glycoproteins." Nat Cell Biol **1**(6): 330-334.

Bagh, M. B., S. Peng, G. Chandra, Z. Zhang, S. P. Singh, N. Pattabiraman, A. Liu and A. B. Mukherjee (2017). "Misrouting of v-ATPase subunit V0a1 dysregulates lysosomal acidification in a neurodegenerative lysosomal storage disease model." Nature Communications **8**(1): 14612.

Bainton, D. F. (1981). "The discovery of lysosomes." J Cell Biol **91**(3 Pt 2): 66s-76s.

Bajaj, L., P. Lotfi, R. Pal, A. d. Ronza, J. Sharma and M. Sardiello (2019). "Lysosome biogenesis in health and disease." Journal of Neurochemistry **148**(5): 573-589.

Bajaj, L., J. Sharma, A. di Ronza, P. Zhang, A. Eblimit, R. Pal, D. Roman, J. R. Collette, C. Booth, K. T. Chang, R. N. Sifers, S. Y. Jung, J. M. Weimer, R. Chen, R. W. Schekman and M. Sardiello (2020). "A CLN6-CLN8 complex recruits lysosomal enzymes at the ER for Golgi transfer." J Clin Invest **130**(8): 4118-4132.

Ballabio, A. (2016). "The awesome lysosome." EMBO Mol Med **8**(2): 73-76.

Ballabio, A. and V. Gieselmann (2009). "Lysosomal disorders: from storage to cellular damage." Biochim Biophys Acta **1793**(4): 684-696.

Barlowe, C. (2003). "Signals for COPII-dependent export from the ER: what's the ticket out?" Trends Cell Biol **13**(6): 295-300.

Barlowe, C. and A. Helenius (2016). "Cargo Capture and Bulk Flow in the Early Secretory Pathway." Annu Rev Cell Dev Biol **32**: 197-222.

Beel, S., M. Moisse, M. Damme, L. De Muynck, W. Robberecht, L. Van Den Bosch, P. Saftig and P. Van Damme (2017). "Progranulin functions as a cathepsin D chaperone to stimulate axonal outgrowth in vivo." Hum Mol Genet **26**(15): 2850-2863.

Bellettato, C. M. and M. Scarpa (2010). "Pathophysiology of neuropathic lysosomal storage disorders." J Inherit Metab Dis **33**(4): 347-362.

Berkovic, S. F., K. L. Oliver, L. Canafoglia, P. Krieger, J. A. Damiano, M. S. Hildebrand, M. Morbin, D. F. Vears, V. Sofia, L. Giuliano, B. Garavaglia, A. Simonati, F. M. Santorelli, A. Gambardella, A. Labate, V. Belcastro, B. Castellotti, C. Ozkara, A. Zeman, J. Rankin, S. E. Mole, U. Aguglia, M. Farrell, S. Rajagopalan, A. McDougall, S. Brammah, F. Andermann, E. Andermann, H. M. Dahl, S. Franceschetti and S. Carpenter (2019). "Kufs disease due to mutation of CLN6: clinical, pathological and molecular genetic features." Brain **142**(1): 59-69.

Best, H. L., A. J. Clare, K. O. McDonald, H. E. Wicky and S. M. Hughes (2021). "An altered secretome is an early marker of the pathogenesis of CLN6 Batten disease." J Neurochem **157**(3): 764-780.

Blott, E. J. and G. M. Griffiths (2002). "Secretory lysosomes." Nat Rev Mol Cell Biol **3**(2): 122-131.

Boonen, M., C. Staudt, F. Gilis, V. Oorschot, J. Klumperman and M. Jadot (2016). "Cathepsin D and its newly identified transport receptor SEZ6L2 can modulate neurite outgrowth." J Cell Sci **129**(3): 557-568.

Braulke, T. and J. S. Bonifacino (2009). "Sorting of lysosomal proteins." Biochim Biophys Acta **1793**(4): 605-614.

Breitling, J. and M. Aebi (2013). "N-linked protein glycosylation in the endoplasmic reticulum." Cold Spring Harb Perspect Biol **5**(8): a013359.

Bronson, R. T., L. R. Donahue, K. R. Johnson, A. Tanner, P. W. Lane and J. R. Faust (1998). "Neuronal ceroid lipofuscinosis (nclf), a new disorder of the mouse linked to chromosome 9." Am J Med Genet **77**(4): 289-297.

Budnik, A. and D. J. Stephens (2009). "ER exit sites – Localization and control of COPII vesicle formation." FEBS Letters **583**(23): 3796-3803.

Buratta, S., B. Tancini, K. Sagini, F. Delo, E. Chiaradia, L. Urbanelli and C. Emiliani (2020). "Lysosomal Exocytosis, Exosome Release and Secretory Autophagy: The Autophagic- and Endo-Lysosomal Systems Go Extracellular." Int J Mol Sci **21**(7).

Camp, L. A., L. A. Verkruyse, S. J. Afendis, C. A. Slaughter and S. L. Hofmann (1994). "Molecular cloning and expression of palmitoyl-protein thioesterase." J Biol Chem **269**(37): 23212-23219.

Cao, Y., J. A. Espinola, E. Fossale, A. C. Massey, A. M. Cuervo, M. E. MacDonald and S. L. Cotman (2006). "Autophagy is disrupted in a knock-in mouse model of juvenile neuronal ceroid lipofuscinosis." J Biol Chem **281**(29): 20483-20493.

Caramelo, J. J. and A. J. Parodi (2008). "Getting in and out from calnexin/calreticulin cycles." J Biol Chem **283**(16): 10221-10225.

Chapman-Smith, A. and J. E. Cronan Jr (1999). "Molecular Biology of Biotin Attachment to Proteins." The Journal of Nutrition **129**(2): 477S-484S.

Chin, J. J., B. Behnam, M. Davids, P. Sharma, W. M. Zein, C. Wang, X. Chepa-Lotrea, W. B. Gallantine, C. Toro, D. R. Adams, C. J. Tifft, W. A. Gahl and M. C. V. Malicdan (2019). "Novel mutations in CLN6 cause late-infantile neuronal ceroid lipofuscinosis without visual impairment in two unrelated patients." Molecular Genetics and Metabolism **126**(2): 188-195.

Coutinho, M. F., M. J. Prata and S. Alves (2012). "Mannose-6-phosphate pathway: a review on its role in lysosomal function and dysfunction." Mol Genet Metab **105**(4): 542-550.

Cox, T. M. and M. B. Cachon-Gonzalez (2012). "The cellular pathology of lysosomal diseases." J Pathol **226**(2): 241-254.

Csala, M., G. Banhegyi and A. Benedetti (2006). "Endoplasmic reticulum: a metabolic compartment." FEBS Lett **580**(9): 2160-2165.

D'Arcangelo, J. G., K. R. Stahmer and E. A. Miller (2013). "Vesicle-mediated export from the ER: COPII coat function and regulation." Biochimica et Biophysica Acta (BBA) - Molecular Cell Research **1833**(11): 2464-2472.

Dancourt, J. and C. Barlowe (2010). "Protein sorting receptors in the early secretory pathway." Annu Rev Biochem **79**: 777-802.

Danilczyk, U. G. and D. B. Williams (2001). "The lectin chaperone calnexin utilizes polypeptide-based interactions to associate with many of its substrates in vivo." J Biol Chem **276**(27): 25532-25540.

Danyukova, T., K. Ariunbat, M. Thelen, N. Brocke-Ahmadinejad, S. E. Mole and S. Storch (2018). "Loss of CLN7 results in depletion of soluble lysosomal proteins and impaired mTOR reactivation." Hum Mol Genet **27**(10): 1711-1722.

De Duve, C., B. C. Pressman, R. Gianetto, R. Wattiaux and F. Appelmans (1955). "Tissue fractionation studies. 6. Intracellular distribution patterns of enzymes in rat-liver tissue." Biochem J **60**(4): 604-617.

De Duve, C. and R. Wattiaux (1966). "Functions of lysosomes." Annu Rev Physiol **28**: 435-492.

Dellas, N., J. Liu, R. C. Botham and G. W. Huisman (2021). "Adapting protein sequences for optimized therapeutic efficacy." Current Opinion in Chemical Biology **64**: 38-47.

di Ronza, A., L. Bajaj, J. Sharma, D. Sanagasetti, P. Lotfi, C. J. Adamski, J. Collette, M. Palmieri, A. Amawi, L. Popp, K. T. Chang, M. C. Meschini, H. E. Leung, L. Segatori, A. Simonati, R. N. Sifers, F. M. Santorelli and M. Sardiello (2018). "CLN8 is an endoplasmic reticulum cargo receptor that regulates lysosome biogenesis." Nat Cell Biol **20**(12): 1370-1377.

Ellgaard, L., N. McCaul, A. Chatsisvili and I. Braakman (2016). "Co- and Post-Translational Protein Folding in the ER." Traffic **17**(6): 615-638.

Elvevold, K., J. Simon-Santamaria, H. Hasvold, P. McCourt, B. Smedsrød and K. K. Sørensen (2008). "Liver sinusoidal endothelial cells depend on mannose receptor-mediated recruitment of lysosomal enzymes for normal degradation capacity." Hepatology **48**(6): 2007-2015.

English, A. R., N. Zurek and G. K. Voeltz (2009). "Peripheral ER structure and function." Current Opinion in Cell Biology **21**(4): 596-602.

Ezaki, J., M. Takeda-Ezaki and E. Kominami (2000). "Tripeptidyl peptidase I, the late infantile neuronal ceroid lipofuscinosis gene product, initiates the lysosomal degradation of subunit c of ATP synthase." J Biochem **128**(3): 509-516.

Fagone, P. and S. Jackowski (2009). "Membrane phospholipid synthesis and endoplasmic reticulum function." J Lipid Res **50 Suppl**: S311-316.

Fass, D. (2012). "Disulfide bonding in protein biophysics." Annu Rev Biophys **41**: 63-79.

Feige, M. J. and L. M. Hendershot (2011). "Disulfide bonds in ER protein folding and homeostasis." Current Opinion in Cell Biology **23**(2): 167-175.

Feige, M. J. and L. M. Hendershot (2011). "Disulfide bonds in ER protein folding and homeostasis." Curr Opin Cell Biol **23**(2): 167-175.

Gao, H., R. M. Boustany, J. A. Espinola, S. L. Cotman, L. Srinidhi, K. A. Antonellis, T. Gillis, X. Qin, S. Liu, L. R. Donahue, R. T. Bronson, J. R. Faust, D. Stout, J. L. Haines, T. J. Lerner and M. E. MacDonald (2002). "Mutations in a novel CLN6-encoded transmembrane protein cause variant neuronal ceroid lipofuscinosis in man and mouse." Am J Hum Genet **70**(2): 324-335.

Gaynor, E. C., S. te Heesen, T. R. Graham, M. Aebi and S. D. Emr (1994). "Signal-mediated retrieval of a membrane protein from the Golgi to the ER in yeast." Journal of Cell Biology **127**(3): 653-665.

Gemmer, M. and F. Förster (2020). "A clearer picture of the ER translocon complex." Journal of Cell Science **133**(3).

Ghosh, P., N. M. Dahms and S. Kornfeld (2003). "Mannose 6-phosphate receptors: new twists in the tale." Nat Rev Mol Cell Biol **4**(3): 202-212.

Gieselmann, V. (1995). "Lysosomal storage diseases." Biochim Biophys Acta **1270**(2-3): 103-136.

Gieselmann, V., A. Hasilik and K. von Figura (1985). "Processing of human cathepsin D in lysosomes in vitro." Journal of Biological Chemistry **260**(5): 3215-3220.

Gorlach, A., P. Klappa and T. Kietzmann (2006). "The endoplasmic reticulum: folding, calcium homeostasis, signaling, and redox control." Antioxid Redox Signal **8**(9-10): 1391-1418.

Graham, J. M. (2002). "Preparation of crude subcellular fractions by differential centrifugation." ScientificWorldJournal **2**: 1638-1642.

Gupta, P., A. A. Soyombo, J. M. Shelton, I. G. Wilkofsky, K. E. Wisniewski, J. A. Richardson and S. L. Hofmann (2003). "Disruption of PPT2 in mice causes an unusual lysosomal storage disorder with neurovisceral features." Proc Natl Acad Sci U S A **100**(21): 12325-12330.

Haltia, M. (2003). "The neuronal ceroid-lipofuscinoses." J Neuropathol Exp Neurol **62**(1): 1-13.

Hardt, R., D. Winter, V. Gieselmann and M. Eckhardt (2018). "Identification of progesterone receptor membrane component-1 as an interaction partner and possible regulator of fatty acid 2-hydroxylase." Biochem J **475**(5): 853-871.

Heine, C., B. Koch, S. Storch, A. Kohlschutter, D. N. Palmer and T. Braulke (2004). "Defective endoplasmic reticulum-resident membrane protein CLN6 affects lysosomal degradation of endocytosed arylsulfatase A." J Biol Chem **279**(21): 22347-22352.

Heine, C., A. Quitsch, S. Storch, Y. Martin, L. Lonka, A. E. Lehesjoki, S. E. Mole and T. Braulke (2007). "Topology and endoplasmic reticulum retention signals of the lysosomal storage disease-related membrane protein CLN6." Mol Membr Biol **24**(1): 74-87.

Ho, A., C. S. Cho, S. Namkoong, U. S. Cho and J. H. Lee (2016). "Biochemical Basis of Sestrin Physiological Activities." Trends Biochem Sci **41**(7): 621-632.

Holopainen, J. M., J. Saarikoski, P. K. J. Kinnunen and I. Järvelä (2001). "Elevated lysosomal pH in neuronal ceroid lipofuscinoses (NCLs)." European Journal of Biochemistry **268**(22): 5851-5856.

Hu, F., T. Padukkavidana, C. B. Vægter, O. A. Brady, Y. Zheng, I. R. Mackenzie, H. H. Feldman, A. Nykjaer and S. M. Strittmatter (2010). "Sortilin-mediated endocytosis determines levels of the frontotemporal dementia protein, progranulin." Neuron **68**(4): 654-667.

Huang da, W., B. T. Sherman and R. A. Lempicki (2009). "Systematic and integrative analysis of large gene lists using DAVID bioinformatics resources." Nat Protoc **4**(1): 44-57.

Huber, L. A. and D. Teis (2016). "Lysosomal signaling in control of degradation pathways." Curr Opin Cell Biol **39**: 8-14.

Hughes, H. and D. J. Stephens (2010). "Sec16A defines the site for vesicle budding from the endoplasmic reticulum on exit from mitosis." Journal of Cell Science **123**(23): 4032-4038.

Iyanagi, T. (2007). "Molecular mechanism of phase I and phase II drug-metabolizing enzymes: implications for detoxification." Int Rev Cytol **260**: 35-112.

Jaiswal, P. K., S. Koul, N. Palanisamy and H. K. Koul (2019). "Eukaryotic Translation Initiation Factor 4 Gamma 1 (EIF4G1): a target for cancer therapeutic intervention?" Cancer Cell International **19**(1): 224.

Jalanko, A. and T. Braulke (2009). "Neuronal ceroid lipofuscinoses." Biochim Biophys Acta **1793**(4): 697-709.

Janda, C. Y., J. Li, C. Oubridge, H. Hernández, C. V. Robinson and K. Nagai (2010). "Recognition of a signal peptide by the signal recognition particle." Nature **465**(7297): 507-510.

Jenkins, R. W., D. Canals, J. Idkowiak-Baldys, F. Simbari, P. Roddy, D. M. Perry, K. Kitatani, C. Luberto and Y. A. Hannun (2010). "Regulated secretion of acid sphingomyelinase: implications for selectivity of ceramide formation." J Biol Chem **285**(46): 35706-35718.

Kall, L., J. D. Storey, M. J. MacCoss and W. S. Noble (2008). "Assigning significance to peptides identified by tandem mass spectrometry using decoy databases." J Proteome Res **7**(1): 29-34.

Kappeler, F., D. R. Klopfenstein, M. Foguet, J. P. Paccaud and H. P. Hauri (1997). "The recycling of ERGIC-53 in the early secretory pathway. ERGIC-53 carries a cytosolic endoplasmic reticulum-exit determinant interacting with COPII." J Biol Chem **272**(50): 31801-31808.

Kerppola, T. K. (2006). "Design and implementation of bimolecular fluorescence complementation (BiFC) assays for the visualization of protein interactions in living cells." Nat Protoc **1**(3): 1278-1286.

Kerppola, T. K. (2008). "Bimolecular fluorescence complementation (BiFC) analysis as a probe of protein interactions in living cells." Annu Rev Biophys **37**: 465-487.

Kerppola, T. K. (2009). "Visualization of molecular interactions using bimolecular fluorescence complementation analysis: characteristics of protein fragment complementation." Chem Soc Rev **38**(10): 2876-2886.

Khan, S. A. and S. C. Tomatsu (2020). "Mucolipidoses Overview: Past, Present, and Future." Int J Mol Sci **21**(18).

Kleizen, B. and I. Braakman (2004). "Protein folding and quality control in the endoplasmic reticulum." Current Opinion in Cell Biology **16**(4): 343-349.

Koike, M., H. Nakanishi, P. Saftig, J. Ezaki, K. Isahara, Y. Ohsawa, W. Schulz-Schaeffer, T. Watanabe, S. Waguri, S. Kametaka, M. Shibata, K. Yamamoto, E. Kominami, C. Peters, K. von Figura and Y. Uchiyama (2000). "Cathepsin D deficiency induces lysosomal storage with ceroid lipofuscin in mouse CNS neurons." J Neurosci **20**(18): 6898-6906.

Kollmann, K., K. Uusi-Rauva, E. Scifo, J. Tyynela, A. Jalanko and T. Braulke (2013). "Cell biology and function of neuronal ceroid lipofuscinosis-related proteins." Biochim Biophys Acta **1832**(11): 1866-1881.

Kollmann, K., K. Uusi-Rauva, E. Scifo, J. Tyynelä, A. Jalanko and T. Braulke (2013). "Cell biology and function of neuronal ceroid lipofuscinosis-related proteins." Biochimica et Biophysica Acta (BBA) - Molecular Basis of Disease **1832**(11): 1866-1881.

Kornfeld, S. (1986). "Trafficking of lysosomal enzymes in normal and disease states." J Clin Invest **77**(1): 1-6.

Kornfeld, S. (1998). "Diseases of abnormal protein glycosylation: an emerging area." J Clin Invest **101**(7): 1293-1295.

Kozlov, G. and K. Gehring (2020). "Calnexin cycle - structural features of the ER chaperone system." FEBS J **287**(20): 4322-4340.

Kudla, J. and R. Bock (2016). "Lighting the Way to Protein-Protein Interactions: Recommendations on Best Practices for Bimolecular Fluorescence Complementation Analyses." Plant Cell **28**(5): 1002-1008.

Kühnel, W. and W. Kühnel (2003). Color atlas of cytology, histology, and microscopic anatomy. Stuttgart ; New York, Thieme.

Kundra, R. and S. Kornfeld (1999). "Asparagine-linked Oligosaccharides Protect Lamp-1 and Lamp-2 from Intracellular Proteolysis *." Journal of Biological Chemistry **274**(43): 31039-31046.

Kurze, A. K., G. Galliciotti, C. Heine, S. E. Mole, A. Quitsch and T. Braulke (2010). "Pathogenic mutations cause rapid degradation of lysosomal storage disease-related membrane protein CLN6." Hum Mutat **31**(2): E1163-1174.

Lamriben, L., J. B. Graham, B. M. Adams and D. N. Hebert (2016). "N-Glycan-based ER Molecular Chaperone and Protein Quality Control System: The Calnexin Binding Cycle." Traffic **17**(4): 308-326.

Lang, C. M., K. Fellerer, B. M. Schwenk, P.-H. Kuhn, E. Kremmer, D. Edbauer, A. Capell and C. Haass (2012). "Membrane Orientation and Subcellular Localization of Transmembrane Protein 106B (TMEM106B), a Major Risk Factor for Frontotemporal Lobar Degeneration *[♦]." Journal of Biological Chemistry **287**(23): 19355-19365.

LeBoeuf, R. C., M. Caldwell, Y. Guo, C. Metz, M. A. Davitz, L. K. Olson and M. A. Deeg (1998). "Mouse glycosylphosphatidylinositol-specific phospholipase D (Gpld1) characterization." Mamm Genome **9**(9): 710-714.

Letovsky, S. and S. Kasif (2003). "Predicting protein function from protein/protein interaction data: a probabilistic approach." Bioinformatics **19**(suppl_1): i197-i204.

Li, C. M., S. B. Hong, G. Kopal, X. He, T. Linke, W. S. Hou, J. Koch, S. Gatt, K. Sandhoff and E. H. Schuchman (1998). "Cloning and characterization of the full-length

cDNA and genomic sequences encoding murine acid ceramidase." Genomics **50**(2): 267-274.

Li, P., J. Li, L. Wang and L. J. Di (2017). "Proximity Labeling of Interacting Proteins: Application of BioID as a Discovery Tool." Proteomics **17**(20).

Lis, H. and N. Sharon (1993). "Protein glycosylation. Structural and functional aspects." Eur J Biochem **218**(1): 1-27.

Liu, G. Y. and D. M. Sabatini (2020). "mTOR at the nexus of nutrition, growth, ageing and disease." Nat Rev Mol Cell Biol **21**(4): 183-203.

Lloyd-Evans, E., H. Waller-Evans, K. Peterneva and F. M. Platt (2010). "Endolysosomal calcium regulation and disease." Biochem Soc Trans **38**(6): 1458-1464.

Mamo, A., F. Jules, K. Dumaresq-Doiron, S. Costantino and S. Lefrancois (2012). "The role of ceroid lipofuscinosis neuronal protein 5 (CLN5) in endosomal sorting." Mol Cell Biol **32**(10): 1855-1866.

Mancias, J. D. and J. Goldberg (2005). "Exiting the endoplasmic reticulum." Traffic **6**(4): 278-285.

McNeil, P. L. and T. Kirchhausen (2005). "An emergency response team for membrane repair." Nat Rev Mol Cell Biol **6**(6): 499-505.

Mellacheruvu, D., Z. Wright, A. L. Couzens, J. P. Lambert, N. A. St-Denis, T. Li, Y. V. Miteva, S. Hauri, M. E. Sardiu, T. Y. Low, V. A. Halim, R. D. Bagshaw, N. C. Hubner, A. Al-Hakim, A. Bouchard, D. Faubert, D. Fermin, W. H. Dunham, M. Goudreault, Z. Y. Lin, B. G. Badillo, T. Pawson, D. Durocher, B. Coulombe, R. Aebersold, G. Superti-Furga, J. Colinge, A. J. Heck, H. Choi, M. Gstaiger, S. Mohammed, I. M. Cristea, K. L. Bennett, M. P. Washburn, B. Raught, R. M. Ewing, A. C. Gingras and A. I. Nesvizhskii (2013). "The CRAPome: a contaminant repository for affinity purification-mass spectrometry data." Nat Methods **10**(8): 730-736.

Mellman, I. (1989). "Organelles observed: lysosomes." Science **244**(4906): 853-854.

Mellman, I., R. Fuchs and A. Helenius (1986). "Acidification of the endocytic and exocytic pathways." Annu Rev Biochem **55**: 663-700.

Meyer-Schwesinger, C. (2021). "Lysosome function in glomerular health and disease." Cell Tissue Res **385**(2): 371-392.

Miller, E. A., T. H. Beilharz, P. N. Malkus, M. C. S. Lee, S. Hamamoto, L. Orci and R. Schekman (2003). "Multiple Cargo Binding Sites on the COPII Subunit Sec24p Ensure Capture of Diverse Membrane Proteins into Transport Vesicles." Cell **114**(4): 497-509.

Miller, W. L. (1988). "Molecular biology of steroid hormone synthesis." Endocr Rev **9**(3): 295-318.

Moerke, N. J., H. Aktas, H. Chen, S. Cantel, M. Y. Reibarkh, A. Fahmy, John D. Gross, A. Degterev, J. Yuan, M. Chorev, J. A. Halperin and G. Wagner (2007). "Small-Molecule Inhibition of the Interaction between the Translation Initiation Factors eIF4E and eIF4G." Cell **128**(2): 257-267.

Mole, S. E., G. Michaux, S. Codlin, R. B. Wheeler, J. D. Sharp and D. F. Cutler (2004). "CLN6, which is associated with a lysosomal storage disease, is an endoplasmic reticulum protein." Exp Cell Res **298**(2): 399-406.

Morgan, J. P., H. Magee, A. Wong, T. Nelson, B. Koch, J. D. Cooper and J. M. Weimer (2013). "A Murine Model of Variant Late Infantile Ceroid Lipofuscinosis Recapitulates

Behavioral and Pathological Phenotypes of Human Disease." PLOS ONE **8**(11): e78694.

Morita, M., L. W. Ler, M. R. Fabian, N. Siddiqui, M. Mullin, V. C. Henderson, T. Alain, B. D. Fonseca, G. Karashchuk, C. F. Bennett, T. Kabuta, S. Higashi, O. Larsson, I. Topisirovic, R. J. Smith, A. C. Gingras and N. Sonenberg (2012). "A novel 4EHP-GIGYF2 translational repressor complex is essential for mammalian development." Mol Cell Biol **32**(17): 3585-3593.

Mumtaz, S. and B. K. Bachhawat (1992). "Enzyme engineering and its application in lysosomal storage disease." Pure and Applied Chemistry **64**(8): 1055-1060.

Navarro, P., M. Trevisan-Herraz, E. Bonzon-Kulichenko, E. Nunez, P. Martinez-Acedo, D. Perez-Hernandez, I. Jorge, R. Mesa, E. Calvo, M. Carrascal, M. L. Hernaez, F. Garcia, J. A. Barcena, K. Ashman, J. Abian, C. Gil, J. M. Redondo and J. Vazquez (2014). "General statistical framework for quantitative proteomics by stable isotope labeling." J Proteome Res **13**(3): 1234-1247.

Newstead, S. and F. Barr (2020). "Molecular basis for KDEL-mediated retrieval of escaped ER-resident proteins – SWEET talking the COPs." Journal of Cell Science **133**(19): jcs250100.

Ng, E. L., B. Q. Gan, F. Ng and B. L. Tang (2012). "Rab GTPases regulating receptor trafficking at the late endosome-lysosome membranes." Cell Biochem Funct **30**(6): 515-523.

Nicchitta, C. V. (2002). "A platform for compartmentalized protein synthesis: protein translation and translocation in the ER." Curr Opin Cell Biol **14**(4): 412-416.

Nita, D. A., S. E. Mole and B. A. Minassian (2016). "Neuronal ceroid lipofuscinoses." Epileptic Disord **18**(S2): 73-88.

Nyfeler, B., S. W. Michnick and H.-P. Hauri (2005). "Capturing protein interactions in the secretory pathway of living cells." Proceedings of the National Academy of Sciences **102**(18): 6350-6355.

Nyfeler, B., S. W. Michnick and H. P. Hauri (2005). "Capturing protein interactions in the secretory pathway of living cells." Proc Natl Acad Sci U S A **102**(18): 6350-6355.

Onyenwoke, R. U. and J. E. Brenman (2015). "Lysosomal Storage Diseases-Regulating Neurodegeneration." J Exp Neurosci **9**(Suppl 2): 81-91.

Owen, C. from https://slideplayer.com/slide/10613641.

Palmer, D. N., I. M. Fearnley, S. M. Medd, J. E. Walker, R. D. Martinus, S. L. Bayliss, N. A. Hall, B. D. Lake, L. S. Wolfe and R. D. Jolly (1989). "Lysosomal storage of the DCCD reactive proteolipid subunit of mitochondrial ATP synthase in human and ovine ceroid lipofuscinoses." Adv Exp Med Biol **266**: 211-222; discussion 223.

Palmieri, M., S. Impey, H. Kang, A. di Ronza, C. Pelz, M. Sardiello and A. Ballabio (2011). "Characterization of the CLEAR network reveals an integrated control of cellular clearance pathways." Hum Mol Genet **20**(19): 3852-3866.

Pappenheimer, A. M. and J. Victor (1946). ""Ceroid" Pigment in Human Tissues." Am J Pathol **22**(2): 395-413.

Parenti, G., G. Andria and A. Ballabio (2015). "Lysosomal storage diseases: from pathophysiology to therapy." Annu Rev Med **66**: 471-486.

Pelletier, M. F., A. Marcil, G. Sevigny, C. A. Jakob, D. C. Tessier, E. Chevet, R. Menard, J. J. Bergeron and D. Y. Thomas (2000). "The heterodimeric structure of

glucosidase II is required for its activity, solubility, and localization in vivo." Glycobiology **10**(8): 815-827.

Perez-Riverol, Y., A. Csordas, J. Bai, M. Bernal-Llinares, S. Hewapathirana, D. J. Kundu, A. Inuganti, J. Griss, G. Mayer, M. Eisenacher, E. Perez, J. Uszkoreit, J. Pfeuffer, T. Sachsenberg, S. Yilmaz, S. Tiwary, J. Cox, E. Audain, M. Walzer, A. F. Jarnuczak, T. Ternent, A. Brazma and J. A. Vizcaino (2019). "The PRIDE database and related tools and resources in 2019: improving support for quantification data." Nucleic Acids Res **47**(D1): D442-D450.

Periquet, M., O. Corti, S. Jacquier and A. Brice (2005). "Proteomic analysis of parkin knockout mice: alterations in energy metabolism, protein handling and synaptic function." Journal of Neurochemistry **95**(5): 1259-1276.

Platt, F. M., B. Boland and A. C. van der Spoel (2012). "Lysosomal storage disorders: The cellular impact of lysosomal dysfunction." Journal of Cell Biology **199**(5): 723-734.

Platt, F. M., A. d'Azzo, B. L. Davidson, E. F. Neufeld and C. J. Tifft (2018). "Lysosomal storage diseases." Nat Rev Dis Primers **4**(1): 27.

Radke, J., W. Stenzel and H. H. Goebel (2015). "Human NCL Neuropathology." Biochim Biophys Acta **1852**(10 Pt B): 2262-2266.

Raiborg, C., E. M. Wenzel and H. Stenmark (2015). "ER-endosome contact sites: molecular compositions and functions." EMBO J **34**(14): 1848-1858.

Rakheja, D. and M. J. Bennett (2018). "Neuronal ceroid-lipofuscinoses." Translational Science of Rare Diseases **3**: 83-95.

Ramirez-Montealegre, D. and D. A. Pearce (2007). "Imaging of late infantile neuronal ceroid lipofuscinosis: a clinical rating scale." Neurology **69**(6): 503-504.

Ramírez, A. S., J. Kowal and K. P. Locher (2019). "Cryo-electron microscopy structures of human oligosaccharyltransferase complexes OST-A and OST-B." Science **366**(6471): 1372-1375.

Raote, I., S. Saxena, F. Campelo and V. Malhotra (2021). "TANGO1 marshals the early secretory pathway for cargo export." Biochimica et Biophysica Acta (BBA) - Biomembranes **1863**(11): 183700.

Reczek, D., M. Schwake, J. Schröder, H. Hughes, J. Blanz, X. Jin, W. Brondyk, S. Van Patten, T. Edmunds and P. Saftig (2007). "LIMP-2 Is a Receptor for Lysosomal Mannose-6-Phosphate-Independent Targeting of β-Glucocerebrosidase." Cell **131**(4): 770-783.

Reinard, T. (2018). Molekularbiologische Methoden 2.0.

Rhinn, H., N. Tatton, S. McCaughey, M. Kurnellas and A. Rosenthal (2022). "Progranulin as a therapeutic target in neurodegenerative diseases." Trends in Pharmacological Sciences **43**(8): 641-652.

Roux, K. J., D. I. Kim, M. Raida and B. Burke (2012). "A promiscuous biotin ligase fusion protein identifies proximal and interacting proteins in mammalian cells." J Cell Biol **196**(6): 801-810.

Ruiz-Canada, C., D. J. Kelleher and R. Gilmore (2009). "Cotranslational and posttranslational N-glycosylation of polypeptides by distinct mammalian OST isoforms." Cell **136**(2): 272-283.

Rus, C.-M., T. Weissensteiner, C. Pereira, I. Susnea, B. D. Danquah, G. Morales Torres, M. E. Rocha, C. Cozma, D. Saravanakumar, S. Mannepalli, K. K. Kandaswamy, S. Di Bucchianico, R. Zimmermann, A. Rolfs, P. Bauer and C. Beetz (2022). "Clinical and genetic characterization of a cohort of 97 CLN6 patients tested at a single center." Orphanet Journal of Rare Diseases **17**(1): 179.

Saito, Y., Y. Ihara, M. R. Leach, M. F. Cohen-Doyle and D. B. Williams (1999). "Calreticulin functions in vitro as a molecular chaperone for both glycosylated and non-glycosylated proteins." EMBO J **18**(23): 6718-6729.

Sardiello, M. and A. Ballabio (2009). "Lysosomal enhancement: a CLEAR answer to cellular degradative needs." Cell Cycle **8**(24): 4021-4022.

Sawiak, S. J., S. R. Perumal, S. R. Rudiger, L. Matthews, N. L. Mitchell, C. J. McLaughlan, C. S. Bawden, D. N. Palmer, T. Kuchel and A. J. Morton (2015). "Rapid and Progressive Regional Brain Atrophy in CLN6 Batten Disease Affected Sheep Measured with Longitudinal Magnetic Resonance Imaging." PLOS ONE **10**(7): e0132331.

Schmidtke, C., S. Tiede, M. Thelen, R. Käkelä, S. Jabs, G. Makrypidi, M. Sylvester, M. Schweizer, I. Braren, N. Brocke-Ahmadinejad, S. L. Cotman, A. Schulz, V. Gieselmann and T. Braulke (2019). "Lysosomal proteome analysis reveals that CLN3-defective cells have multiple enzyme deficiencies associated with changes in intracellular trafficking." J Biol Chem **294**(24): 9592-9604.

Schroder, B., C. Wrocklage, C. Pan, R. Jager, B. Kosters, H. Schafer, H. P. Elsasser, M. Mann and A. Hasilik (2007). "Integral and associated lysosomal membrane proteins." Traffic **8**(12): 1676-1686.

Schroder, B. A., C. Wrocklage, A. Hasilik and P. Saftig (2010). "The proteome of lysosomes." Proteomics **10**(22): 4053-4076.

Schwake, M., B. Schroder and P. Saftig (2013). "Lysosomal membrane proteins and their central role in physiology." Traffic **14**(7): 739-748.

Seehafer, S. S. and D. A. Pearce (2006). "You say lipofuscin, we say ceroid: defining autofluorescent storage material." Neurobiol Aging **27**(4): 576-588.

Settembre, C., A. Fraldi, D. L. Medina and A. Ballabio (2013). "Signals from the lysosome: a control centre for cellular clearance and energy metabolism." Nat Rev Mol Cell Biol **14**(5): 283-296.

Settembre, C., A. Fraldi, D. L. Medina and A. Ballabio (2013). "Signals from the lysosome: a control centre for cellular clearance and energy metabolism." Nature Reviews Molecular Cell Biology **14**(5): 283-296.

Shepherd, V., P. Schlesinger and P. Stahl (1983). Receptors for Lysosomal Enzymes and Glycoproteins. Current Topics in Membranes and Transport. A. Kleinzeller and B. R. Martin, Academic Press. **18:** 317-338.

Shibata, Y., G. K. Voeltz and T. A. Rapoport (2006). "Rough sheets and smooth tubules." Cell **126**(3): 435-439.

Sleat, D. E., H. Lackland, Y. Wang, I. Sohar, G. Xiao, H. Li and P. Lobel (2005). "The human brain mannose 6-phosphate glycoproteome: a complex mixture composed of multiple isoforms of many soluble lysosomal proteins." Proteomics **5**(6): 1520-1532.

Solda, T., C. Galli, R. J. Kaufman and M. Molinari (2007). "Substrate-specific requirements for UGT1-dependent release from calnexin." Mol Cell **27**(2): 238-249.

Staudt, C., E. Puissant and M. Boonen (2016). "Subcellular Trafficking of Mammalian Lysosomal Proteins: An Extended View." Int J Mol Sci **18**(1).

Storch, S. and T. Braulke (2005). Transport of Lysosomal Enzymes. Lysosomes. Boston, MA, Springer US**:** 17-26.

Tanaka, Y., G. Suzuki, T. Matsuwaki, M. Hosokawa, G. Serrano, T. G. Beach, K. Yamanouchi, M. Hasegawa and M. Nishihara (2017). "Progranulin regulates lysosomal function and biogenesis through acidification of lysosomes." Hum Mol Genet **26**(5): 969-988.

Tang, C. H., J. W. Lee, M. G. Galvez, L. Robillard, S. E. Mole and H. A. Chapman (2006). "Murine cathepsin F deficiency causes neuronal lipofuscinosis and late-onset neurological disease." Mol Cell Biol **26**(6): 2309-2316.

Terman, A. and U. T. Brunk (2004). "Lipofuscin." Int J Biochem Cell Biol **36**(8): 1400-1404.

Thelen, M., M. Damme, M. Schweizer, C. Hagel, A. M. Wong, J. D. Cooper, T. Braulke and G. Galliciotti (2012). "Disruption of the autophagy-lysosome pathway is involved in neuropathology of the nclf mouse model of neuronal ceroid lipofuscinosis." PLoS One **7**(4): e35493.

Thelen, M., D. Winter, T. Braulke and V. Gieselmann (2017). "SILAC-Based Comparative Proteomic Analysis of Lysosomes from Mammalian Cells Using LC-MS/MS." Methods Mol Biol **1594**: 1-18.

Thor, F., M. Gautschi, R. Geiger and A. Helenius (2009). "Bulk Flow Revisited: Transport of a Soluble Protein in the Secretory Pathway." Traffic **10**(12): 1819-1830.

Tsuboi, K., Y. X. Sun, Y. Okamoto, N. Araki, T. Tonai and N. Ueda (2005). "Molecular characterization of N-acylethanolamine-hydrolyzing acid amidase, a novel member of the choloylglycine hydrolase family with structural and functional similarity to acid ceramidase." J Biol Chem **280**(12): 11082-11092.

Ungewickell, A., C. Hugge, M. Kisseleva, S. C. Chang, J. Zou, Y. Feng, E. E. Galyov, M. Wilson and P. W. Majerus (2005). "The identification and characterization of two phosphatidylinositol-4,5-bisphosphate 4-phosphatases." Proc Natl Acad Sci U S A **102**(52): 18854-18859.

van Diggelen, O. P., J. L. Keulemans, B. Winchester, I. L. Hofman, S. L. Vanhanen, P. Santavuori and Y. V. Voznyi (1999). "A rapid fluorogenic palmitoyl-protein thioesterase assay: pre- and postnatal diagnosis of INCL." Mol Genet Metab **66**(4): 240-244.

van Meel, E. and J. Klumperman (2008). "Imaging and imagination: understanding the endo-lysosomal system." Histochem Cell Biol **129**(3): 253-266.

van Veen, S., S. Martin, C. Van den Haute, V. Benoy, J. Lyons, R. Vanhoutte, J. P. Kahler, J. P. Decuypere, G. Gelders, E. Lambie, J. Zielich, J. V. Swinnen, W. Annaert, P. Agostinis, B. Ghesquière, S. Verhelst, V. Baekelandt, J. Eggermont and P. Vangheluwe (2020). "ATP13A2 deficiency disrupts lysosomal polyamine export." Nature **578**(7795): 419-424.

Varnaitė, R. and S. A. MacNeill (2016). "Meet the neighbors: Mapping local protein interactomes by proximity-dependent labeling with BioID." PROTEOMICS **16**(19): 2503-2518.

Vitner, E. B., F. M. Platt and A. H. Futerman (2010). "Common and uncommon pathogenic cascades in lysosomal storage diseases." J Biol Chem **285**(27): 20423-20427.

Wang, J., L. L. Molday, T. Hii, J. A. Coleman, T. Wen, J. P. Andersen and R. S. Molday (2018). "Proteomic Analysis and Functional Characterization of P4-ATPase Phospholipid Flippases from Murine Tissues." Sci Rep **8**(1): 10795.

Watson, P., A. K. Townley, P. Koka, K. J. Palmer and D. J. Stephens (2006). "Sec16 defines endoplasmic reticulum exit sites and is required for secretory cargo export in mammalian cells." Traffic **7**(12): 1678-1687.

Wattiaux, R., M. Wibo and P. Baudhuin (1963). "[Effect of the injection of Triton WR 1339 on the hepatic lysosomes of the rat]." Arch Int Physiol Biochim **71**: 140-142.

Westrate, L. M., J. E. Lee, W. A. Prinz and G. K. Voeltz (2015). "Form follows function: the importance of endoplasmic reticulum shape." Annu Rev Biochem **84**: 791-811.

Wheeler, R. B., J. D. Sharp, R. A. Schultz, J. M. Joslin, R. E. Williams and S. E. Mole (2002). "The gene mutated in variant late-infantile neuronal ceroid lipofuscinosis (CLN6) and in nclf mutant mice encodes a novel predicted transmembrane protein." Am J Hum Genet **70**(2): 537-542.

Williams, D. B. (2006). "Beyond lectins: the calnexin/calreticulin chaperone system of the endoplasmic reticulum." J Cell Sci **119**(Pt 4): 615-623.

Winchester, B., A. Vellodi and E. Young (2000). "The molecular basis of lysosomal storage diseases and their treatment." Biochem Soc Trans **28**(2): 150-154.

Wu, S., Z. Li, J. Han and S. Han (2011). "Dual colored mesoporous silica nanoparticles with pH activable rhodamine-lactam for ratiometric sensing of lysosomal acidity." Chem Commun (Camb) **47**(40): 11276-11278.

Yamanaka, S., O. N. Johnson, F. Norflus, D. J. Boles and R. L. Proia (1994). "Structure and expression of the mouse beta-hexosaminidase genes, Hexa and Hexb." Genomics **21**(3): 588-596.

Zaidi, N., A. Maurer, S. Nieke and H. Kalbacher (2008). "Cathepsin D: A cellular roadmap." Biochemical and Biophysical Research Communications **376**(1): 5-9.

Zanetti, G., K. B. Pahuja, S. Studer, S. Shim and R. Schekman (2012). "COPII and the regulation of protein sorting in mammals." Nature Cell Biology **14**(1): 20-28.

8 Appendix

8.1 List of identified biotinylated proteins with the N-terminal BioID construct by mass spectrometry

Listed are the Accessions of proteins, which have at least 4 of possible 6 sample/control abundance ratios surpassing the cut-off of 2						
A0FGR8	P05556	P42167	P63104	Q5SQN1	Q93008	Q9NSD9
A2RRP1	P06493	P42566	P63244	Q5UIP0	Q96A33	Q9NV66
A6NKT7	P06709	P43304	P78344	Q5VV42	Q96A49	Q9NVP1
O00264	P07197	P43307	P84157	Q6KB66	Q96A65	Q9NWW5
O00303	P08195	P46060	Q00341	Q6P2Q9	Q96AG4	Q9NXE4
O00400	P08238	P46108	Q01469	Q6Y7W6	Q96BR5	Q9NZC7
O00425	P08240	P46109	Q02413	Q7KZF4	Q96C36	Q9NZI8
O00571	P0CG47	P48029	Q02952	Q7Z2W4	Q96G23	Q9NZJ5
O14641	P0CG48	P48444	Q04637	Q7Z3J3	Q96HY6	Q9NZT1
O14715	P0DJD0	P48634	Q04721	Q7Z417	Q96I24	Q9P035
O14966	P0DJD1	P48741	Q07065	Q7Z739	Q96JB5	Q9P0L0
O14976	P0DMV8	P49257	Q07960	Q86UE4	Q96S66	Q9P246
O15027	P11142	P49327	Q09666	Q86UL3	Q96SK2	Q9P2E9
O15173	P11717	P49368	Q12769	Q86UP2	Q99460	Q9UBF2
O15371	P11940	P49790	Q12800	Q86XL3	Q99536	Q9UBM7
O15498	P12270	P49792	Q13283	Q86Y07	Q99666	Q9UGP8
O15523	P13797	P49959	Q13435	Q8IWZ3	Q9BSJ8	Q9UHB9
O43396	P14618	P50226	Q13501	Q8IYD1	Q9BTX1	Q9ULH7
O43432	P15170	P50402	Q13573	Q8IZH2	Q9BVP2	Q9UN86
O60488	P15311	P50990	Q13586	Q8N4V1	Q9BZF1	Q9UNE7
O60503	P15924	P51148	Q13619	Q8N511	Q9C0C9	Q9UNF1
O75179	P16435	P51149	Q14008	Q8N5K1	Q9C0E8	Q9UPQ9
O75369	P17066	P51572	Q14126	Q8NBN3	Q9H089	Q9UQR0
O75396	P17706	P51648	Q14145	Q8NC51	Q9H0A0	Q9Y265
O75475	P18031	P52292	Q14157	Q8NEN9	Q9H0U4	Q9Y266
O75534	P20340	P52948	Q14168	Q8NF37	Q9H2J7	Q9Y2H6
O75643	P20700	P53985	Q14247	Q8NFQ8	Q9H2M9	Q9Y2J2
O75694	P21333	P54578	Q14315	Q8TCG1	Q9H361	Q9Y2U8
O75787	P22735	P54652	Q14677	Q8TCJ2	Q9H3N1	Q9Y2Z0
O75844	P23588	P55010	Q14739	Q8TCT9	Q9H3P7	Q9Y385
O94874	P25685	P55036	Q14789	Q8WUM0	Q9H5V9	Q9Y394
O94901	P27797	P55084	Q14839	Q8WUM4	Q9H8Y8	Q9Y4P3
O95292	P27824	P55209	Q15717	Q8WVM8	Q9H910	Q9Y520
O95573	P30519	P55786	Q15738	Q8WWK9	Q9HBM0	Q9Y5A9
O95613	P31939	P58107	Q15758	Q8WWM7	Q9HCU5	Q9Y5M8
O95721	P34931	P61011	Q15907	Q8WXH0	Q9HD20	Q9Y5Z9
P00167	P35579	P61081	Q16850	Q8WYP5	Q9HDC5	Q9Y679
P00387	P35613	P61254	Q4KMQ2	Q92526	Q9NPA0	Q9Y6I9
P00558	P37802	P62491	Q58FF7	Q92575	Q9NPI1	Q9Y6M1
P02786	P39023	P62820	Q5HYI8	Q92616	Q9NQC3	Q9Y6M7
P04264	P40939	P62826	Q5JRA6	Q92879	Q9NR30	
P05067	P42166	P62987	Q5JTV8	Q92928	Q9NS69	

8.2 List of identified biotinylated proteins with the C-terminal BioID construct by mass spectrometry

Listed are the Accessions of proteins, which have at least 4 of possible 6 sample/control abundance ratios surpassing the cut-off of 2						
A6NKT7	P07814	P23246	P55010	Q14008	Q6Y7W6	Q9BVA1
A6NNZ2	P07900	P23284	P55036	Q14157	Q71U36	Q9BXJ9
O00425	P08195	P24928	P55795	Q14247	Q7KZF4	Q9BXS4
O00571	P08238	P25815	P58107	Q14315	Q7Z2W4	Q9BYJ9
O14715	P08865	P26639	P60468	Q14532	Q7Z3J3	Q9C075
O15027	P09651	P27797	P60842	Q14533	Q7Z417	Q9H0L4
O15173	P09874	P27824	P61011	Q14568	Q7Z739	Q9H307
O15523	P09936	P30101	P61978	Q14692	Q7Z7L1	Q9H3N1
O43432	P0CG47	P31942	P62826	Q14697	Q86UE4	Q9HC84
O60884	P0CG48	P31943	P62913	Q14839	Q86UP2	Q9NPA0
O75179	P0DJD0	P31948	P62987	Q15005	Q8IUD2	Q9NQI0
O75533	P0DJD1	P34931	P63244	Q15149	Q8IXB1	Q9NSB2
O75534	P0DMV8	P35998	P68104	Q15154	Q8IZH2	Q9NWW5
O75787	P0DP04	P37802	P68363	Q15155	Q8N1G4	Q9NZC7
O75844	P0DPH7	P39023	P68371	Q15233	Q8N511	Q9NZI8
O76011	P11021	P42167	P69849	Q15323	Q8NBS9	Q9P2E9
O76024	P11142	P43243	P78344	Q15365	Q8NC51	Q9ULH7
O95229	P11233	P43307	P78371	Q15366	Q8NFQ8	Q9UN86
O95613	P11234	P46060	P80303	Q15417	Q8TCJ2	Q9UPQ9
O95793	P13637	P46108	P84103	Q15758	Q8TCT9	Q9Y265
P00338	P13639	P46781	P98088	Q16352	Q8WWM7	Q9Y285
P01782	P13667	P48444	Q00341	Q3ZCM7	Q92598	Q9Y2G8
P01876	P14314	P48634	Q01469	Q58FF3	Q92616	Q9Y2J2
P02545	P14625	P49257	Q04637	Q58FF7	Q92766	Q9Y2U8
P02766	P14923	P49327	Q05639	Q58FF8	Q92769	Q9Y385
P03973	P15880	P49792	Q08211	Q5JPE7	Q93008	Q9Y450
P04083	P15924	P49959	Q09666	Q5JSZ5	Q96A33	Q9Y4H2
P05023	P16615	P50402	Q13085	Q5JTV8	Q96JH7	Q9Y4L1
P05164	P17844	P50990	Q13151	Q5SW79	Q96S66	Q9Y4P3
P06709	P17987	P50993	Q13263	Q5VTE0	Q99614	Q9Y5A9
P06727	P18583	P51572	Q13283	Q68D06	Q99666	Q9Y6M1
P07195	P20930	P51991	Q13347	Q6P5S2	Q99733	
P07197	P21333	P52272	Q13435	Q6PEY2	Q9BQE3	
P07437	P22102	P54652	Q13885	Q6UWP8	Q9BTX1	

8.3 List of identified biotinylated proteins with the BioID-mFA2H construct by mass spectrometry

Listed are the Accessions of proteins, which have at least 4 of possible 6 sample/control abundance ratios surpassing the cut-off of 2						
A6NKT7	P0CG48	P46060	P84157	Q6Y7W6	Q92575	Q9P2E9
O14715	P0DJD0	P46109	Q04637	Q7L5A8	Q96A33	Q9UBF2
O15027	P0DJD1	P48444	Q09666	Q7Z2W4	Q96HY6	Q9UHB9
O95292	P13646	P49327	Q14126	Q7Z3J3	Q96JB5	Q9ULH7
O95573	P16435	P49792	Q14137	Q86UE4	Q99666	Q9UPQ9
P05089	P21333	P49959	Q14247	Q86UP2	Q9BSJ8	Q9Y2U8
P06709	P31948	P50402	Q14315	Q86XL3	Q9BTX1	
P07197	P37802	P51648	Q14739	Q8NFQ8	Q9H089	
P08240	P42166	P52948	Q5HYI8	Q8WXH0	Q9HDC5	
P0CG47	P42167	P62987	Q5JTV8	Q8WYP5	Q9NQC3	

8.4 List of identified proteins with the N-terminal BioID construct by mass spectrometry using 2h as biotin incubation time

Listed are the Accessions of proteins, which have at least 4 of possible 6 sample/control abundance ratios surpassing the cut-off of 2					
O75439	P0CG47	P23246	P42167	P62987	Q6Y7W6
P00390	P0CG48	P31943	P50402	Q04637	Q9NZC7
P06709	P21333	P42166	P55795	Q14739	Q9Y446

9 List of Figures

10 List of Tables

11 Acknowledgment

First and foremost, I thank Prof. Dr. Volkmar Gieselmann for giving me the opportunity to work on this interesting topic and supporting me throughout my thesis with his professional competence and careful considerations. Particularly I appreciate that his door was always open and I am very grateful for his supportive guidance and approachability.

Furthermore, I thank Prof. Dr. Oliver Gruß for his readiness to supervise and assess this thesis as well as his helpful suggestions and valuable impulses during this project. I also want to thank Prof. Dr. Thomas Becker for his kindness in giving me the possibility to continue and complete my thesis.

Special thanks are directed to Dr. Melanie Thelen for her dedicated mentoring, which had a huge impact in promoting my project. I am grateful to her for sharing her extremely profound insights in this topic, motivating discussions and giving me the best possible support. Moreover, I thank Simone Mausbach for showing me the ropes, helping me to get acquainted with the whole laboratory and being always addressable. I am also grateful for her technical support, especially in the tritosome isolation and TMT-labeling. I also want to express my gratitude to Dr. Edgar Kaade for helping me with his experience and the western blots showing the enrichment in the tritosome fractions. Overall, I thank the whole working group for a supportive and pleasant working environment and also cherish the fun and memorable moments, which made work a lot easier.

Another thanks belongs to Marc Sylvester, who I want to acknowledge for his assistance in mass spectrometry related questions and for conducting the mass spectrometry measurements.

At this point I also want to thank all members of the Institute for Biochemistry and Molecular Biology Bonn for the good cooperation and positive working atmosphere.

Finally, I like to show my deep gratitude to those, who supported me during the thesis and encouraged me when things did not always go as supposed to. I couldn’t have done it without you.